INVESTIGATIONS INTO NEW METHODS OF ANALYSIS BY ATOMIC AND MOLECULAR FLUORESCENCE AND FLAME EMISSION

by

Ronald Frederick Suddendorf

A Dissertation Submitted to the Faculty of the

DEPARTMENT OF CHEMISTRY

In Partial Fulfillment of the Requirements
For the Degree of

DOCTOR OF PHILOSOPHY

In the Graduate College

THE UNIVERSITY OF ARIZONA

1 9 7 6

THE UNIVERSITY OF ARIZONA

GRADUATE COLLEGE

I hereby recommend that this dissertation prepared under my direction by Ronald Frederick Suddendorf

entitled Investigations into New Methods of Analysis by Atomic and Molecular Fluorescence and Flame Emission

be accepted as fulfilling the dissertation requirement of the degree of Doctor of Philosophy

M Bonner Denton 5-3-76

Dissertation Director Date

After inspection of the final copy of the dissertation, the following members of the Final Examination Committee concur in its approval and recommend its acceptance:*

M Bonner Denton	5-3-76
Dantus Fernando	May 3, 1976
M F Dunker	5/3/76
Walter B. Miller	3 May 76
G. K. Vemulapalli	3 May 76

*This approval and acceptance is contingent on the candidate's adequate performance and defense of this dissertation at the final oral examination. The inclusion of this sheet bound into the library copy of the dissertation is evidence of satisfactory performance at the final examination.

STATEMENT BY AUTHOR

This dissertation has been submitted in partial fulfillment of requirements for an advanced degree at The University of Arizona and is deposited in the University Library to be made available to borrowers under rules of the Library.

Brief quotations from this dissertation are allowable without special permission, provided that accurate acknowledgment of source is made. Requests for permission for extended quotation from or reproduction of this manuscript in whole or in part may be granted by the head of the major department or the Dean of the Graduate College when in his judgment the proposed use of the material is in the interests of scholarship. In all other instances, however, permission must be obtained from the author.

SIGNED: Ronald Frederick Judd

ACKNOWLEDGMENTS

The author wishes to express his appreciation and thanks to Dr. M. Bonner Denton for the encouragement, help, and guidance that he has given throughout this work.

The author would also like to thank the chemistry faculty, especially the Analytical Division, for their help and guidance.

TABLE OF CONTENTS

TABLE OF CONTENTS--Continued

LIST OF ILLUSTRATIONS

LIST OF ILLUSTRATIONS--Continued

LIST OF ILLUSTRATIONS--Continued

LIST OF ILLUSTRATIONS--Continued

LIST OF ILLUSTRATIONS--Continued

LIST OF ILLUSTRATIONS--Continued

LIST OF TABLES

ABSTRACT

Investigations are described into the design, construction and evaluation of a premixed oxygen-hydrogen burner for the analysis of small sample volumes by flame emission and atomic fluorescence. Data are presented showing gas flow rates and maximum allowable burner temperature to produce a safe and stable premixed flame of either oxygen-hydrogen or oxygen-acetylene. A special one-hole insert burner was constructed which allowed the safe acquisition of this data as both a function of exit port diameter and burner temperature.

The sample introduction method, which is based on pulsed ultrasonic nebulization, includes the capability to change samples without extinguishing the flame. Included in the study is the effect of pulse time and sample volume on the emission intensity. Such data are valuable in determining the optimum operating conditions for a given analysis. The accuracy of this method is demonstrated by the analysis of NBS liver samples.

The parameters affecting sensitivity of fluorescence analysis with laser excitation was also studied. Included was an investigation into the effect of monochromator position and slit width on the background and fluorescence intensity. The conditions to obtain maximum sensitivity were then determined by running working curves and detection limits under different experimental conditions. The design and construction of

a pulse amplifier and its effect on laser excited molecular fluorescence is also discussed.

CHAPTER 1

INTRODUCTION

Many areas of research today require trace metal analysis techniques which not only possess good sensitivity, but which can be conveniently used with small sample volumes. The development of new sample introduction methods have been promoted by workers in such areas as biomedical and pollution research, where sample volumes may often be limited. Of the three commonly used atomic methods of analysis ; atomic absorption, flame emission and atomic fluorescence, probably the greatest number and variety of sample introduction techniques have been developed for atomic absorption spectrometry. This is partly the result of atomic absorption being used on a more routine basis today than either flame emission or atomic fluorescence techniques.

One of the first atomic absorption atomizers capable of handling small volume samples was the Lvov Furnace (46). This device consists of a heated hollow graphite tube through which radiation from a hollow cathode lamp is passed. An electrode, mounted below a hole in the tube, holds the sample to be analyzed and is heated producing atomic vapor in the graphite tube and the resulting absorption of radiation is measured. This device has several drawbacks, the first being that the tube must be purged with either argon or nitrogen to remove all oxygen. This prevents

the tube from burning when it is heated. Another drawback is that sample changing is tedious and time consuming.

Another tube type atomizer has been designed by Massmann (47, 48). This consists of a hollow graphite tube mounted horizontally with a small sample introduction port at the top. Sample is then placed in the tube by way of this introduction port using a micropipet. The tube is then purged of oxygen and heated to 2,600°C in a few seconds and the absorption which occurred is then measured. With this design, sample volumes in the range of 5 to 200 μl could be used.

The Massmann modification of the basic Lvov graphite tube furnace is available commercially from Perkin-Elmer Corporation (known commercially as the Heated Graphite Atomizer or HGA). This model can operate with sample volumes from 1 to 100 μl which are introduced to the graphite tube through a 2 mm hole at the top of the tube. The atomizer has a water jacket which is used to dissipate heat after a run. With this system as many as 40 samples can be run in one hour.

In addition to the nonflame methods just described, several small volume methods have been devised for atomic absorption using a flame as the primary atomization source. The tantalum boat (36, 62) is an example of a commonly used small volume introduction method. With this technique a sample is placed on a tantalum boat, allowed to dry and then pushed into the flame where atomization takes place. The boat is positioned just below the hollow cathode beam so as to produce a maximum atomic concentration at the beam. Sample volumes used with this method are typically 1 ml although smaller volumes can be used. One problem that

occurs with this method is a lack of precision. If the sample is not reproducibly placed on the boat, then a different distribution of atomic vapor will occur in each atomization step. Also the boat has a tendency to change shape after repeated use and this also affects the precision of the method.

The Delves Cup (11) was developed for the analysis of lead in whole blood. In addition to requiring only 10 μl of sample, it is a rapid and sensitive technique. It consists of an absorption tube constructed from nickel which is fastened above a three-slot burner. The sample is placed in a small nickel cup which is positioned in a wire loop. The cup is then placed in the flame below an entrance port in the nickel tube. As atomic vapor flows from the cup into the tube, the absorption of radiation is measured.

Although the methods described so far work quite well for atomic absorption they are not readily adaptable for analysis by flame emission. For example, the Lvov furnace and Massmann graphite tube do not produce a large enough atomic population in the excited state to make analysis by emission possible with these techniques. The tantalum boat and Delves cup techniques are used with an air acetylene flame. Although it would be possible to do flame emission with these techniques, the best flame emission analysis is usually carried out in much hotter flames. Because of these restrictions, the small volume analysis methods developed for atomic absorption are not readily adaptable for analysis by flame emission. Several methods have been developed for analysis of small sample volumes by flame emission which use design characteristics different from those for atomic absorption.

One of the first small sample volume methods for analysis by flame emission was the use of a platinum wire (59, 60, 61) of 0.38 mm thick which was bent to form a loop of 2.54 mm in diameter. A sample to be analyzed was placed on the loop and allowed to dry. The loop was then inserted into an air-methane flame and the emission intensity was integrated. The total emission intensity could then be related to the atomic concentration in the sample. Using this method as little as 10^{-3} μl of sample could be analyzed.

Muller (52) used the platinum wire method for the analysis of sodium and potassium in nerve fibers. The calibration curve for potassium ranged from 10^{-9} moles to 10^{-14} moles. The calibration curve was constructed by applying different volumes of a given concentration on the wire. At the lower end of the curve a greater scatter in the data points occurred presumably because of the difficulty in reproducibly placing the small sample volumes on the wire.

Additional work done with this technique has included the development of a system to reproducibly place the wire loop in a flame (54). This consisted of mounting the wire loop on a rotatable arm which was activated by a solenoid. In work done with this system, the hydrogen-air entrained flame was used. The air flowing around the flame was purified by passing it through a filter. This eliminated any dust particles from getting into the flame and resulted in a decrease in background noise. A dual channel detector system was employed to monitor both the sodium and potassium emission lines. An interference filter and a selenium photoelement were used for the sodium channel and an

interference filter and semiconductor element for the potassium channel. An integrating circuit was used with each channel. Reproducibility was quite good with this particular system; for 3×10^{-10} mole of sodium in a 2×10^{-3} µl volume a relative standard deviation of 1.7% was found. In the case of 10^{-11} mole of potassium in 2×10^{-3} µl a relative standard deviation of 3.3% was observed.

A different approach to the analysis of small sample volumes was taken by Solomon and Caton (64). These workers machined a sample cup from lucite which had a total volume of 1 ml. A sample to be analyzed was placed in the cup and the capillary tube from a Beckman total consumption burner was then inserted into the sample cup. The sample was aspirated and the resulting emission observed. For 1 ml sample volumes of 100 n moles sodium a standard deviation of 0.6% was found, for 6 n moles of potassium a standard deviation of 1.5% was observed. Detection limits obtained by this method were 0.2 ppb for sodium and 1.0 ppb for potassium. This system was eventually used on sample volumes as small as 1 µl for the analysis of sodium and potassium in single kidney tubules.

Exley and Sproat (18) used a microcup which held a sample volume of 100 µl and was treated with silicone fluid to reduce surface tension and therefore allowed all of the sample to be aspirated. By modifying a Beckman DU flame spectrometer and adding a circuit to electrically integrate the total flame emission they were able to make the device 1000 times more sensitive than before. In addition, samples dissolved in acetone increased the sensitivity by a factor of 60,000.

Ultimate detection limits were found to be 3×10^{-13} g for sodium and 10^{-10} g for magnesium. The improved detection limits using acetone as a solvent is the result of a greatly improved aspiration rate and an increased rate of desolvation. One problem associated with the use of small volumes of acetone is that it quickly evaporates. As a result of this an error of $\pm$ 5% was found when using acetone as a solvent.

A third type of device used for emission analysis is a helium-glow photometer (68). This method is based on the fact that electrical excitation of helium at atmospheric pressure through the use of a high voltage radio frequency field produces excited state helium atoms. The helium atoms then transfer their energy to other atoms causing them to reach an excited state and emit radiation. A sample to be analyzed is placed on an iridium wire and inserted into a cavity containing the helium. The radio frequency field is applied by an electrode mounted outside a quartz emission chamber. The emitted light is passed through a filter and monitored by a photomultiplier tube. Using this method volumes from 2 to 10 n 1 containing 10^{-11} to 10^{-13} moles of an element can be determined.

Although the methods for analysis by flame emission just described do operate with small volumes, they are not as quick and easy to use as those methods for atomic absorption. For example, the use of a platinum loop requires a great deal of operator skill to reproducibly place the sample on the loop. A sample not placed in the same position each time will be vaporized and atomized at a different rate and thus will not be reproducible. The helium glow photometer suffers from the

same problem of sample placement and also requires a greater amount of time to change samples. In addition, these methods do not employ high temperature flames which can result in an increase in vaporization interferences. Also these methods do not supply the necessary energy to excite a large population of the available atoms which can result in poor sensitivity.

There are several characteristics which should be possessed by a system for the analysis of small volume samples by flame emission. Ideally, the flame should be of a high temperature. This serves several purposes. First it allows for the rapid desolvation and atomization of the sample. This fact is important in reducing both chemical and physical interferences in the flame. The use of a high temperature flame also provides enough excitation energy to the atomic vapor to produce a more intense emission signal. Several flames are suitable for this purpose including oxygen-hydrogen, oxygen-acetylene and nitrous oxide-acetylene. The merits of each flame have been discussed elsewhere in detail (26, 27). The primary advantage of an oxygen-hydrogen flame is its low background emission spectra. This allows for wider slit widths to be used with the monochromator and thus increase the amount of light passing through the monochromator. The acetylene flames have the advantage of producing a more reducing environment and as a result help to prevent oxide and hydroxide formation in the flame.

The system should also have the capability to analyze samples quickly and easily. The wire loop method of analysis does not handle samples quickly since the solution must be allowed to dry after it is

applied to the wire. The technique of aspirating a "plug" of sample through a total consumption burner is quick, but it does not make effective use of the total available sample volume. The name "total consumption" burner is somewhat of a misnomer since this burner converts less than 50% of its total uptake of salt species into a useable vaporized form (30). Therefore, aspirating a small sample volume through a pneumatic nebulizer is a quick way to run samples, but it does not make effective use of the total sample volume and thus results in less than optimum sensitivity. For this reason any new methods should not only be quick and easy to use, but should make efficient use of the total available sample.

The ultimate goal of any new analytical technique is that it be simple enough to be used on a routine basis for analysis. Therefore, it should yield reproducible results with a minimum of operator training and skill. The method should be free from contamination and also changes in sensitivity as a result of prolonged use.

Because the methods currently available for analysis of small sample volumes by atomic absorption are not readily adapted to flame emission, and since those techniques now available for analysis by flame emission have severe limitations it was decided to design, construct and evaluate a system for the analysis of small sample volumes by flame emission and atomic fluorescence. The system to be used was to meet the criteria outlined above and would be based on the use of ultrasonic nebulization as the means of sample introduction.

CHAPTER 2

BURNING PARAMETERS OF PREMIXED OXYGEN-HYDROGEN AND OXYGEN-ACETYLENE FLAMES

Background

In recent years premixed laminar flow flames have enjoyed increasing popularity over turbulent flames due to their lower flicker, reduced rise velocities, increased dimensional stability and improved homogeneity. Such flames have become the standard for routine analysis by atomic absorption (AA) and are gaining acceptance by workers employing flame emission (FE) and atomic fluorescence (AF).

Choosing the optimum flame composition for performing a given analysis depends not only on the technique employed (emission, absorption, or fluorescence), but also on the element to be determined and the nature of other species which may be present. The investigator must consider the chemical environment produced by a particular gas mixture, temperature, background emission, the presence or absence of quenching species and the availability of a burner design capable of safe, stable operation with that mixture.

The primary function of a flame in flame emission spectroscopy is to produce free atoms and to provide the necessary energy to place those atoms in an excited state. The major processes occurring in a flame are diagrammed in Figure 1. As the solution containing a metallic

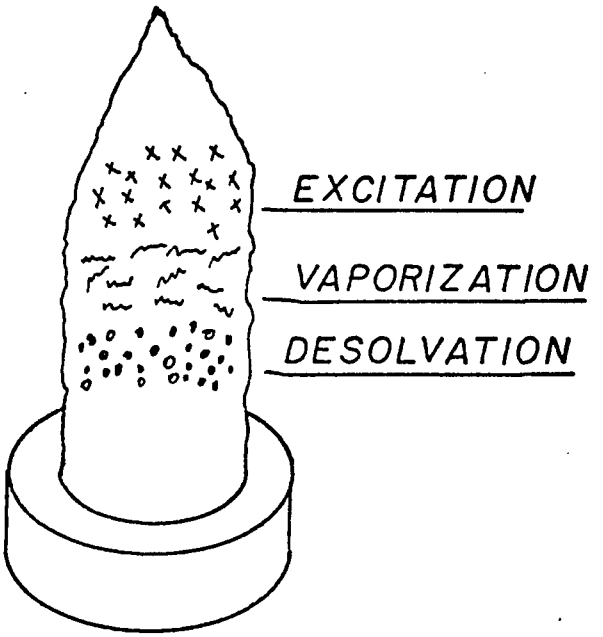

Figure 1. Processes occurring within an ideal flame.

salt is sprayed into the flame the first process to occur is the desolvation of the solvent. This is simply the boiling away of the solvent to form a salt particle. If solvent remains trapped in the salt particle, dehydration of the particle occurs next. Following this atomization of the solid particle occurs, if any molecular species have formed in the flame they are also dissociated to the atomic form. Once atomization has occurred the atomic species are placed in an excited state through collisions with high energy species within the flame. Finally, emission of line radiation takes place.

The degree to which the processes described above are complete depends to a great extent on the characteristics of the flame. For example, a very hot flame will be more efficient at producing atoms in the excited state than will a cooler flame. A high temperature flame will also be more efficient at producing a high concentration of free atoms. Although high temperature flames may solve the problems of atomization and excitation they can introduce other problems. At higher flame temperatures the number of atoms which become ionized increases and thus reduces the number of neutral atoms available for emission.

Table 1 lists the theoretical temperature, measured temperature and burning velocity of several commonly used flames in flame spectrochemical analysis. As can be seen from this table the premixed oxygen-hydrogen flame has a temperature of between 2550°C and 2700°C, thus it is one of the hottest flames listed. In addition to the high temperature, this flame possesses a very low background emission. The only significant background emission occurs at the wavelengths of 2811Å, 3064Å and

Table 1. Temperatures and burning velocities of common premixed flames.*

Fuel	Oxidant	Temperature (°C)		Burning Velocity (cm/sec)
		Theoret.	Meas.	
Acetylene	Air	2050	2125-2400	160-266 (160)
Acetylene	Oxygen	3110	3060-3135	800-2480 (1100)
Acetylene	Nitrous oxide	--	2600-2800	160
Hydrogen	Air	2115	2000-2050	320-440
Hydrogen	Oxygen	2690	2550-2700	900-3680 (2000)
Methane	Air	1955	1875	70
Methane	Oxygen	2720	2670	5502 (?)
Natural Gas	Air	1840	1700-1900	55
Natural Gas	Oxygen	2800	2740	--

* Taken from Dean and Rains (10).

3428Å (26). Between the wavelengths of 3300Å to 6000Å the background is very low. Because of this few interferences, as a result of background emission, occur when using this flame. Therefore, it is possible to open the slits to a wider diameter and view a greater area of the flame. Using wider slit widths allows more light to be collected and helps to lower the detection limits obtainable with this flame (26).

Owing to the small number of combustion products formed an oxygen-hydrogen flame produces a weak background intensity. Some of the reactions which occur in an oxygen-hydrogen flame are listed below (35).

$$H_2 + O_2 \rightarrow H + HO_2$$

$$H + O_2 \rightarrow OH + O$$

$$OH + H_2 \rightarrow H + H_2O$$

$$O + H_2 \rightarrow H + OH$$

Another interesting characteristic of the oxygen-hydrogen flame is its high electron concentration, which can shift the ionization equilibria of metals. The electron concentration of oxygen-hydrogen flames containing carbon compounds is characterized by the following reactions (16, 41, 45, 58).

$$C_2 + OH = CO + CH$$

$$CH + O = CHO^+ + e^-$$

$$CHO^+ + H_2O = CO + H_3O^+$$

This can be a very important effect when measuring low concentrations of alkali and alkaline earth metals which have a high degree of ionization in hot flames.

In contrast to the low background emission of an oxygen-hydrogen flame, the oxygen-acetylene flame possesses a very intense background. This is the result of the large variety of combustion products formed in an oxygen-acetylene flame. Some of the products which have been identified are (9, 24): O_2, N_2, CO_2, CO, H_2O, C_2H_2, CH_3CH, CHO, CH, CH_2, CH_3, C_2H, C_2, C_3, C_5, H_2, H, O, OH, O_2H, CHO^+, $C_2O_2H^+$, $C_3H_3^+$, NO^+, CO^+, OH^+, H_2O^+, H_3O^+, $H_5O_2^+$, $H_7O_3^+$. Some of the reactions in the oxidation of acetylene are described below (5, 17, 25, 28, 38, 51).

$$H + O_2 \rightarrow OH + O$$

$$OH + C_2H_2 \rightarrow H_2O + C_2H$$

$$O + C_2H_2 \rightarrow OH + C_2H$$

$$C_2H + C_2H_2 \rightarrow C_4H_2 + H$$

$$C_2H + O_2 \rightarrow CO_2 + CH^*$$

$$CH^* + O \rightarrow CO^* + H$$

$$C_2H + O \rightarrow CO + CH^*$$

Although the temperature of the oxygen-acetylene flame is about 400°C hotter than the oxygen-hydrogen flame, the major advantage of acetylene flames are their greater reducing character. This is especially useful for elements which form stable monoxides. The reducing character of this flame helps to prevent oxide formation and thus increase the sensitivity which is obtained with this flame.

The major drawback to using oxygen-acetylene and oxygen-hydrogen flame is their very high burning velocity which complicates burner design.

It is possible to use other oxidants with these fuels such as air or nitrous oxide, but these flames operate at lower temperatures. Because of these problems a study was undertaken to determine the conditions necessary to produce a safe and stable premixed oxygen-hydrogen and oxygen acetylene flame.

The production of a stable, premixed flame supported on top of a burner head depends on several factors. On ignition, the fuel-oxidizer mixture forms a reaction zone or flame front which assumes the parabolic velocity distribution of the unburned gases and starts moving toward the source of the mixture--in this case, the burner orifice. If the flame propagation velocity, termed the burning velocity, is less than the velocity of the expanding gases, the flame will lift off or blow off the burner head. However, if the burning velocity exceeds the escape velocity of the combustible gases, the flame will travel down through the burner orifice and ignite the mixture below the burner head, causing flashback.

Between the two extremes of blow off and flashback the flame may be viewed as self-propagating in that the burning velocity is balanced by the flow velocity of the gas mixture. In general, the burning velocity is uniform over most of the flame front but drops to zero near the port walls as a result of quenching by the walls. The quenching effect of the cool port walls prevents flashback even though the flow velocity approaches zero at the wall. If not for this boundary quenching effect, the flame would always flash back. A short distance from the wall, known as the quenching distance, the burning velocity of the gas mixture

increases. Flashback may be prevented in this area by keeping the flow velocity of the gas greater than the burning velocity (Figure 2). However, if the flow rate drops below the burning velocity of the gas mixture in any part of the flame or if the burner head temperature becomes high enough to lower quenching by the port walls sufficiently, flashback will occur.

Additionally, under certain conditions of pressure (43, 49) when a combustible mixture is compressed suddenly its burning velocity may be greatly increased over that observed under normal conditions. This phenomenon, known as detonation, is initiated when a portion of the gas mixture is compressed causing its temperature to increase to the point of ignition. The resulting detonation wave compresses the adjacent gas mixture to the ignition point and thus the flame front propagates rapidly throughout the gas mixture.

For laminar flow the velocity of the gas mixture must exceed a specific value near the burner port to prevent flashback; this specific value, called the critical boundary velocity gradient (g_F) was found by Lewis and Von Elbe (43, 44) to be given by

$$\lim_{r \to R} \left(\frac{-dV}{dr}\right) = g_F = \frac{4V_F}{\pi R^3} \qquad (1)$$

where V is the gas velocity, R is the exit port radius and V_F is the total gas flow at which the gas velocity curve meets the burning velocity curve (Figure 2) and r is the variable radius coordinate.

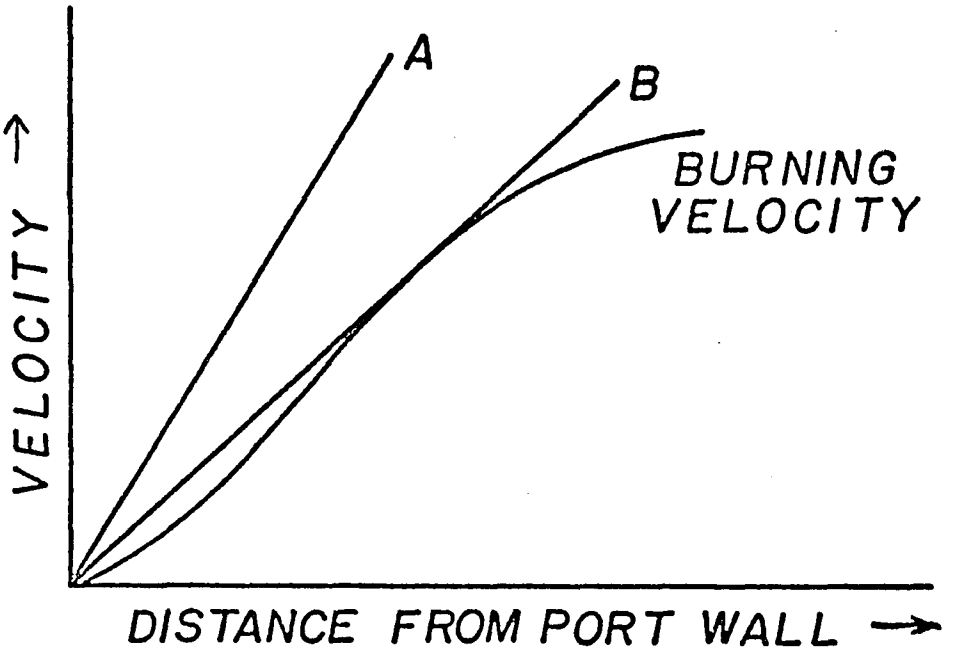

Figure 2. Conditions at which flashback will occur. -- A = no flashback; B = point at which flashback will occur.

If the exit port diameter is large compared to the distance over which the wall exerts a cooling effect on the flame, theoretically the values of g_F will be identical (31, 67). As the exit port diameter becomes smaller, the effect of quenching by the port walls becomes more pronounced. In this situation both the burning velocity profile of the gas mixture and heat transfer to the burner top are changed such that lower gas flow rates will still support a stable flame. Eventually a diameter of the exit port (defined as the quenching diameter) is reached which will not allow passage of the flame front through the orifice at any flow rate.

The burner head temperature also assumes an important role in preventing flashback (1, 20). The port wall not only changes the flow velocity and burning velocity, but with the cold wall of the burner there is the additional effect of cooling the reaction gas. This plays an important part in preventing flashback by reducing the activation energies of the chain carrier reactions within the gas mixture (23, 44). Most burners used in flame spectrometry today operate at temperatures much greater than room temperature. Flashback data which represent the effects of both port diameter and burner head temperature should be valuable in the design of new burners which either reduce or eliminate the possibility of flashback.

A simple "one hole" insert burner design is used which has proven useful in determining quenching distances and critical boundary velocity gradients as a function of burner head temperature. Data are presented

for designing improved burners employing premixed oxygen-hydrogen (O_2-H_2) and oxygen-acetylene (O_2-C_2H_2) gases.

Burner

The burner used to determine flashback parameters should meet certain specifications. It should be sturdily built to withstand the pressure of explosion. It should be designed so as to reproduce the operating conditions of conventional burners used in flame spectrometry, such as burner temperature and mixing and preheating of the fuel and oxidant. In addition, the burner should be flexible enough to allow the effect of various exit port diameters and different operating temperatures to be easily investigated. Such a burner was specially designed and built for the study of flashback parameters.

The burner consisted of three parts: base, head, and removable plug (Figure 3). The base is designed to provide efficient mixing and to ensure proper preheating of the gas mixture. Fuel and oxidant are mixed in a high turbulence region and routed to a small plenum chamber the size of which was held small (2.5 cm^3) to limit the violence of the flashback explosion.

A spring compressed "pop-off" valve is incorporated in the base of the burner to release excess pressure during flashback. Preheating of the gas mixture is accomplished by flowing each gas through a five-inch long copper tube prior to entering the mixing chamber. The temperature of the tubes is maintained at the same temperature as the rest of the burner.

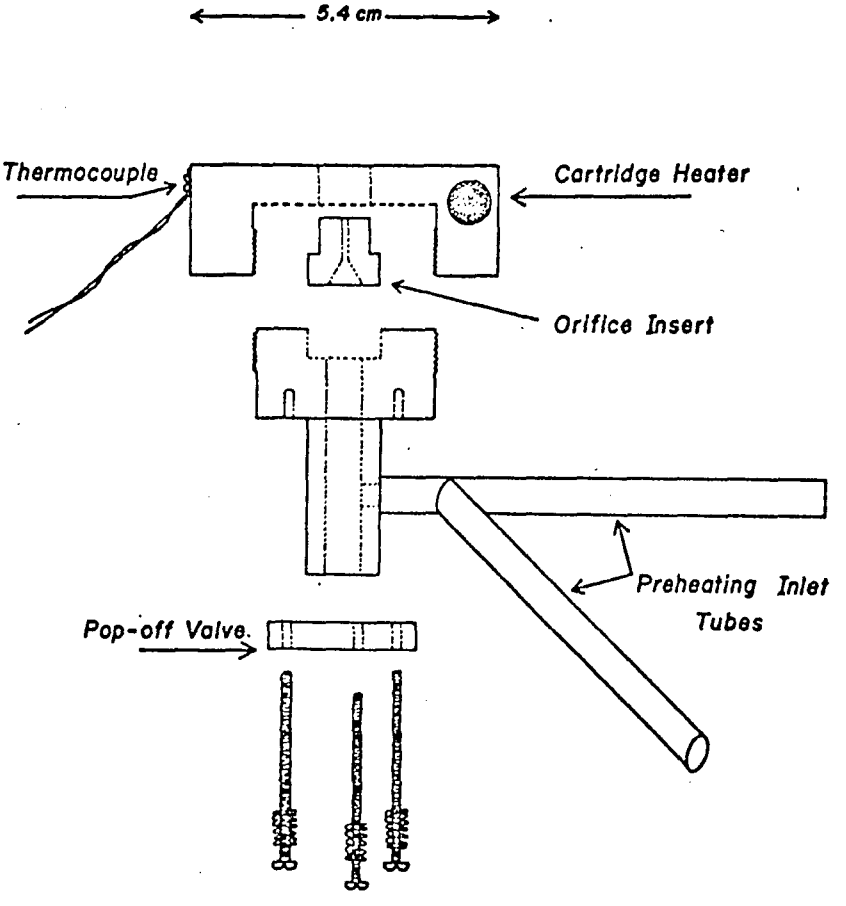

Figure 3. Cross section view of the one-hole insert burner.

Most burners used in flame spectrometry operate at temperatures much greater than room temperature. Since the heat transferred to a burner head by a single hole will be only a fraction of that produced by a functional multihole burner used in an analysis, the head of the burner incorporated a cartridge heater capable of producing temperatures in excess of 600^{o}K. This allowed determining burning parameters at various different head temperatures, independent from other variables such as gas flow rate, composition, etc. Head temperature was monitored using an iron-constantan thermocouple and gauge (Assembly Products, Inc., Chesterland, Ohio). Power to the heater is controlled by use of a variac.

One of the most convenient and economical features of the described burner is the use of a single-hole removable plug, similar to that reported by Berlad and Potter (3). In the present design, a cylindrical brass plug with a base diameter of 1.5 cm and an exit orifice drilled in the center is held firmly between the base and the head. This design allows flashback data to be taken quickly with a number of different exit port diameters and a minimum amount of machine shop work.

Gas Supply and Flow Meters

Gas flow rates were measured using a soap-film flow meter and corrected for temperature and the vapor pressure of water. The burner offered very low resistance to gas flow, thereby eliminating the necessity of any further compressibility corrections for the flow rate. Oxygen and hydrogen were supplied by double stage regulators (Model 22025-1, Matheson Co., East Rutherford, New Jersey 07073) and acetylene

by a single stage regulator, Model 8-P. Flow rates were controlled by micrometer needle valves (Nuclear Products Co., Cleveland, Ohio).

Measurement of Parameters

To obtain flashback, the fuel (H_2 or C_2H_2) and oxygen rates were set to produce a stable flame. Either fuel or oxidant flow was then slowly changed until flashback occurred. Burner head temperature was controlled to better than $5^{o}C$ for all measurements.

The corrected flow rates were used to calculate the fuel-oxidant ratio, total flow through the exit port, and the critical boundary velocity gradient.

Results

The effect of port diameter on the total gas flow at flashback versus the fuel-oxidant ratio for oxyhydrogen and oxyacetylene flames is illustrated in Figures 4 through 9. As the port diameter is decreased the total flow at flashback also decreases as a result of the increased quenching effect of the port wall at small diameters.

Figures 10 through 15 are plots of the critical boundary velocity gradient versus fuel-oxidant ratio calculated from Equation 1 for the data in Figures 4 through 9. The effect of port diameter is again seen in these figures. With the smaller port diameters a decrease in the diameter results in an increase in the critical boundary velocity gradient. Results similar to these have been observed for other gas mixtures (31, 44) and may be explained with the help of Figure 2. As the port diameter is decreased, the burning velocity of the gas mixture

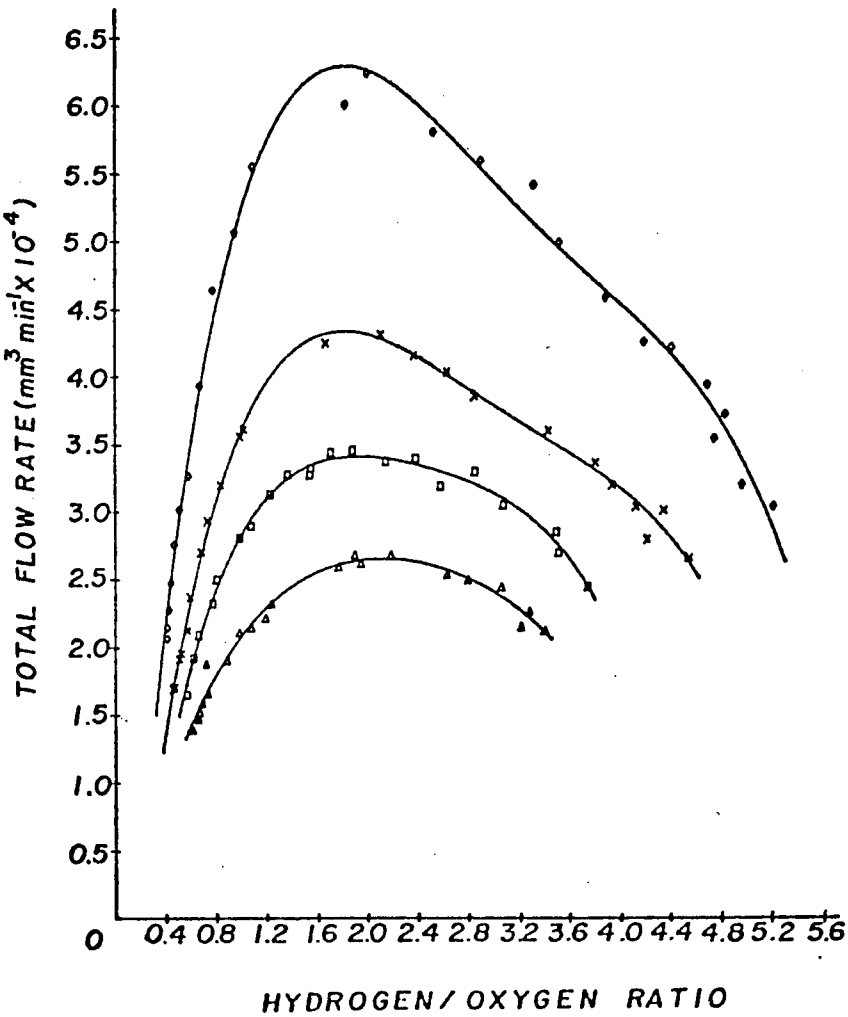

Figure 4. Total flow at flashback for oxygen-hydrogen flame. Burner temperature: 573°K. -- Port diameters: △ = 0.572 mm; □ = 0.660 mm; X = 0.742 mm; ◇ = 0.812 mm.

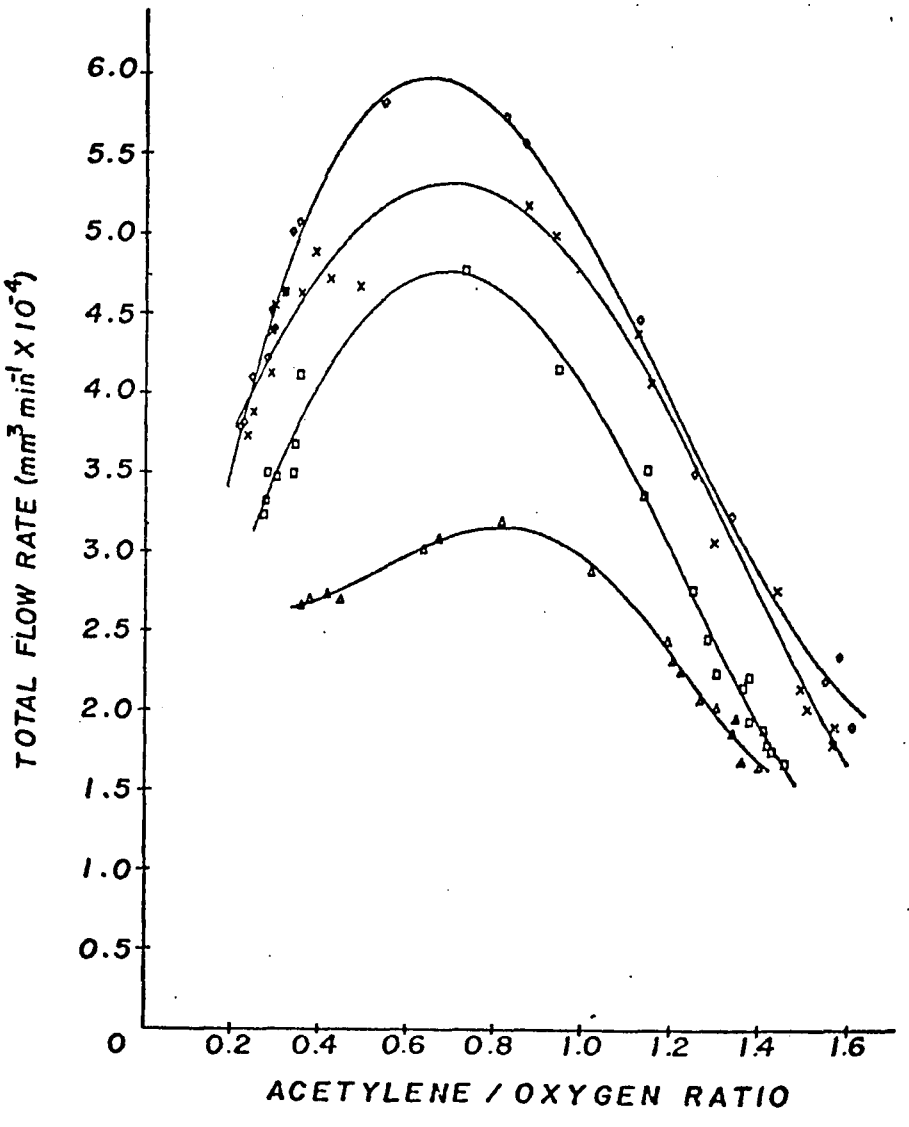

Figure 5. Total flow at flashback for oxygen-acetylene flame. Burner temperature: 573°K. -- Port diameters: △ = 0.508; □ = 0.533 mm; X = 0.572 mm; ◊ = 0.610 mm.

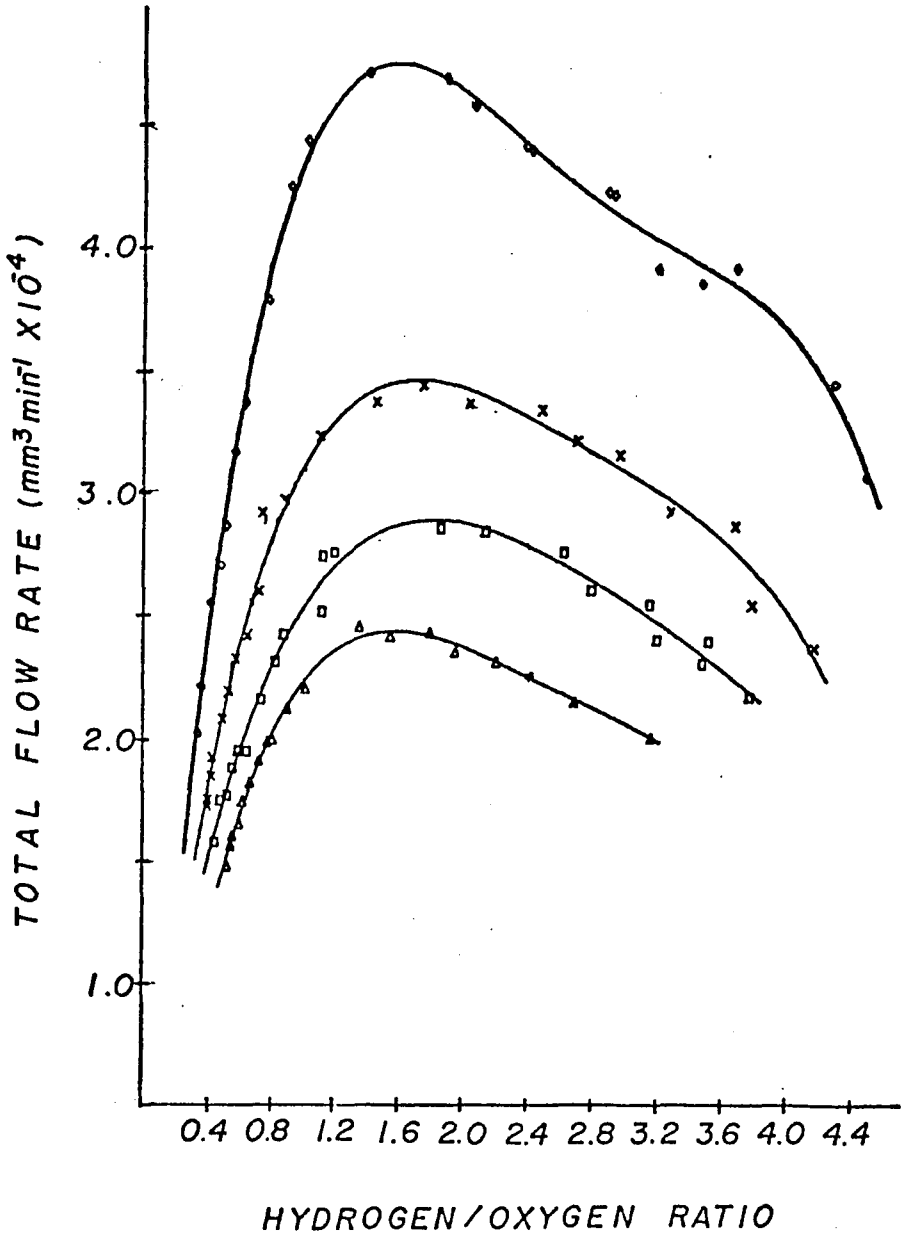

Figure 6. Total flow at flashback for oxygen-hydrogen flame. Burner temperature: 473°K. -- Port diameters: △ = 0.572 mm; □ = 0.660 mm; X = 0.742 mm; ◇ = 0.812 mm.

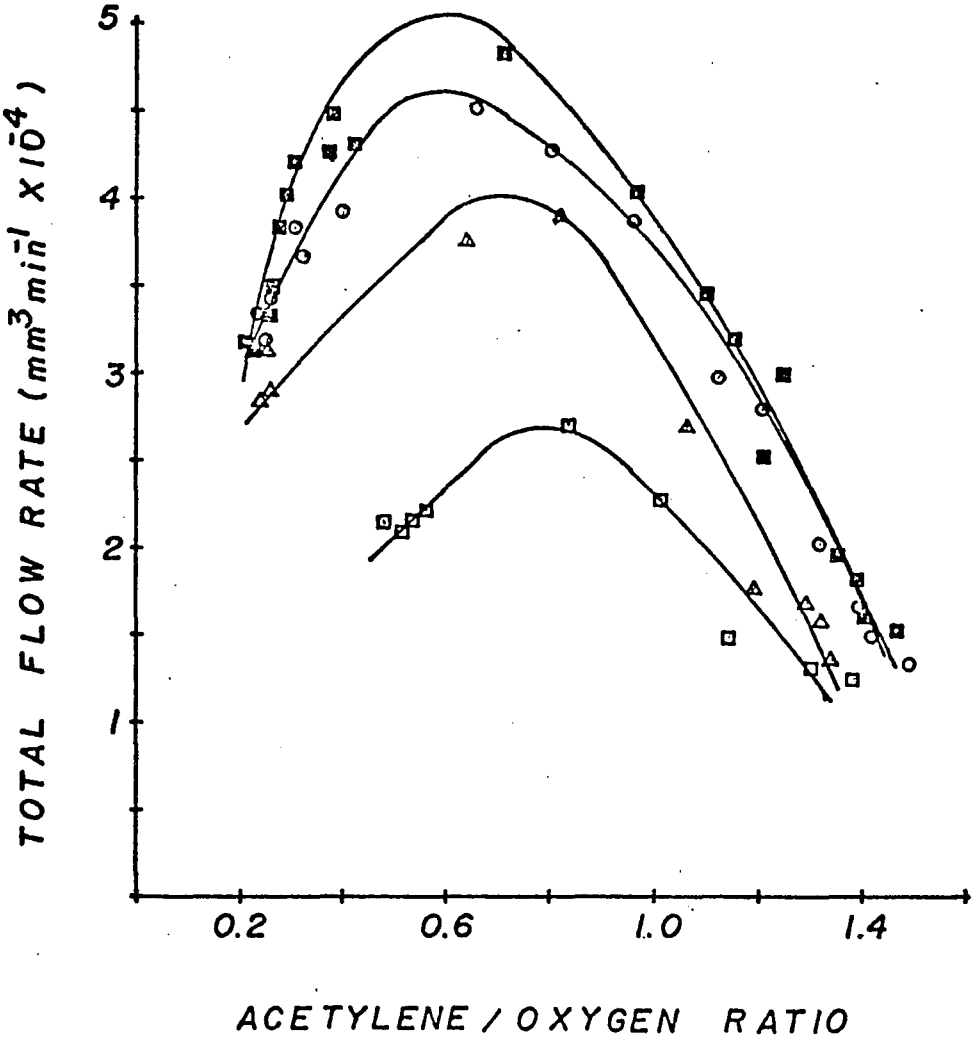

Figure 7. Total flow at flashback for oxygen-acetylene flame. Burner temperature: 473°K. -- Port diameters: □ = 0.508 mm; △ = 0.533 mm; ○ = 0.572 mm; ■ = 0.610 mm.

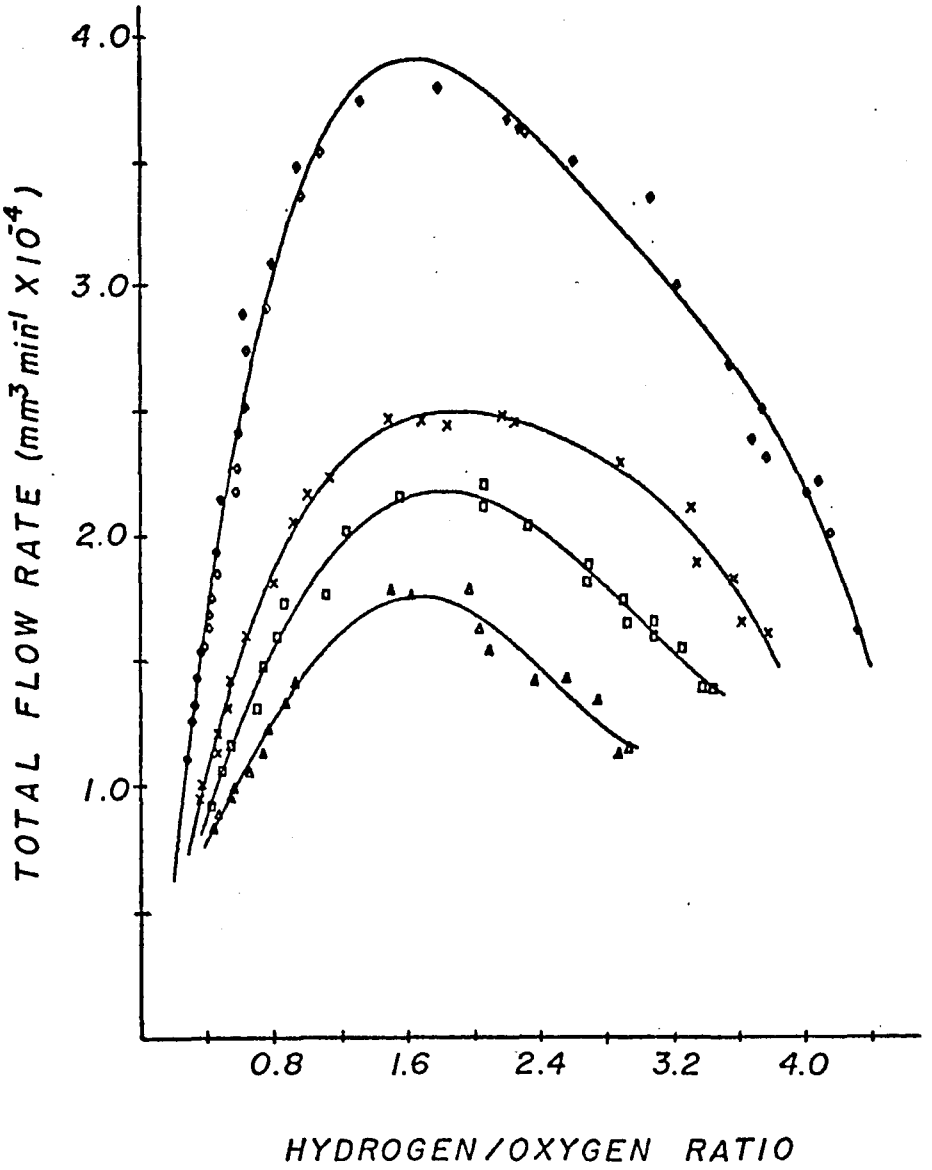

Figure 8. Total flow at flashback for oxygen-hydrogen flame. Burner temperature: 373°K. -- Port diameters: △ = 0.572 mm; □ = 0.660 mm; X = 0.742 mm; ◇ = 0.812 mm.

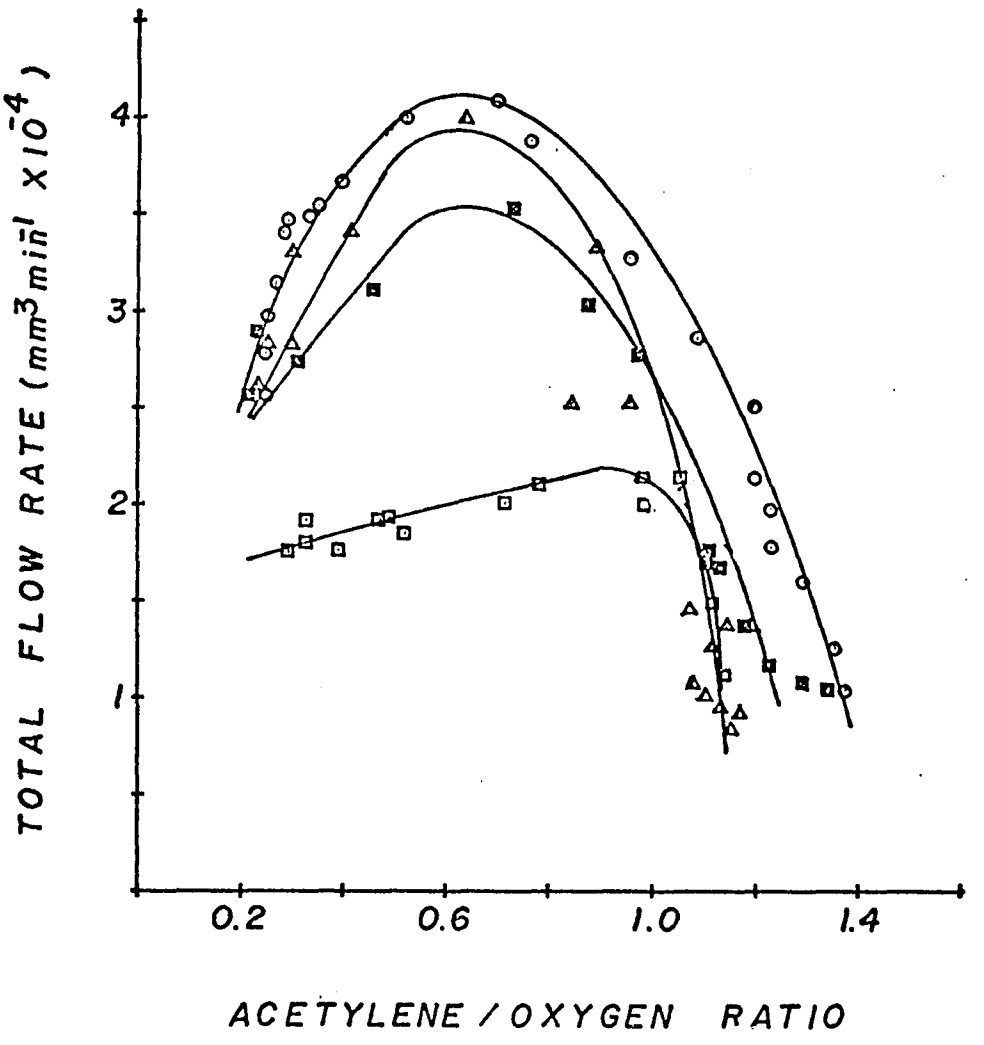

Figure 9. Total flow at flashback for oxygen-acetylene flame. Burner temperature: 373°K. -- Port diameters: □ = 0.508 mm; ■ = 0.533 mm; △ = 0.572 mm; ○ = 0.610 mm.

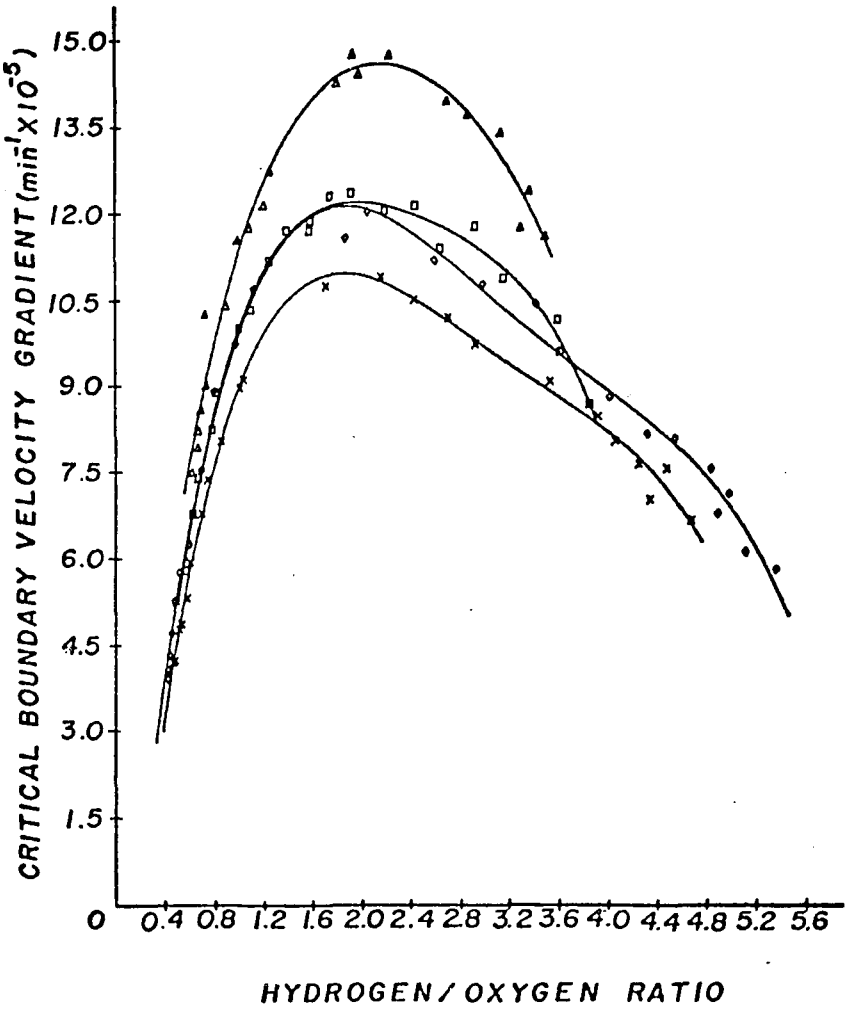

Figure 10. Critical boundary velocity gradient at flashback for oxygen-hydrogen flame. Burner temperature: 573°K.--Port diameters: △ = 0.572 mm: □ = 0.660 mm; X = 0.742 mm; ◇ = 0.812 mm.

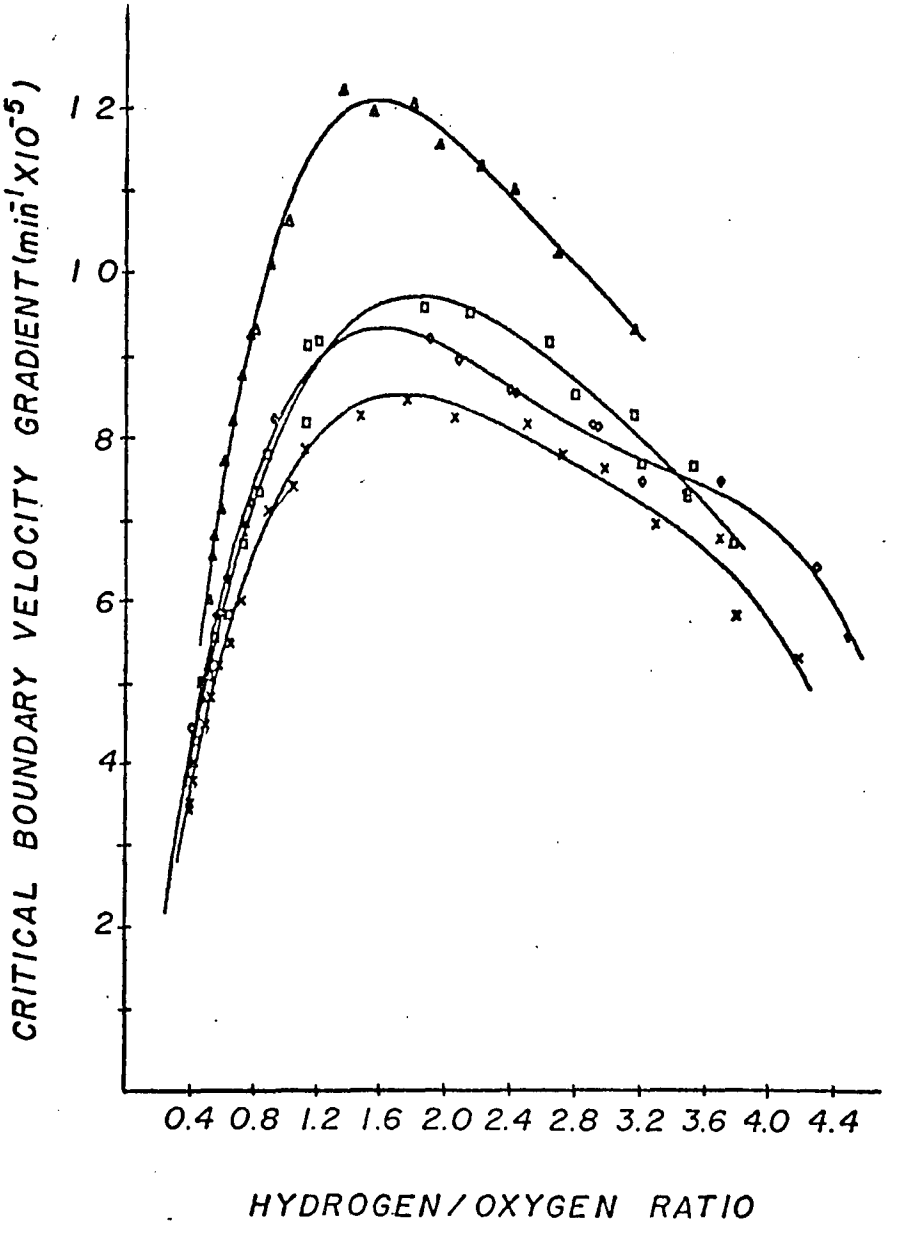

Figure 11. Critical boundary velocity gradient at flashback for oxygen-hydrogen flame. Burner temperature: 473°K.--Port diameters: △ = 0.572 mm; □ = 0.660 mm; X = 0.742 mm; ◇ = 0.812 mm.

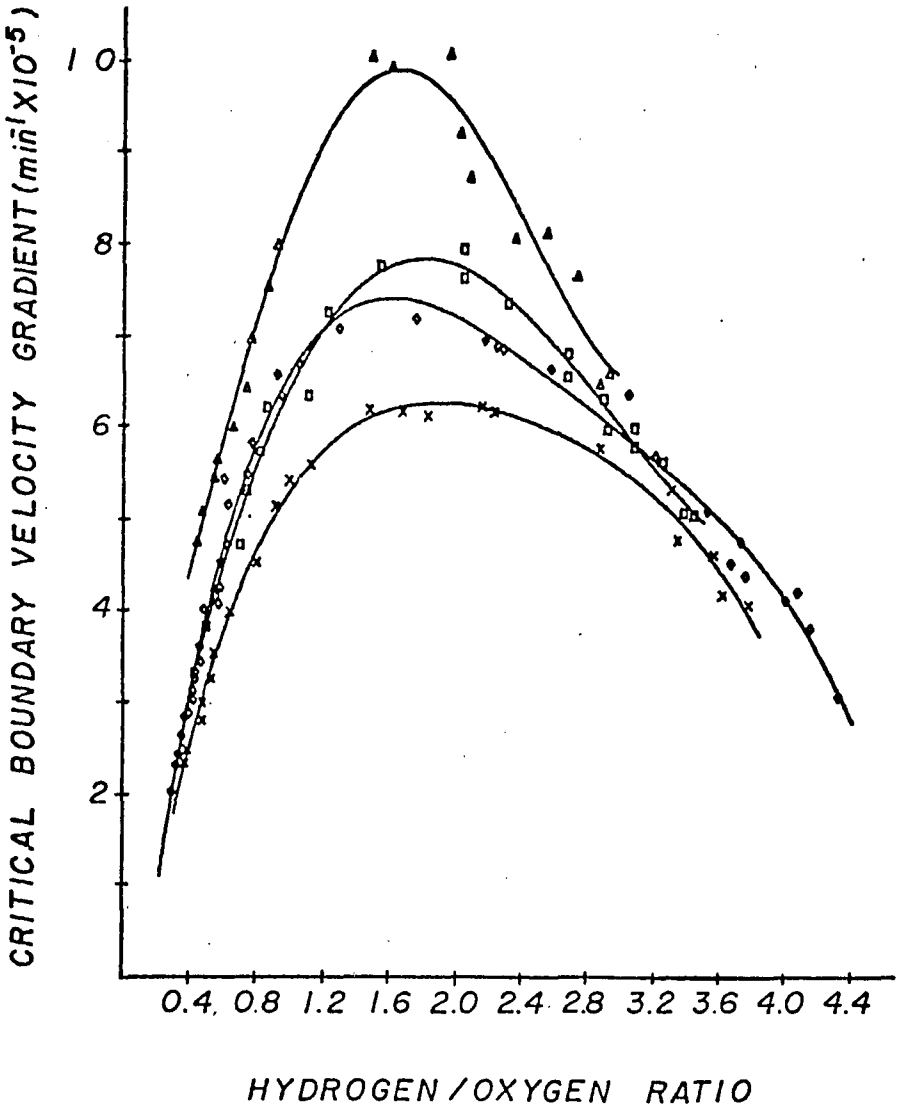

Figure 12. Critical boundary velocity gradient at flashback for oxygen-hydrogen flame. Burner temperature: 373°K.-- Port diameters: △ = 0.572 mm; □ = 0.660 mm; X = 0.742 mm; ◇ = 0.812 mm.

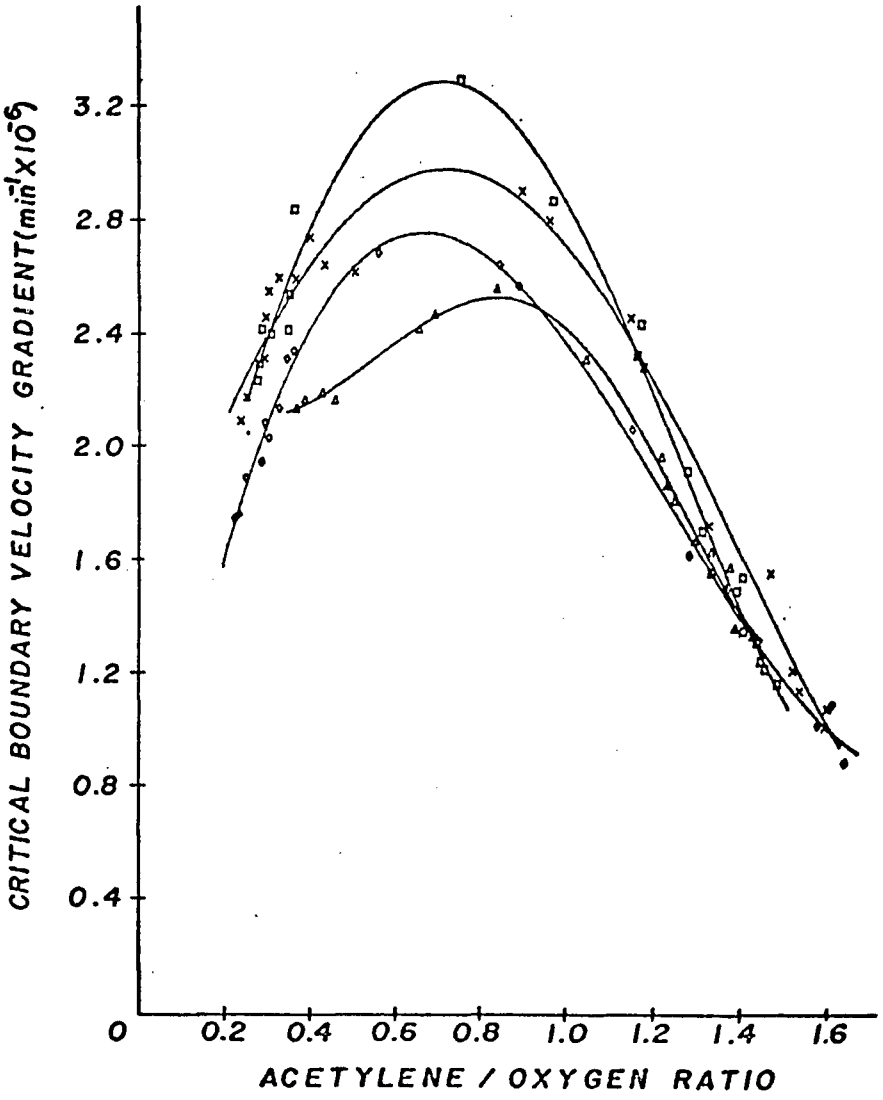

Figure 13. Critical boundary velocity gradient at flashback for oxygen-acetylene flame. Burner temperature: 573°K.--Port diameters: △ = 0.508 mm; □ = 0.533 mm; X = 0.572 mm; ◇ = 0.610 mm.

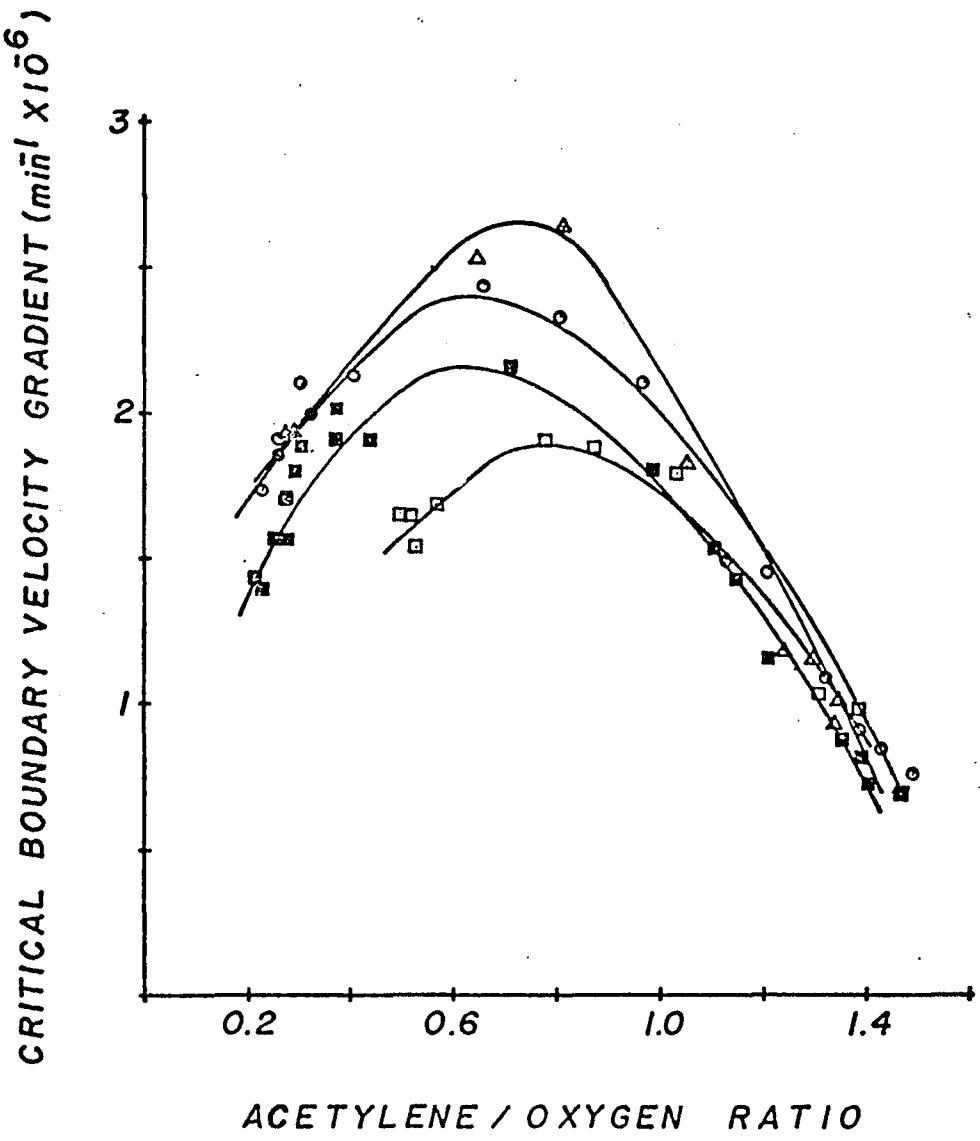

Figure 14. Critical boundary velocity gradient at flashback for oxygen-acetylene flame. Burner temperature: 473°K.--Port diameters: □ = 0.508 mm; ■ = 0.610 mm; ○ = 0.572 mm; △ = 0.533 mm.

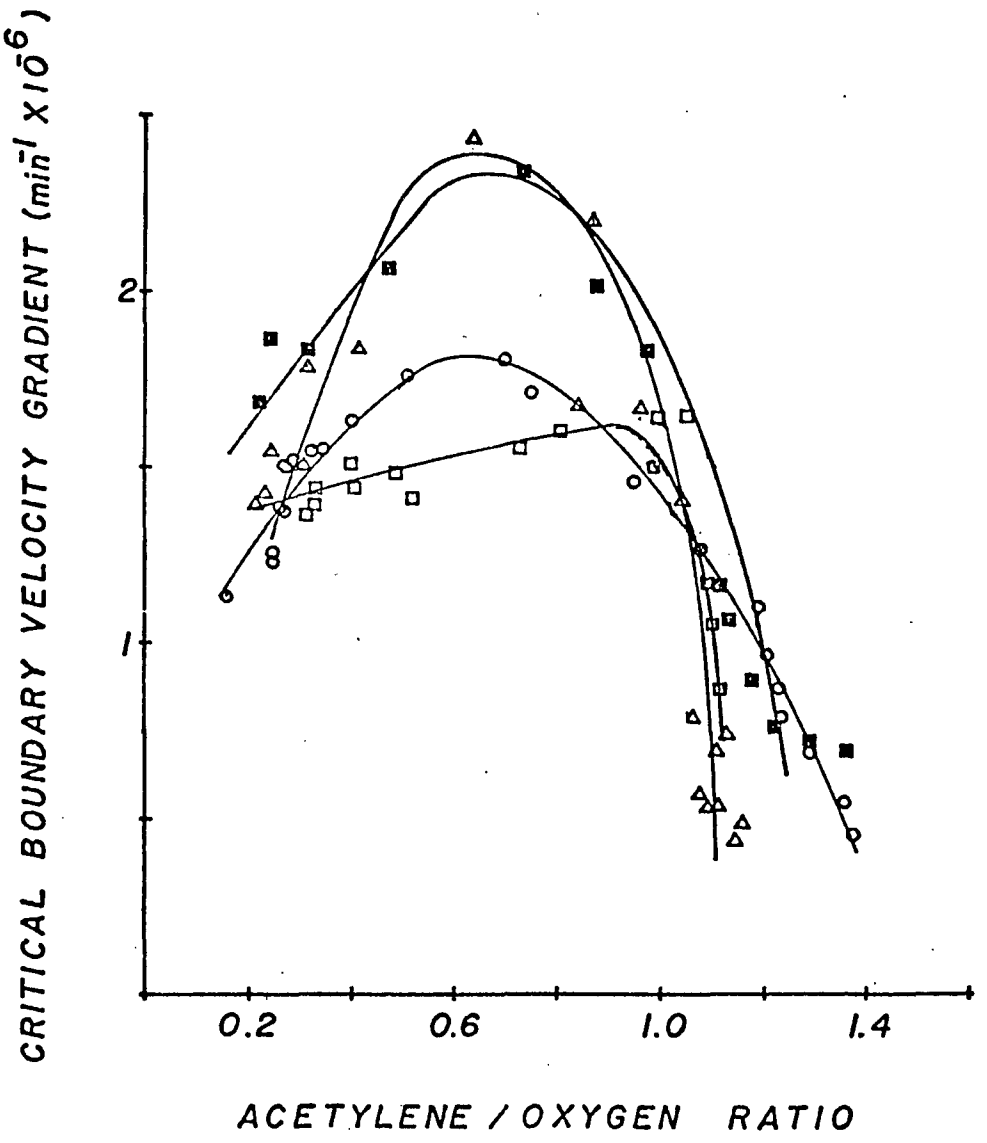

Figure 15. Critical boundary velocity gradient at flashback for oxygen-acetylene flame. Burner temperature: 373°K.--Port diameters: ○ = 0.610 mm; △ = 0.572 mm; □ = 0.508 mm; ■ = 0.533 mm.

decreases slightly. If the value of R^3 changes faster than the total flow rate to prevent flashback, the value of g will increase with decreasing port diameter. However, once the port diameter approaches the quenching distance the burning velocity of the gas mixture will decrease much faster than the value of R^3 and g will then decrease as R approaches the quenching distance. This latter effect is seen in Figure 10 for a port diameter of 0.572 mm.

Since the quenching effect of a burner wall can be attributed to its ability to cool the gas mixture, resulting in the destruction of chain carrier reactions, an increase in burner head temperature will reduce the wall's quenching effect. By controlling the temperature of the burner head it was possible to investigate the change in quenching as a function of temperature. Figures 16 through 23 show the effect of temperature at $373^{o}K$, $473^{o}K$ and $573^{o}K$ on the total gas flow rate at which flashback occurs and the effect on the critical boundary velocity gradient. It can be seen in Figures 16 through 23 that as the temperature is raised the total flow rate required to prevent flashback increases. This demonstrates that the heat transfer to the burner port wall decreases as the difference in flame temperature and burner port temperature decreases. As would be expected, the critical boundary velocity gradient also increases as the temperature increases as shown in Figures 24 through 31.

In designing a burner for flame spectrometry it is desirable to reduce, or ideally to completely eliminate, the possibility of flashback. By studying a number of different port diameters it has been possible to experimentally determine the diameter necessary to prevent flashback.

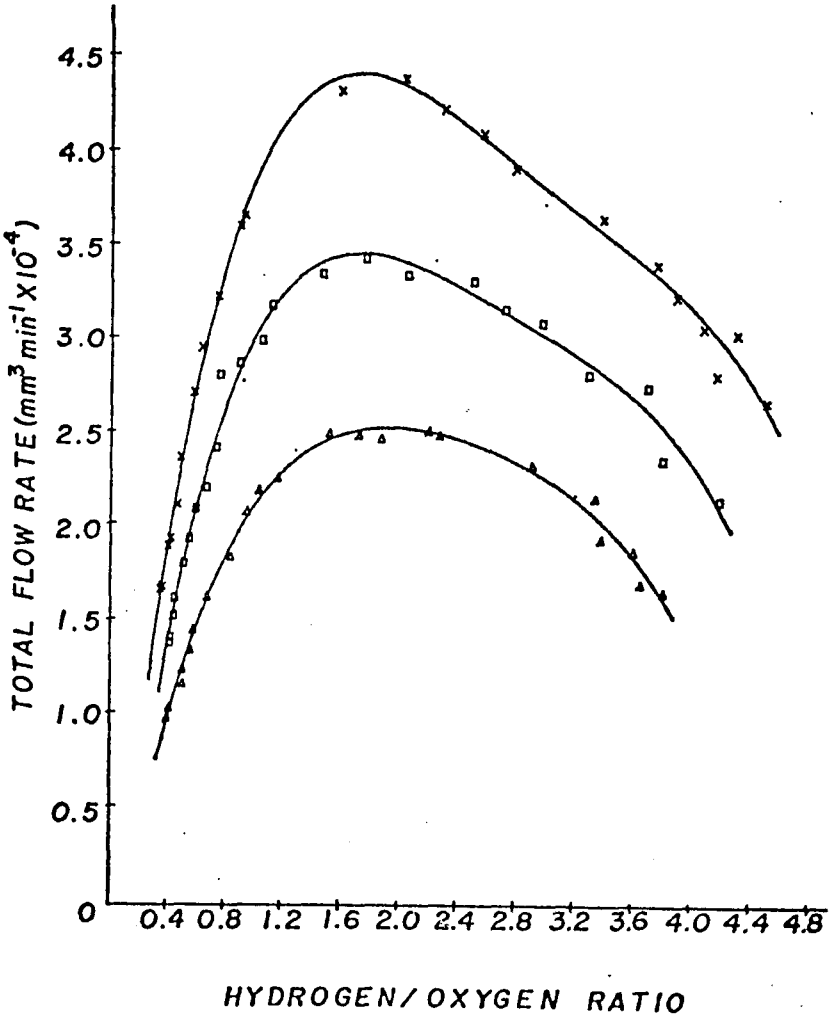

Figure 16. Variation of flow rate at flashback as a function of temperature I. -- Port diameter: 0.742 mm. Burner temperature: △ = 373°K; □ = 473°K; X = 573°K.

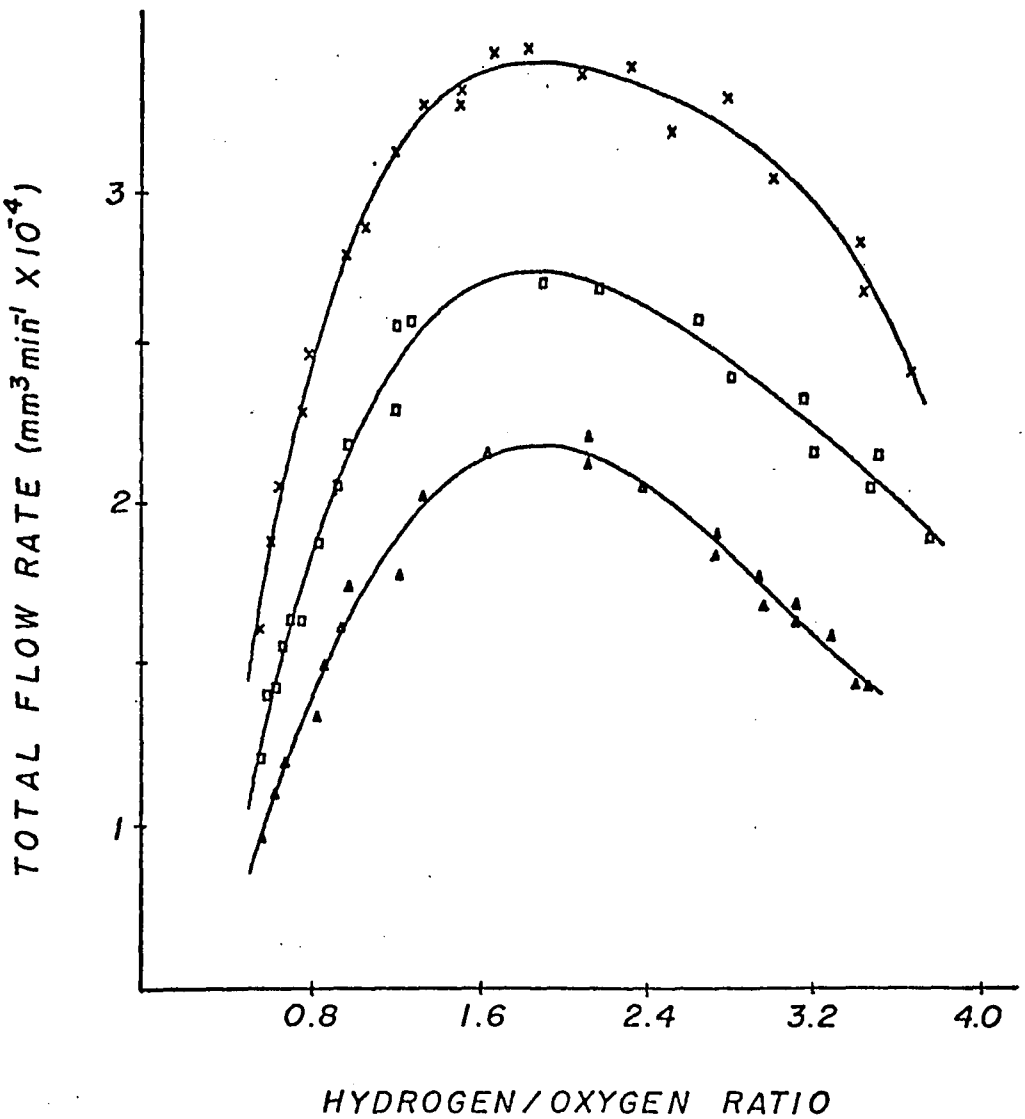

Figure 17. Variation of flow rate at flashback as a function of temperature II. -- Port diameter: 0.660 mm. Burner temperature: △ = 373°K; □ = 473°K; X = 573°K.

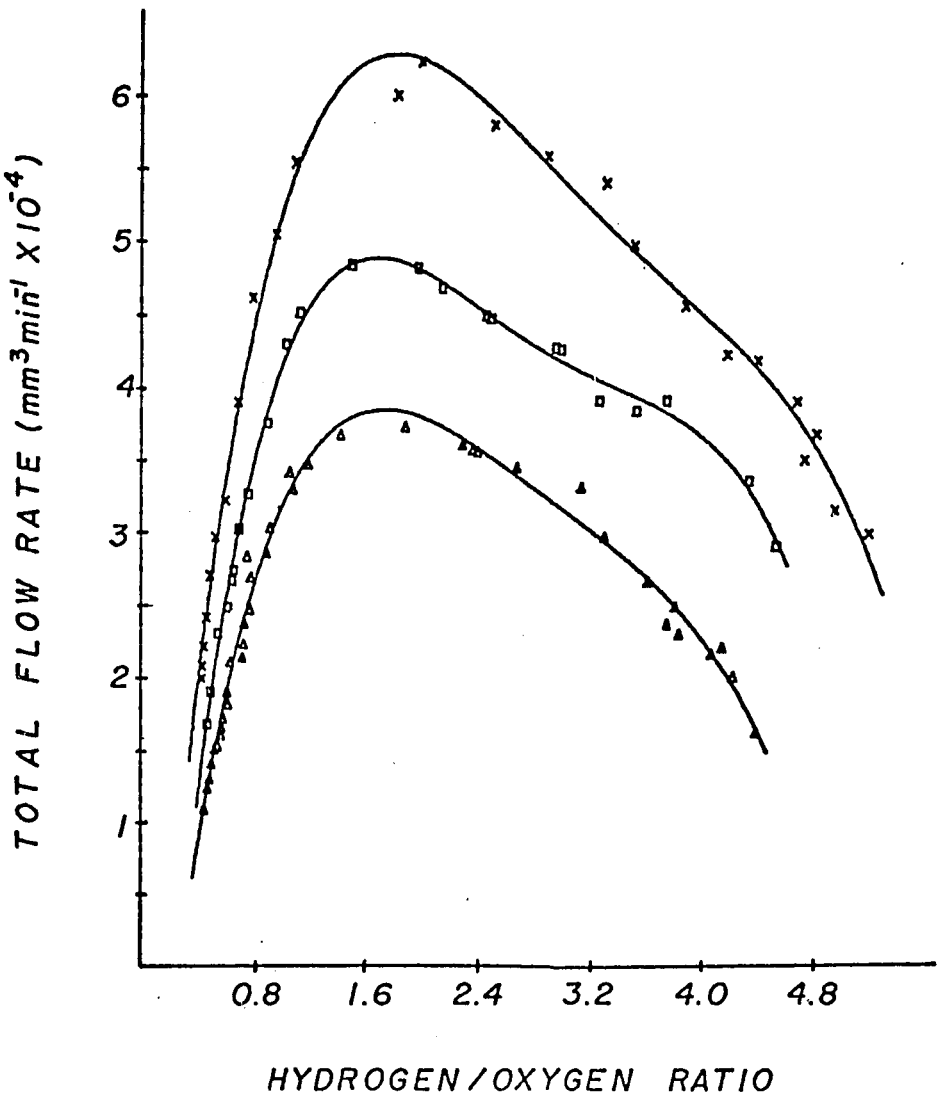

Figure 18. Variation of flow rate at flashback as a function of temperature III. -- Port diameter: 0.812 mm. Burner temperature: △ = 373°K; □ = 473°K; X = 573°K.

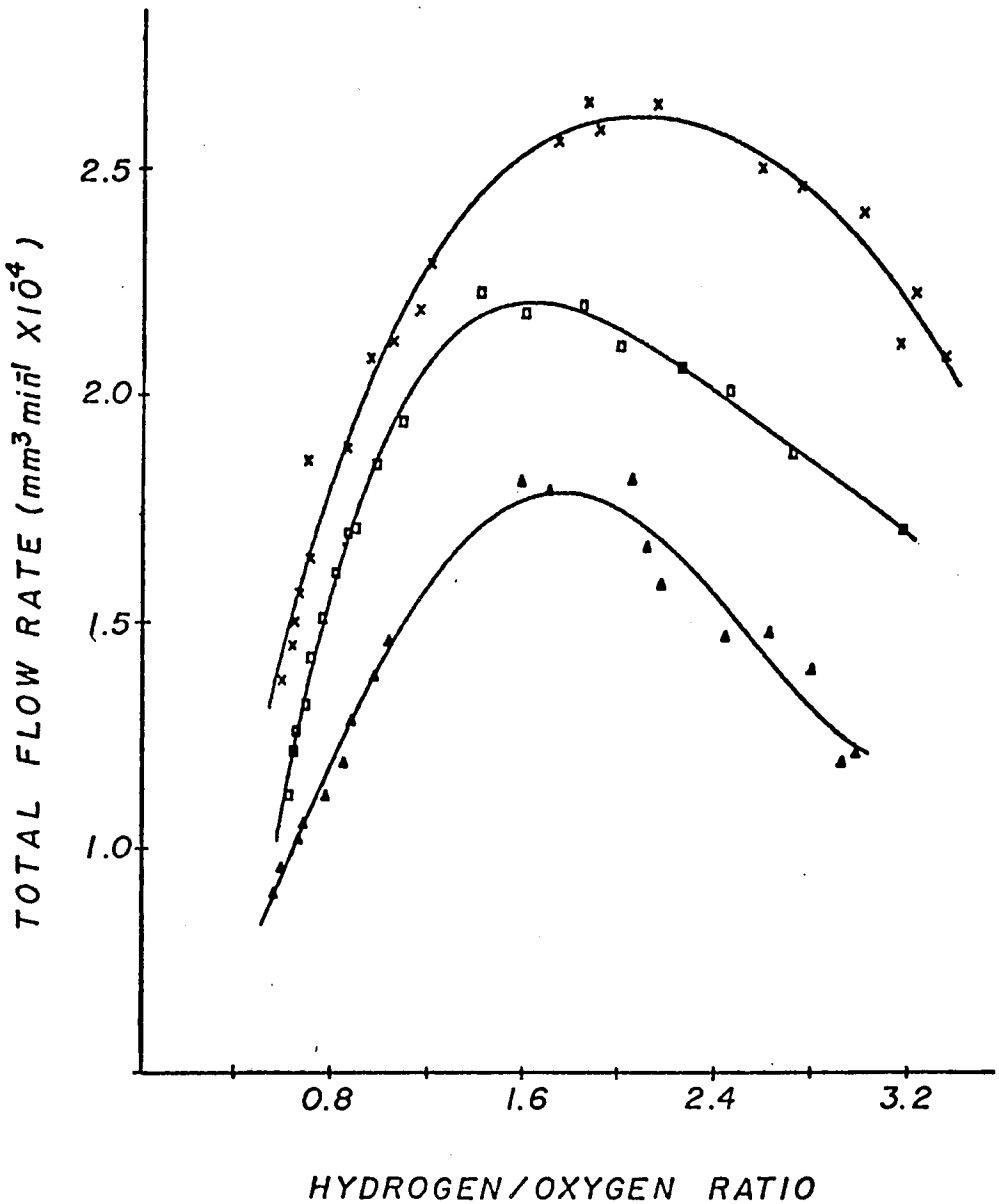

Figure 19. Variation of flow rate at flashback as a function of temperature IV. -- Port diameter: 0.572 mm. Burner temperature: △ = 373°K; □ = 473°K; X = 573°K.

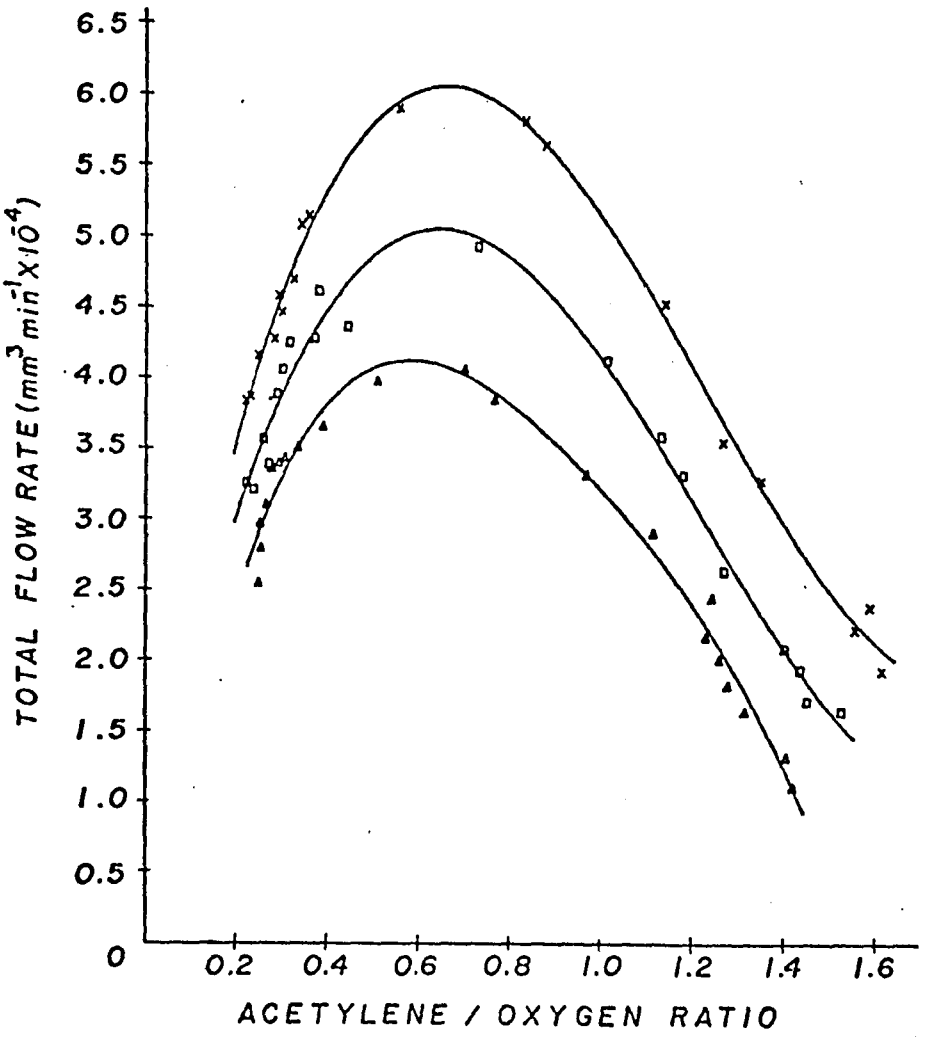

Figure 20. Variation of flow rate at flashback as a function of temperature V. -- Port diameter: 0.610 mm. Burner temperature: △ = 373°K; □ = 473°K; X = 573°K.

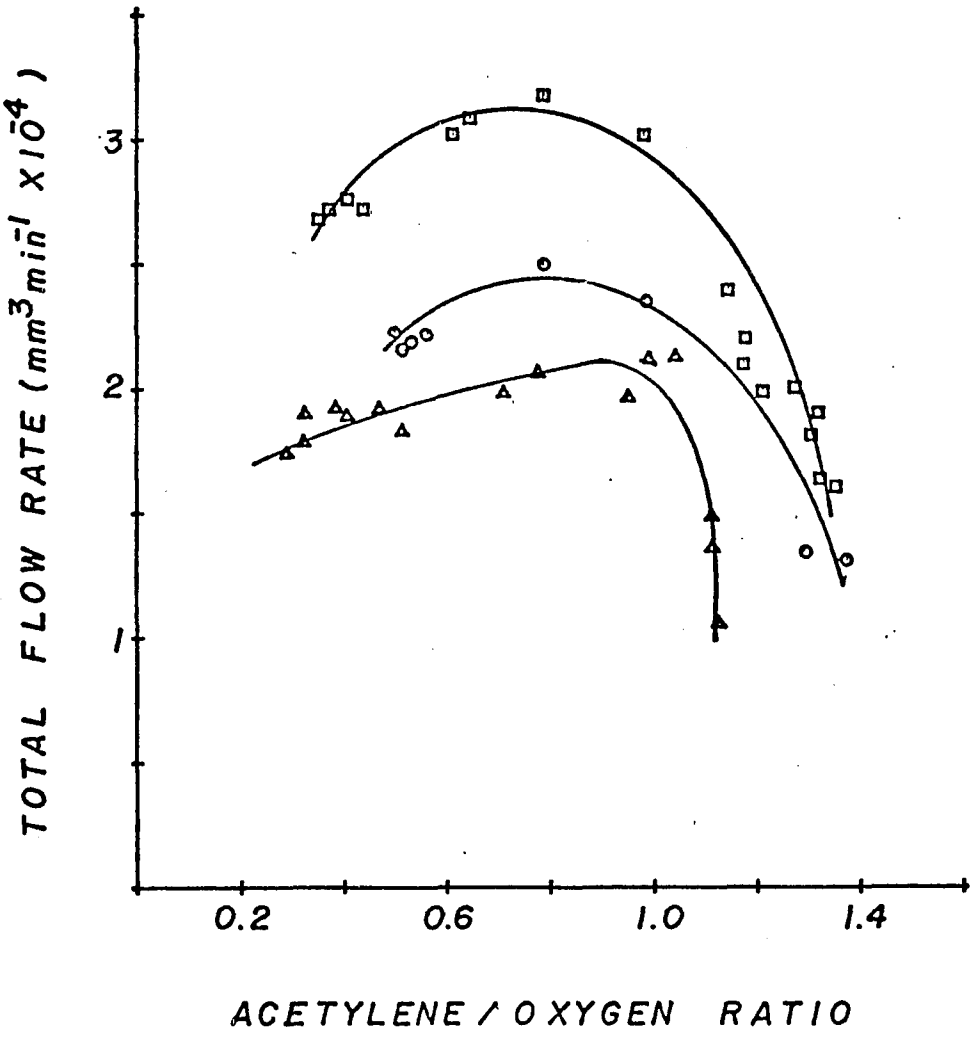

Figure 21. Variation of flow rate at flashback as a function of temperature VI. -- Port diameter: 0.508 mm. Burner temperature: △ = 373°K; ○ = 473°K; □ = 573°K.

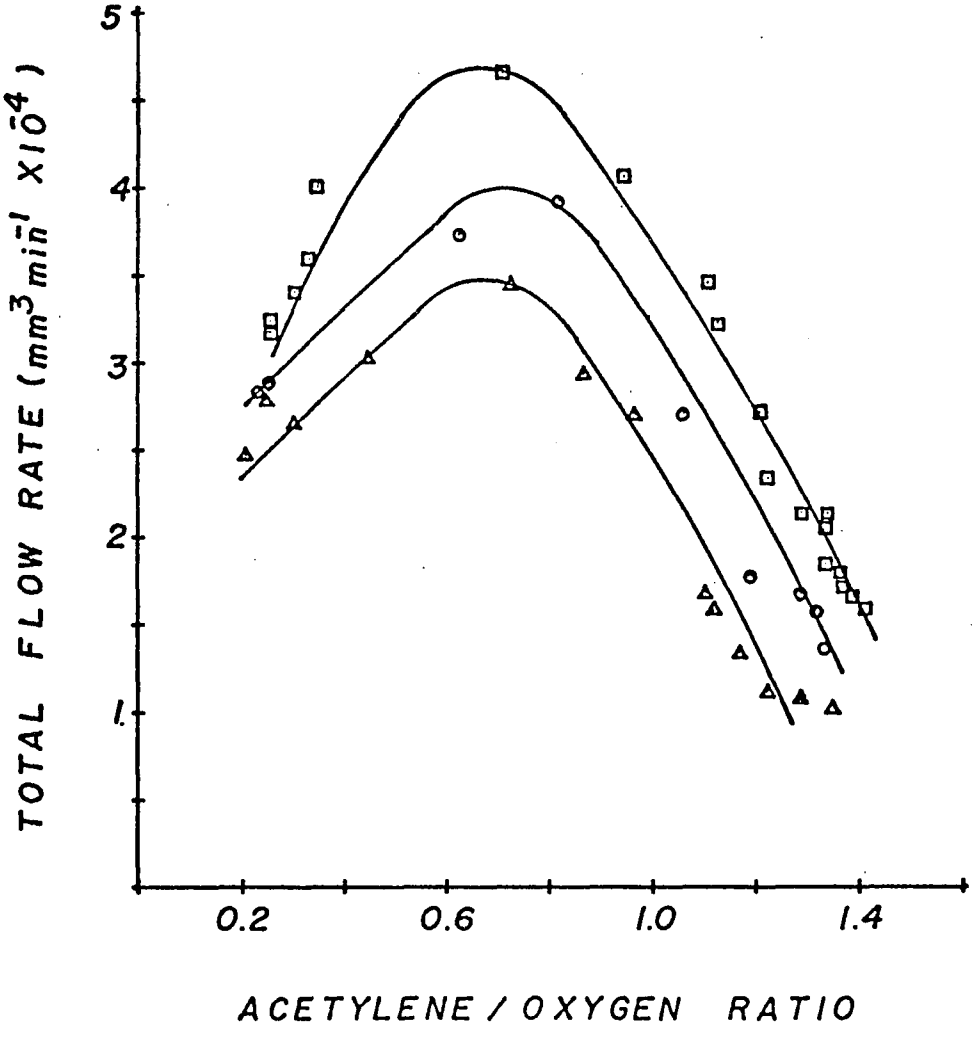

Figure 22. Variation of flow rate at flashback as a function of temperature VII. -- Port diameter: 0.533 mm. Burner temperature: △ = 373°K; ○ = 473°K; □ = 573°K.

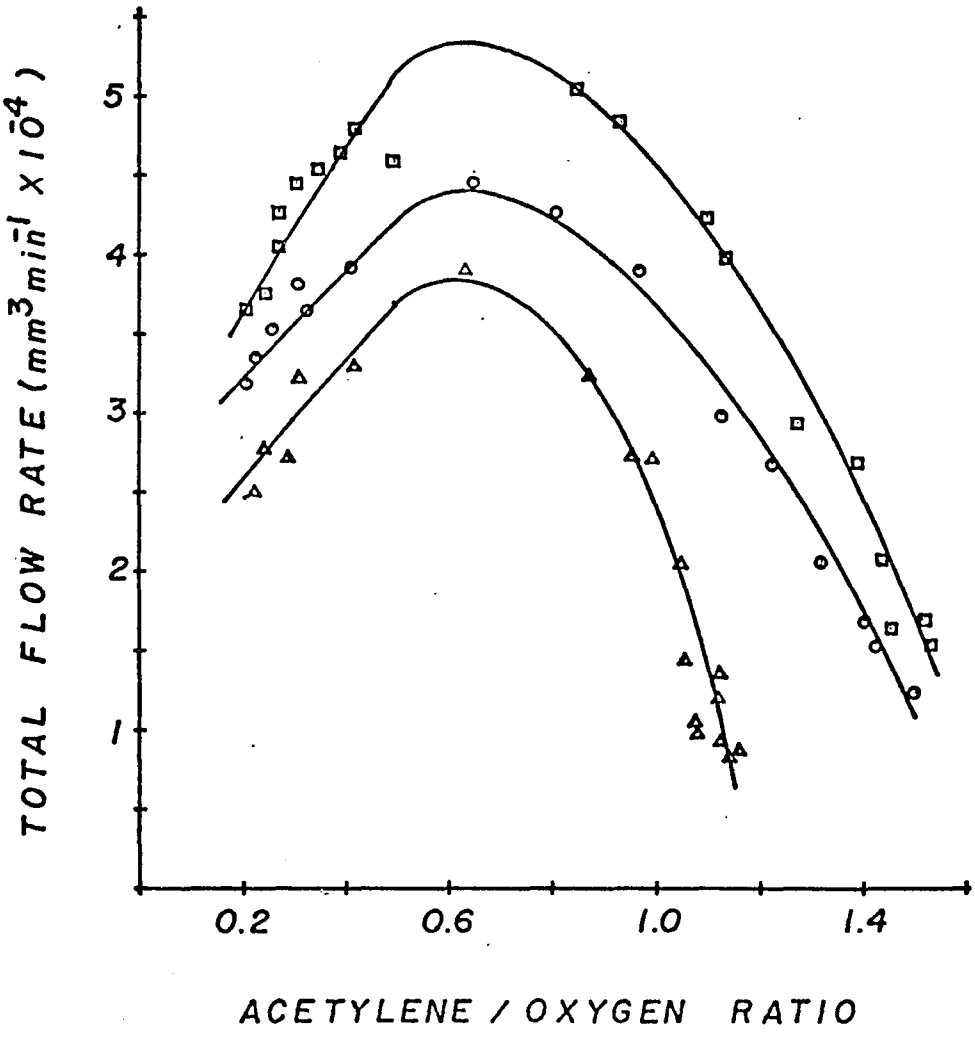

Figure 23. Variation of flow rate at flashback as a function of temperature VIII.-- Port diameter: 0.572 mm. Burner temperature: △ = 373°K; ○ = 473°K; □ = 573°K.

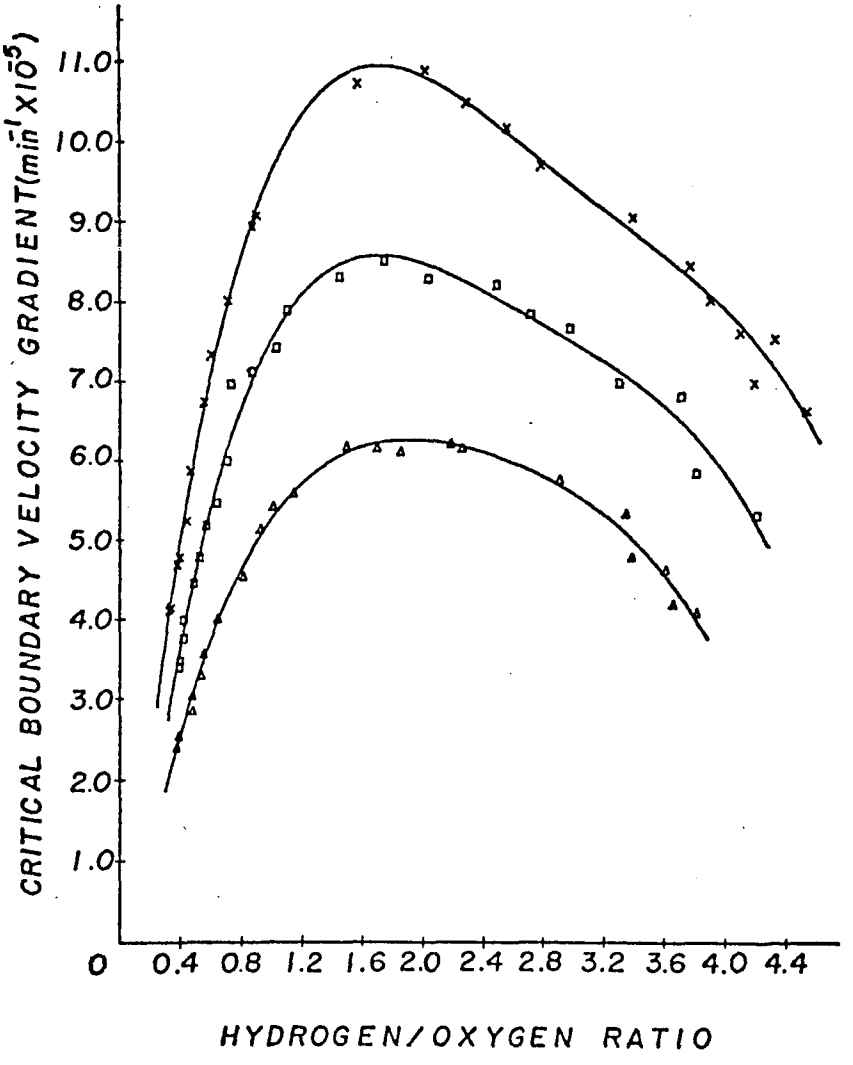

Figure 24. Variation of critical boundary velocity gradient as a function of temperature I.-- Port diameter: 0.742 mm. Burner temperature: △ = 373°K; □ = 473°K; X = 573°K.

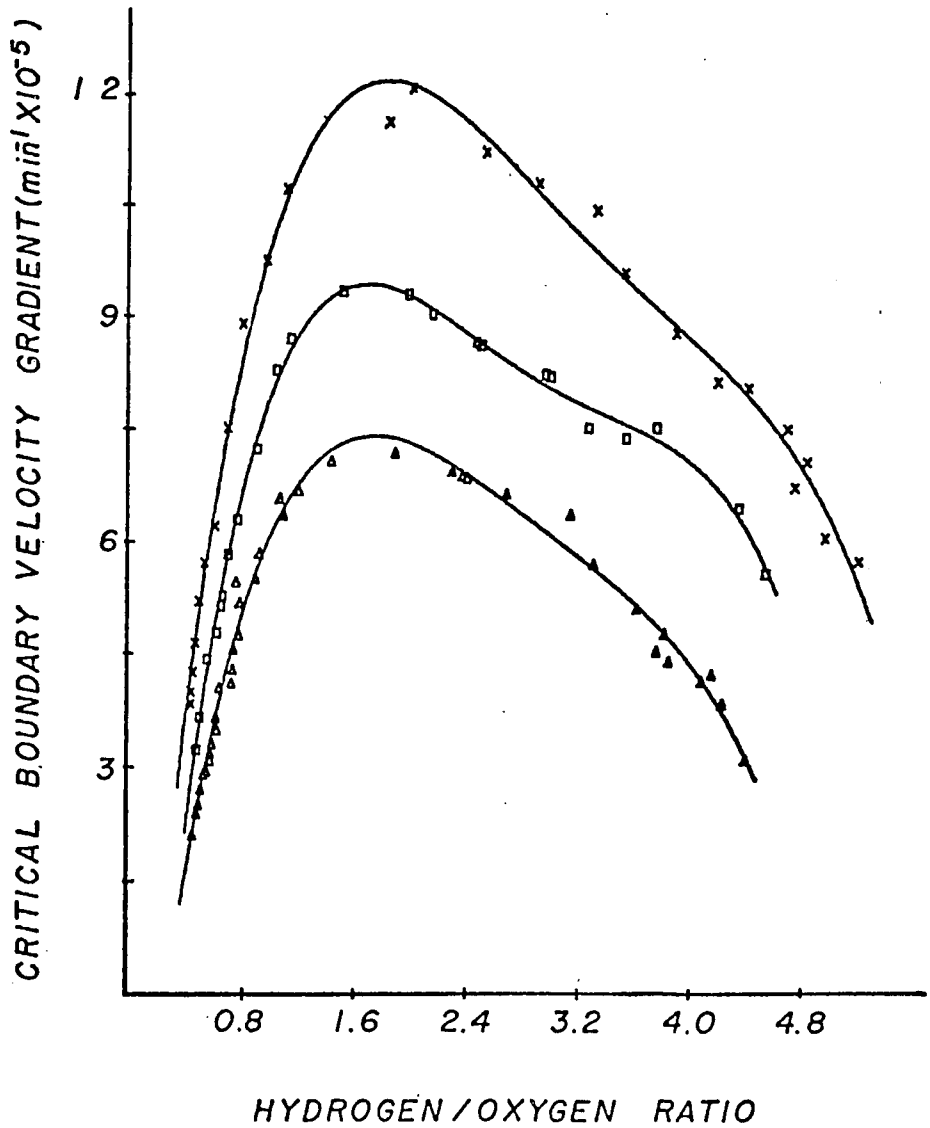

Figure 25. Variation of critical boundary velocity gradient as a function of temperature II. -- Port diameter: 0.812 mm. Burner temperature: △ = 373°K; □ = 473°K; X = 573°K.

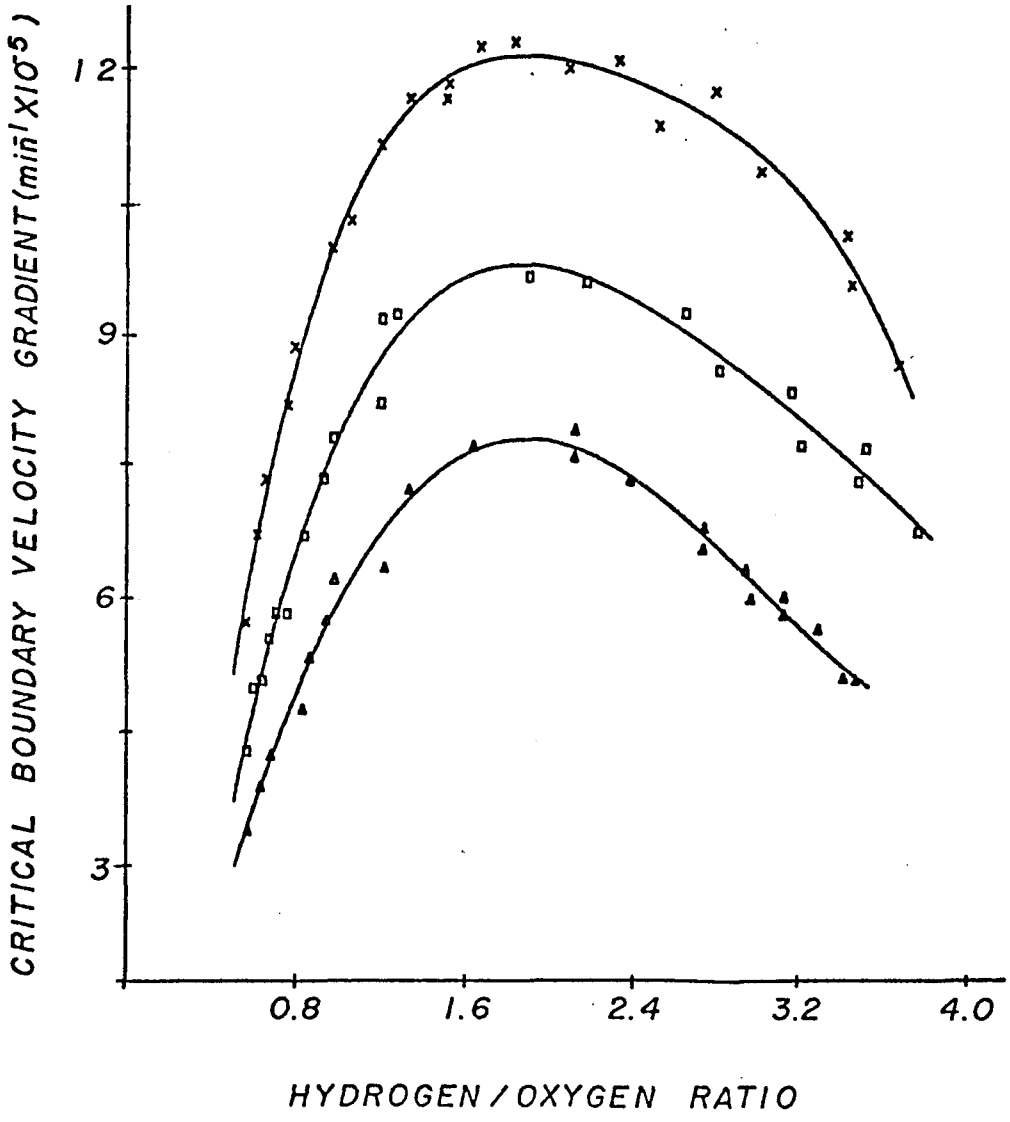

Figure 26. Variation of critical boundary velocity gradient as a function of temperature III. -- Port diameter 0.660 mm. Burner temperature: △ = 373°K; □ = 473°K; X = 573°K.

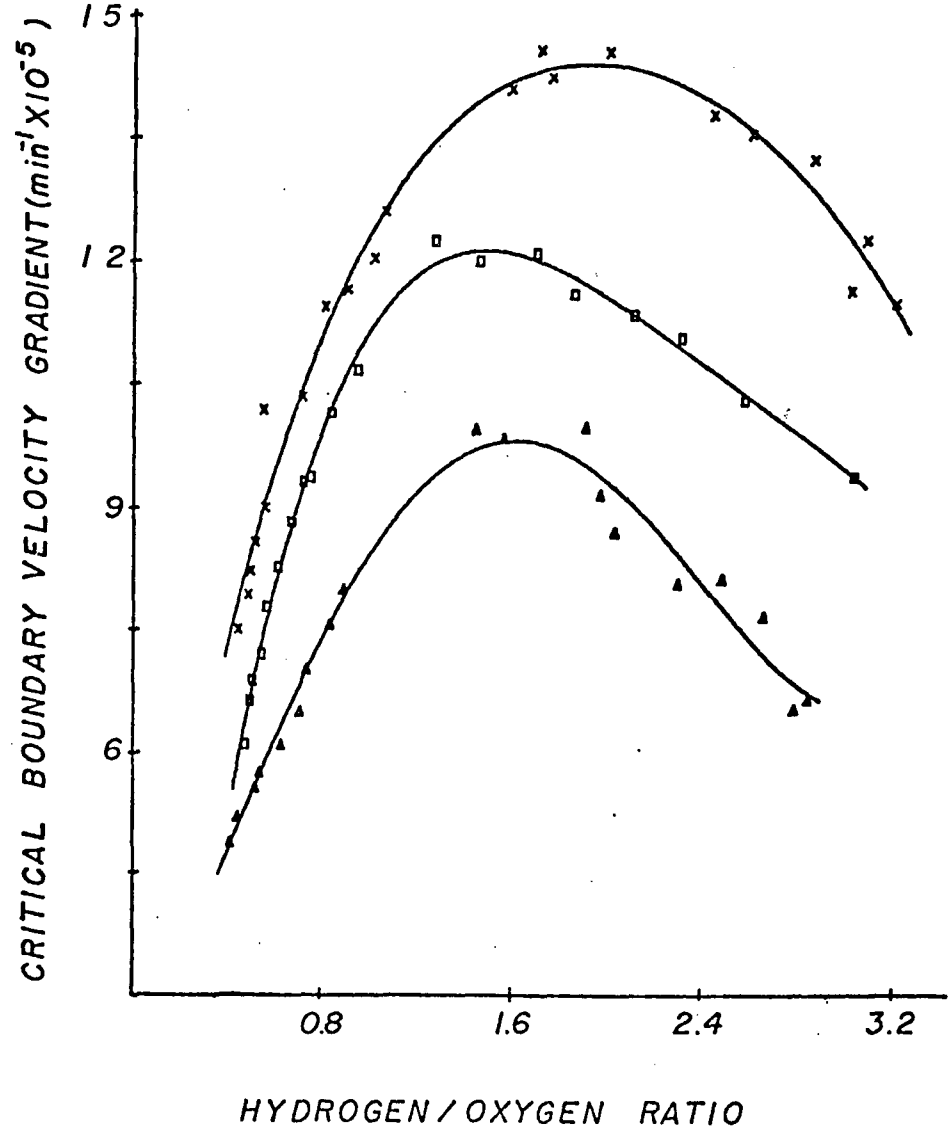

Figure 27. Variation of critical boundary velocity gradient as a function of temperature IV. -- Port diameter: 0.572 mm. Burner temperature: △ = 373°K; □ = 473°K; X = 573°K.

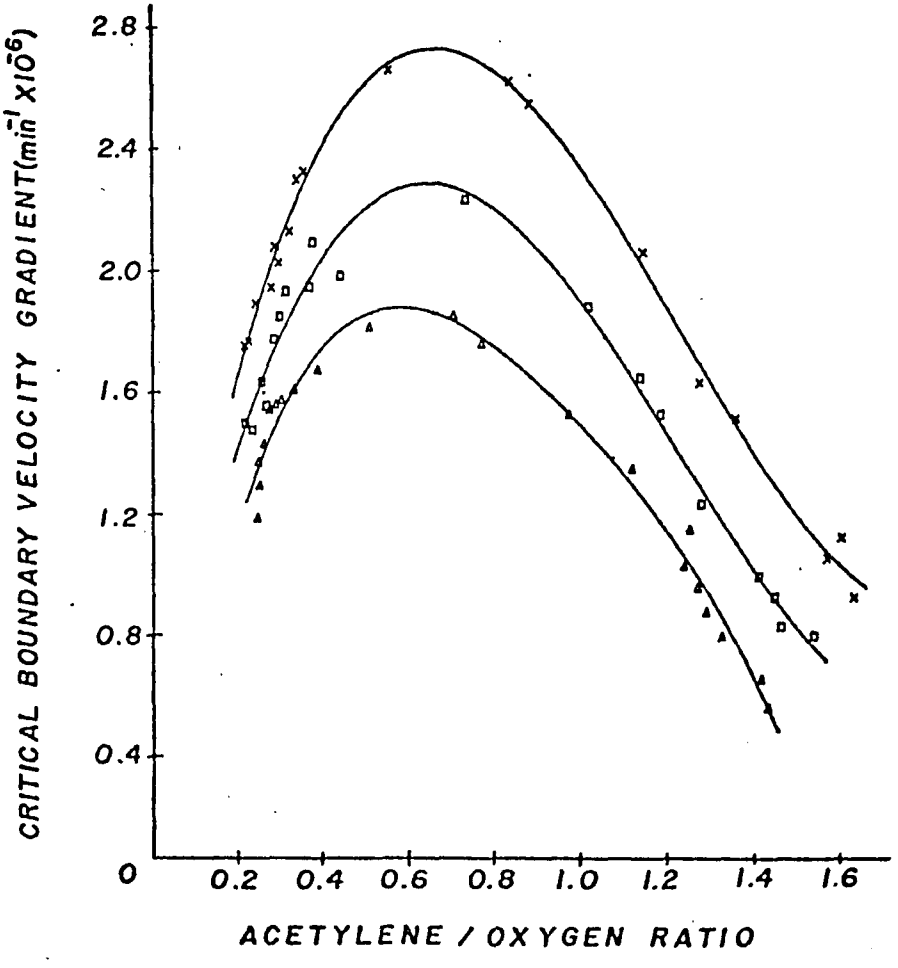

Figure 28. Variation of critical boundary velocity gradient as a function of temperature V. -- Port diameter: 0.610 mm. Burner temperature: △ = 373°K; □ = 473°K; X = 573°K.

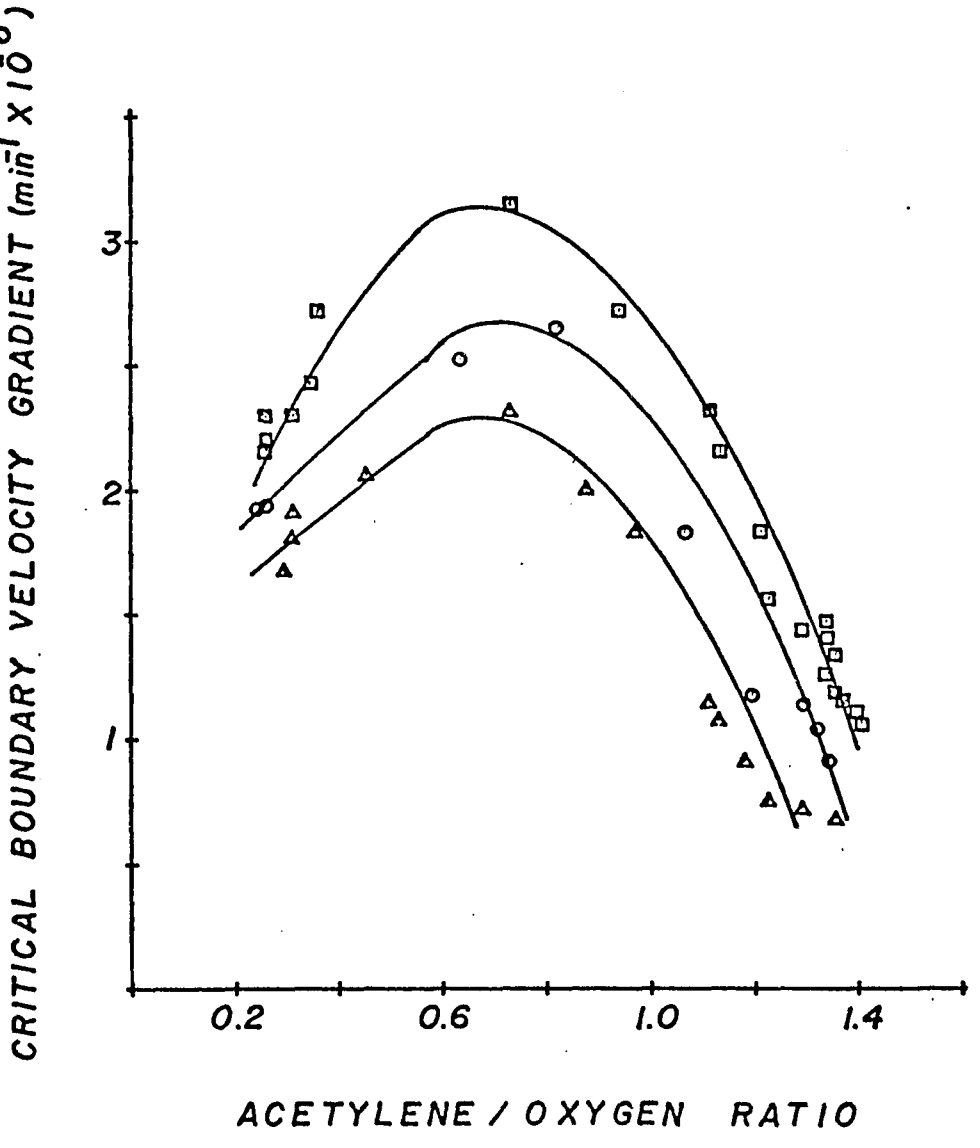

Figure 29. Variation of critical boundary velocity gradient as a function of temperature VI. -- Port diameter: 0.533 mm. Burner temperature: △ = 373°K; ○ = 473°K; □ = 573°K.

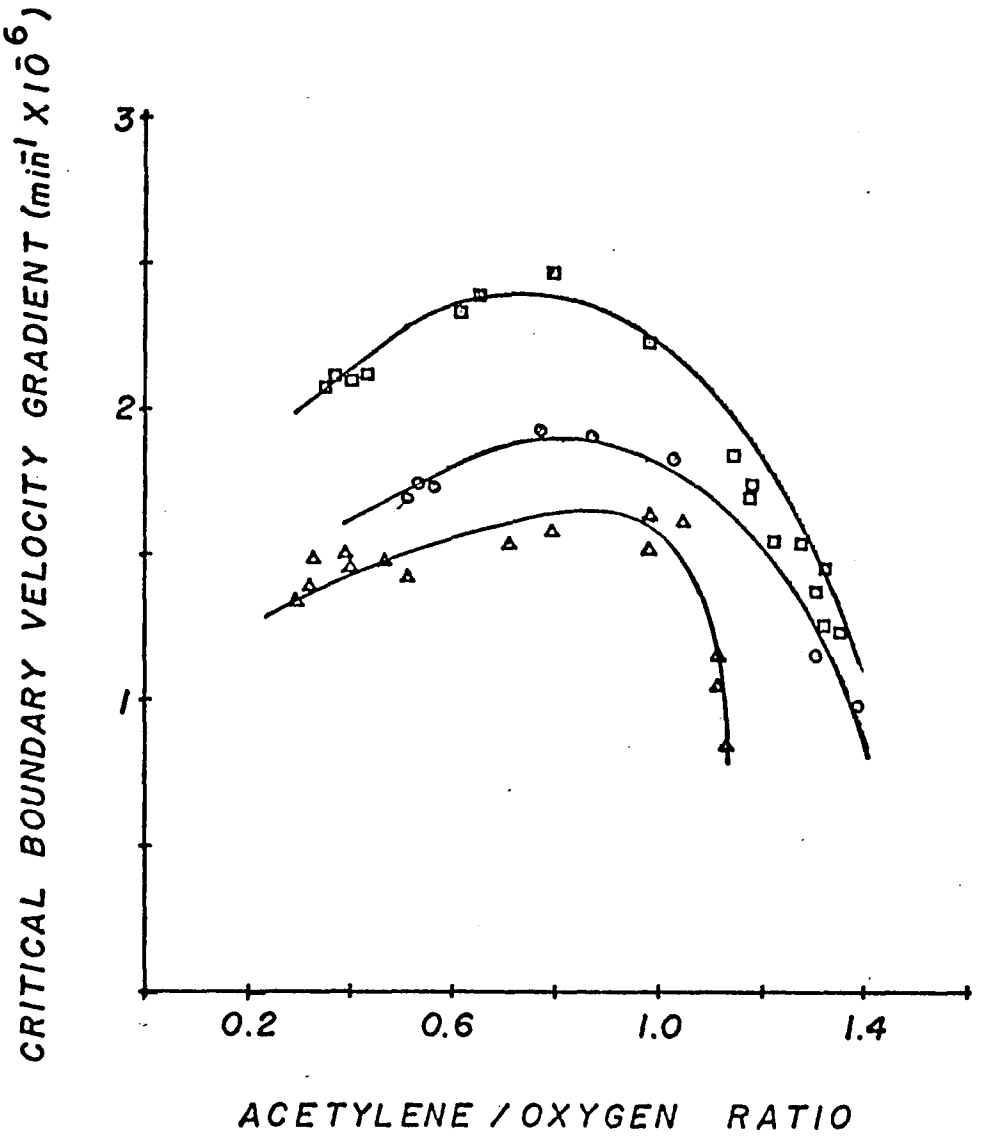

Figure 30. Variation of critical boundary velocity gradient as a function of temperature VII. -- Port diameter: 0.508 mm. Burner temperature: △ = 373°K; ○ = 473°K; □ = 573°K.

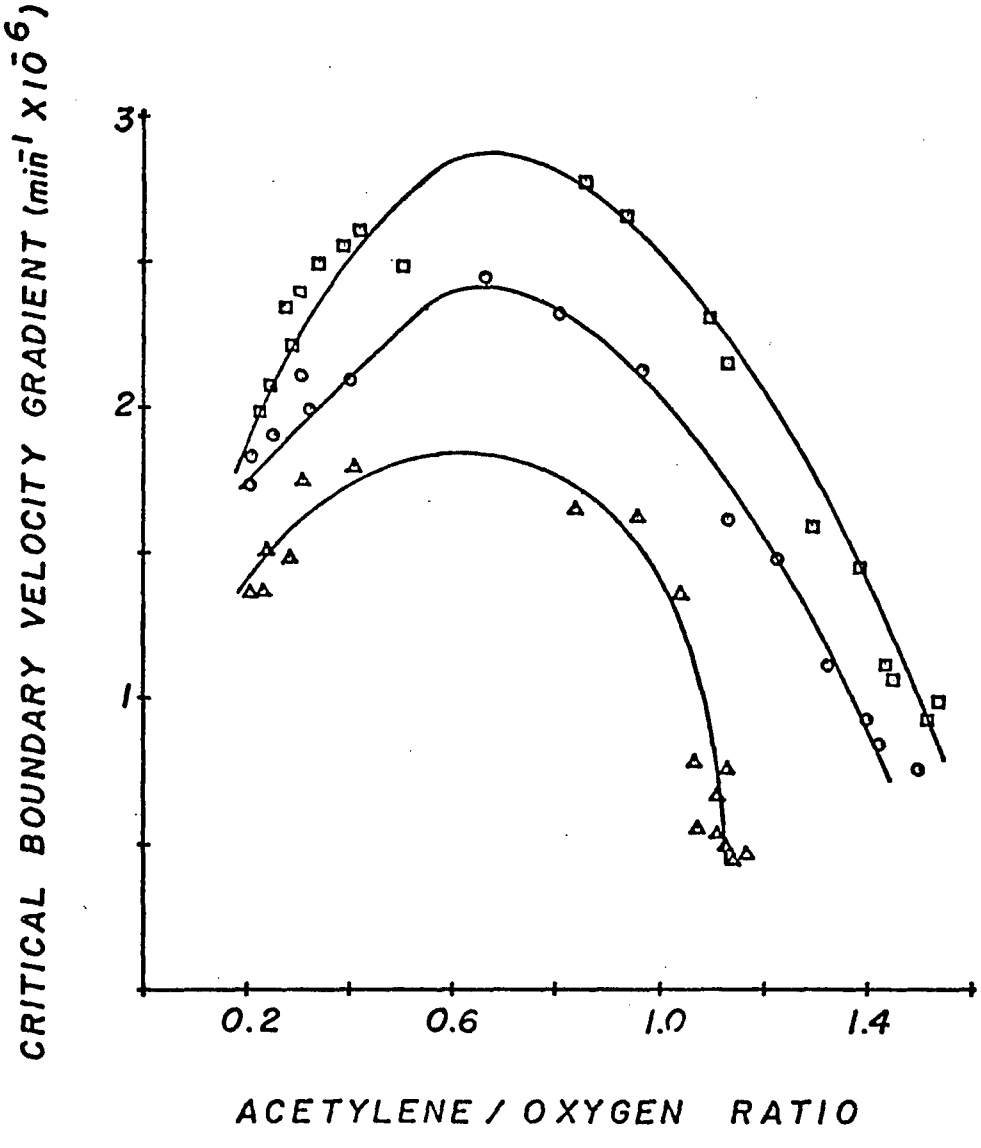

Figure 31. Variation of critical boundary velocity gradient as a function of temperature VIII. -- Port diameter: 0.572 mm. Burner temperature: △ = 373°K; ○ = 473°K; □ = 573°K.

With the burner head at 573°K no flashback was found to occur with port diameters of 0.368 mm or smaller for an oxyhydrogen flame. With an oxyacetylene flame at the same head temperature flashback was prevented with a port diameter of 0.406 mm.

It would appear that the problem of flashback with oxyhydrogen and oxyacetylene flames can be solved by simply using suitably small diameter exit ports. This can be accomplished either through drilling suitably small holes or assembling a number of stainless steel capillaries (2). However, when actually analyzing a solution with a burner design utilizing the small diameter necessary to completely prevent flashback, salt deposits may form within the port and impede the free passage of the analyte aerosol and support gases to the flame. Thus, although the flashback problem may be solved in this manner a new problem of sample passage can be created.

It is suggested that with the data presented here suitable burners can be constructed which would possess reduced flashback probability, but yet allow free sample passage to the flame. For example, from Figure 4 it is possible to construct a safe burner for oxyhydrogen using 0.572 mm diameter exit ports which would possess relative freedom from flashback. In addition, the exit port is large enough to allow the analyte to pass freely to the flame with the implementation of one of the newer sample introduction techniques such as high frequency ultrasonic nebulization (14, 15, 39). In other techniques, such as the single droplet technique described by Hieftje and Malmstadt (32, 33) holes smaller than the quenching diameter could be employed in order to totally eliminate flashback problems.

As temperature has been shown to be a significant factor in preventing flashback, a burner should incorporate suitable cooling devices. The two most common methods of cooling a burner are the extensive use of cooling fins or the use of a water cooling system. The incorporation of such cooling devices can significantly reduce the possibility of flashback and should be considered in the design of any burner.

The construction of a burner which may be safely operated with premixed oxyhydrogen or oxyacetylene has been shown to depend on a number of parameters, including exit port diameter, fuel-oxidant ratio, and the burner head temperature. By carefully evaluating the operating parameters for a particular application, a burner which can be safely operated with oxyhydrogen or oxyacetylene may be constructed with the help of the data presented here.

CHAPTER 3

SYSTEM DESCRIPTION AND OPERATION OF PULSE ULTRASONIC NEBULIZATION

Ultrasonic Nebulization

The use of ultrasonic nebulization as a sample introduction technique for flame spectroscopy has been reported in numberous publications (12, 14, 15, 39). The primary advantage of ultrasonic nebulization is in the very fine and dense aerosol that is produced. Small aerosol droplets help to minimize vaporization interferences in a flame and also allow more efficient passage of the sample through small exit ports into the flame. Unlike pneumatic nebulizers where the total aerosol production is dependent on the gas flow rate, the ultrasonic nebulizer produces aerosol independent of the gas flow rate. This is a major advantage in low flow systems such as premixed burners and inductively coupled plasmas.

At the heart of an ultrasonic nebulizer is a piezoceramic transducer. Piezoceramic transducers are constructed from ferroelectric materials. Ferroelectrics are defined as consisting of regions of homogeneous polarization, although the direction of this polarization may be different. The regions of homogeneous polarization are known as ferroelectric domains. Between each domain there is an area known as a domain wall. It is in the domain wall that the direction of polarization changes.

There are two subdivisions of ferroelectrics. In the first, spontaneous polarization can occur along only one axis. A simplified diagram of this class is shown in the first part of Figure 32. The domains are orientated either parallel or antiparallel to each other. Rochelle salt KH_2PO_4 and $(NH_4)_2SO_4$ are members of this class of ferroelectrics (37).

In the second class spontaneous polarization can occur along several different axes. This class is shown in the second part of Figure 32. One of the most common members of this class is barium titanate. It is important to note that ferroelectrics in this class are not necessarily piezoelectric in the unpolarized state. The individual domains do exhibit piezoelectric properties, but effects in the material as a whole readily cancel any over-all effect.

In order to better visualize the procedure by which a ferroelectric material of the second class can be made to exhibit useful piezoelectric properties it is necessary to consider a simplified structure of a ferroelectric crystal as in Figure 33. In this figure the dark circles are ions with a negative charge and the light circles represent ions with a positive charge. The positively charged ions are on a horizontal line between two negatively charged ions. The positively charged ion will always lie closer to one of the negatively charged ions than to the other. Thus there will be an electric dipole which is represented by an arrow, the head of which points in the positive direction of the polarization. A crystal in which one dipole orientation predominates over another results in the crystal being spontaneously

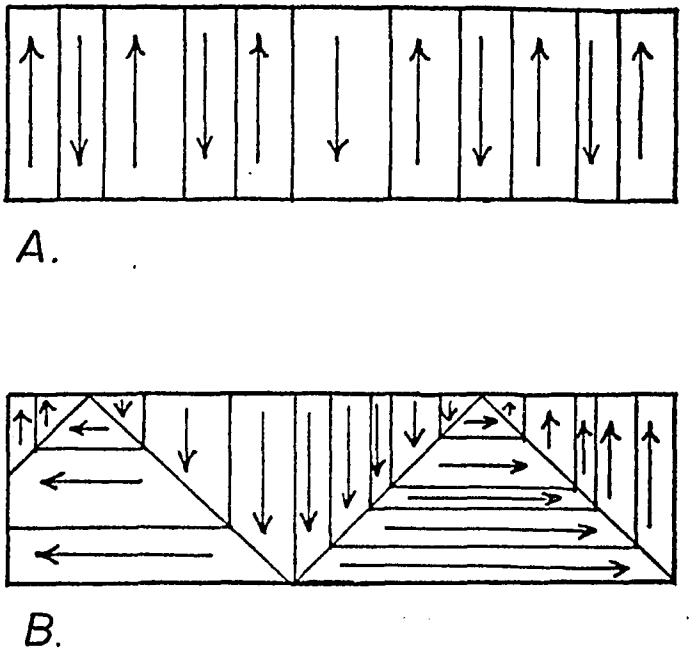

Figure 32. Representation of two classes of ferroelectrics. -- A = domains orientated parallel or antiparallel to each other; B = domains along several different axes.

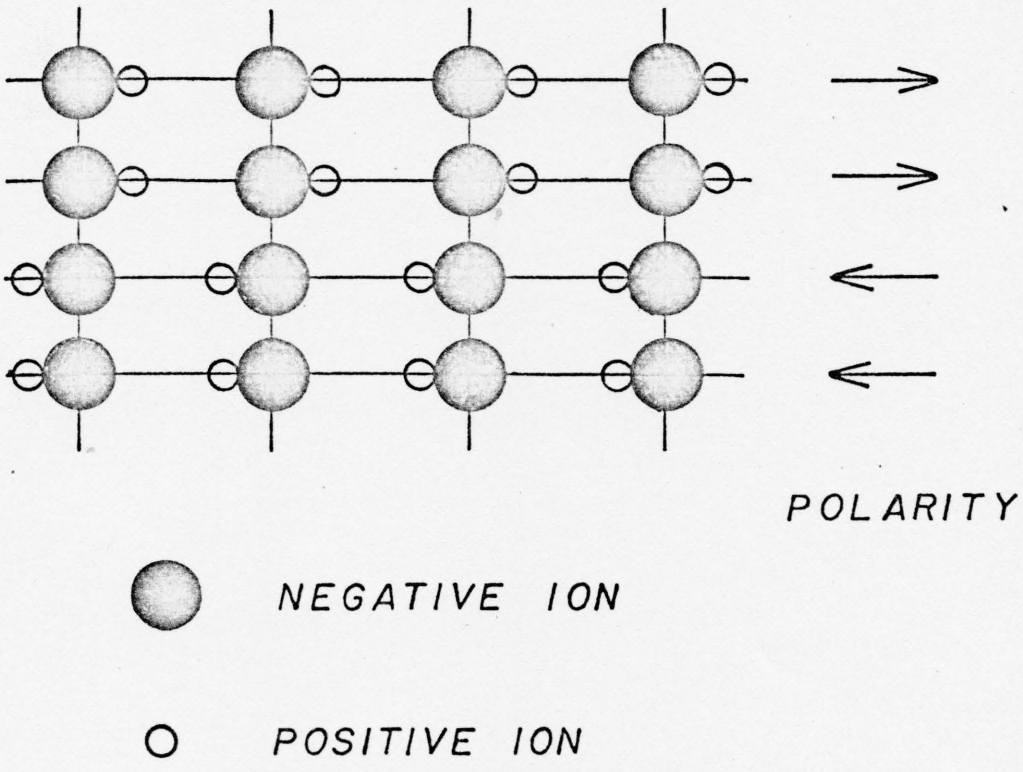

Figure 33. Representation of a ferroelectric with spontaneous polarization occurring in two different directions.

polarized. The degree of polarization is measured in terms of dipole moment per unit volume.

If a crystal possessed an equal number of domains orientated to the right and to the left, the over-all polarization of the crystal would be zero. An electric field applied in the positive direction will result in a linear relationship between the polarization (P) and the applied field strength (E) as shown by the line AB in Figure 34 (35). Increasing the field strength will result in some of the negative domains switching over in the positive direction with a rapid increase in polarization (BC), until a state is reached in which all domains are aligned in the positive direction (CD) and the crystal is of one domain.

If the potential is decreased the polarization will not return to zero but to a position represented by path DE. When the field is totally removed a polarization (AE) will remain aligned in the positive direction.

If a negative field is next applied, the over-all polarization of the material will be reversed. The value of the potential to make P equal to zero is called the coercive field (AF). Continued decrease in potential will align the dipoles in the negative direction (FG). The cycle can then be completed by again applying a positive potential. This entire cycle is known as a hysteresis loop. Thus a ferroelectric material can be polarized by applying a potential to any desired axis.

A ferroelectric such as barium titanate does not exhibit piezoelectric properties in its natural form. However, if the material is

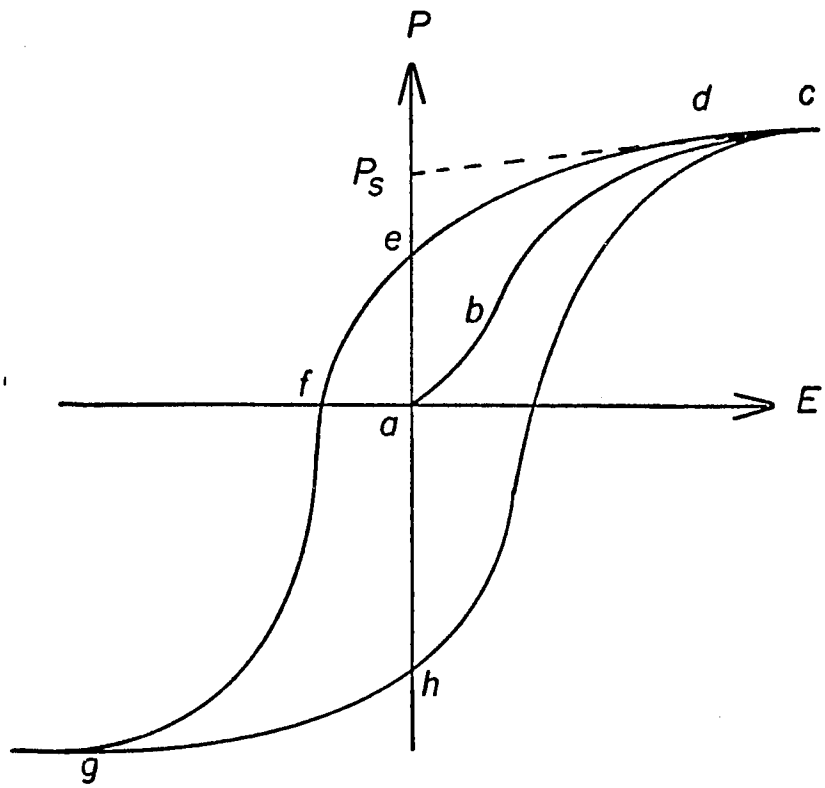

Figure 34. Typical hysteresis loop for a piezoceramic transducer.

heated to a temperature above its Curie point such that the electrostructive forces normally present disappear, and if a strong potential is applied to the crystal it will become polarized or poled. At this point the temperature is lowered below the Curie point and the potential is removed. The barium titanate is now polarized and does exhibit piezoelectric properties. A diagram of the normal position of ions in a barium titanate crystal lattice is shown in Figure 35. The arrows point to the ion positions when the crystal is polarized.

If a piezoelectric ceramic such as barium titanate, after it has been poled, is placed in a radio frequency field the transducer will experience strains across the surface of the material in the form of expansions and contractions. These strains will be in step with the applied field. For example, if the applied field is changing at a rate of 1 MHz the transducer will oscillate at 1 MHz. This is represented in Figure 36.

Placing a liquid on a rapidly oscillating transducer such as this will result in the production of a very dense but fine aerosol. A picture of an ultrasonic nebulizer in operation can be seen in Figure 37. The aerosol droplet size is dependent upon the frequency of operation (16, 41, 45). At 1 MHz the droplet size ranges from 4 to 7 microns in diameter with the principal size being 5.5 microns. At 3 MHz the range is 1 to 3 microns in diameter with the majority being 2 microns in diameter.

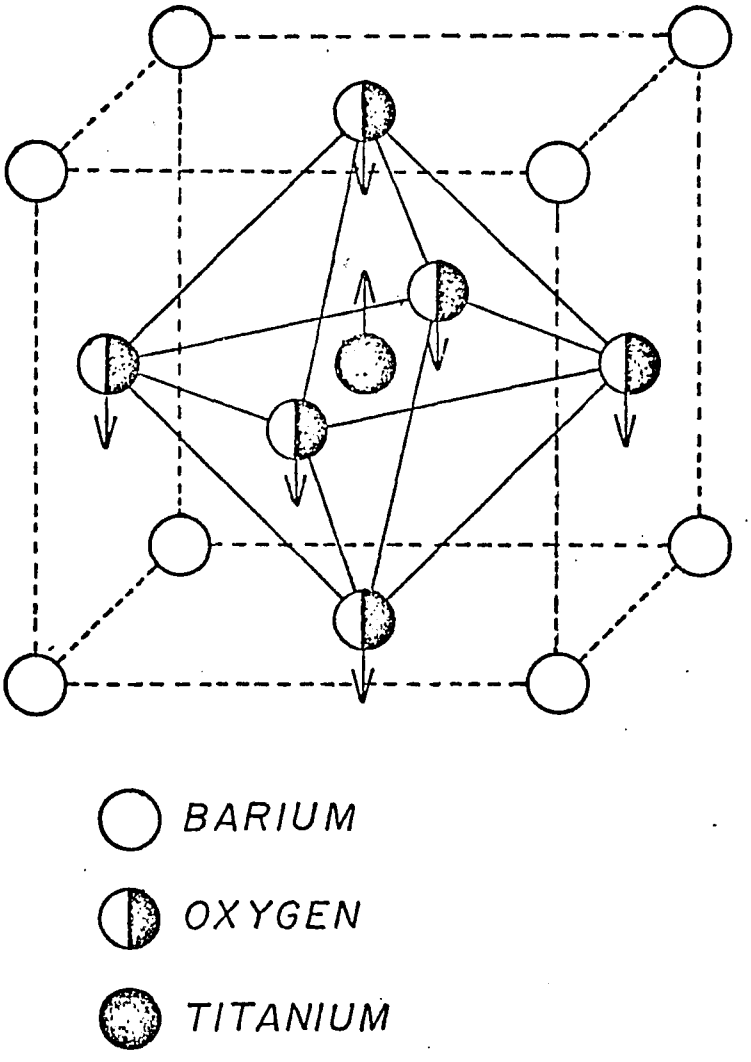

Figure 35. Structure of barium titanate showing position of atoms in both the polarized and unpolarized conditions. -- In the polarized condition each atom is in the position shown by the appropriate arrow.

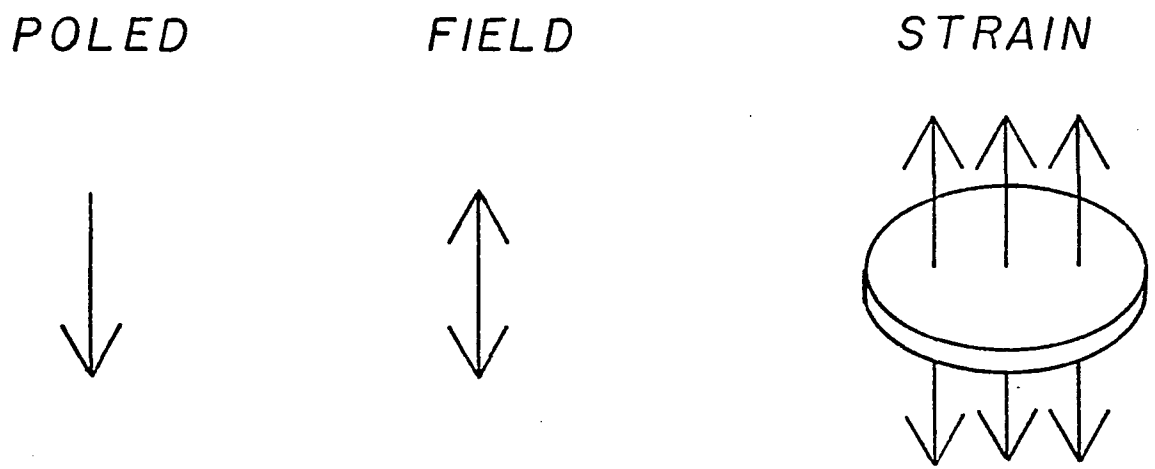

Figure 36. Direction of strain across the surface of a piezoceramic transducer when placed in an R-F field.

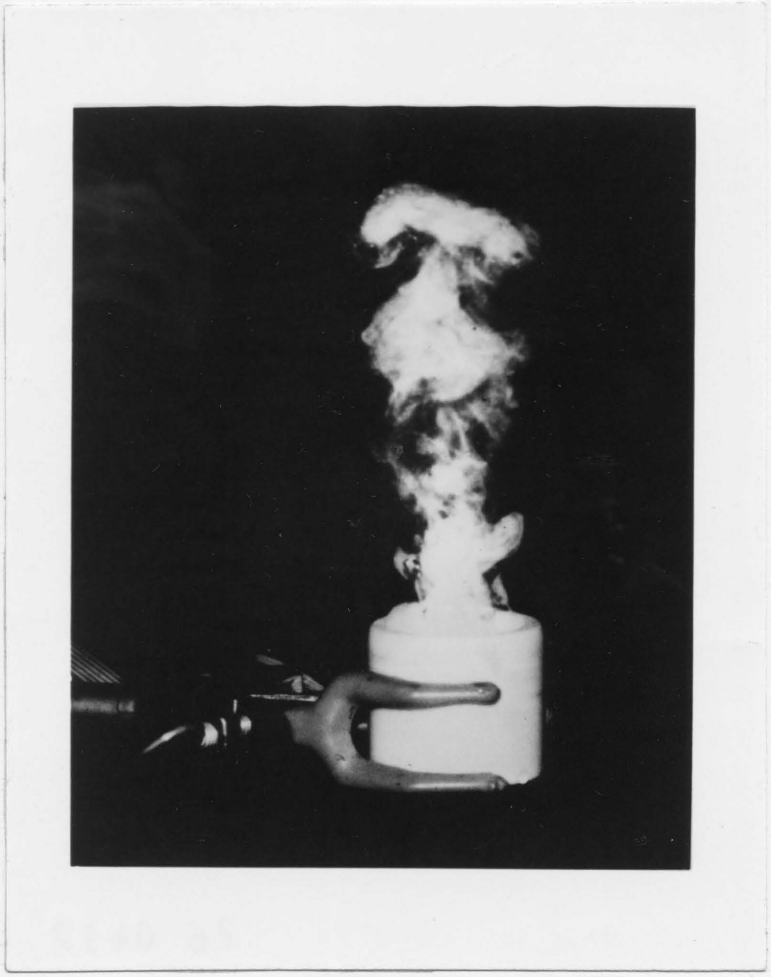

Figure 37. Photograph of ultrasonic nebulizer producing aerosol from an aqueous sample.

Burner-Nebulizer Assembly

Construction details of the nebulizer-sample cup assembly can be seen in Figure 38. The sample cup is constructed from Teflon and serves to both hold the liquid sample and house the piezoceramic transducer. Two electrodes are mounted on the bottom of the transducer in a coaxial arrangement. The center electrode makes contact with a spring mounted in the base of the sample cup which provides the radio frequency field to the transducer. The outer electrode is a ground to complete the circuit. A rubber "O" ring is placed both above and below the transducer to prevent the sample solution from leaking around the sides of the assembly and corroding the electrodes. A figure of the electrodes and their relationship to the transducer can be seen in Figure 39.

The entire nebulizer sample cup assembly is then press fit into a swivel base, which itself is mounted to the base of the burner by a spring loaded shoulder bolt as shown in Figure 40. The burner is constructed from brass with the burner head being 1 cm thick and utilizing 25 holes of 0.5 mm in diameter spaced 1.5 mm apart. The burner is surrounded by fins providing 250 cm^2 of surface area for cooling. Fuel and oxidizer enter the mixing chamber of the burner through a single entrance port to insure complete mixing.

One of the outstanding features this burner arrangement offers is the ability to change samples without extinguishing the flame. This is done by initially placing the sample cup under the sample introduction port and applying the sample to the transducer by means of an Eppendorf microsyringe (Brinkman Instruments, Westburn, N. Y. 11590). With the

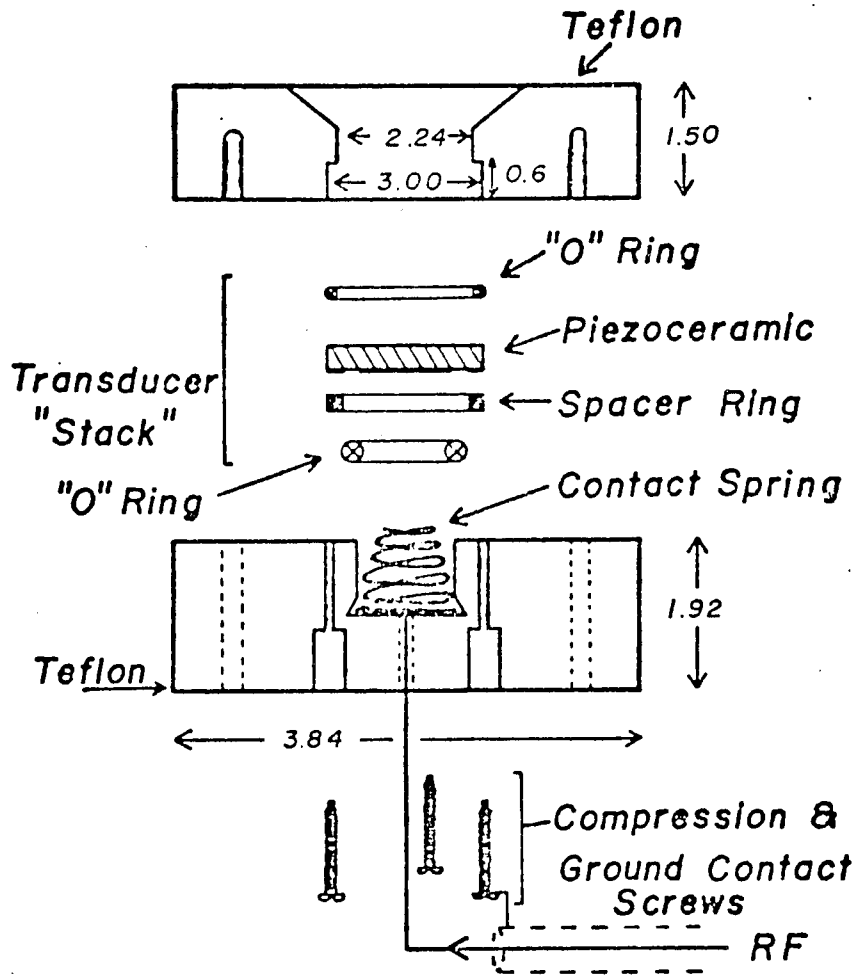

Figure 38. Detailed view of nebulizer-sample cup assembly. -- All dimensions are in cm.

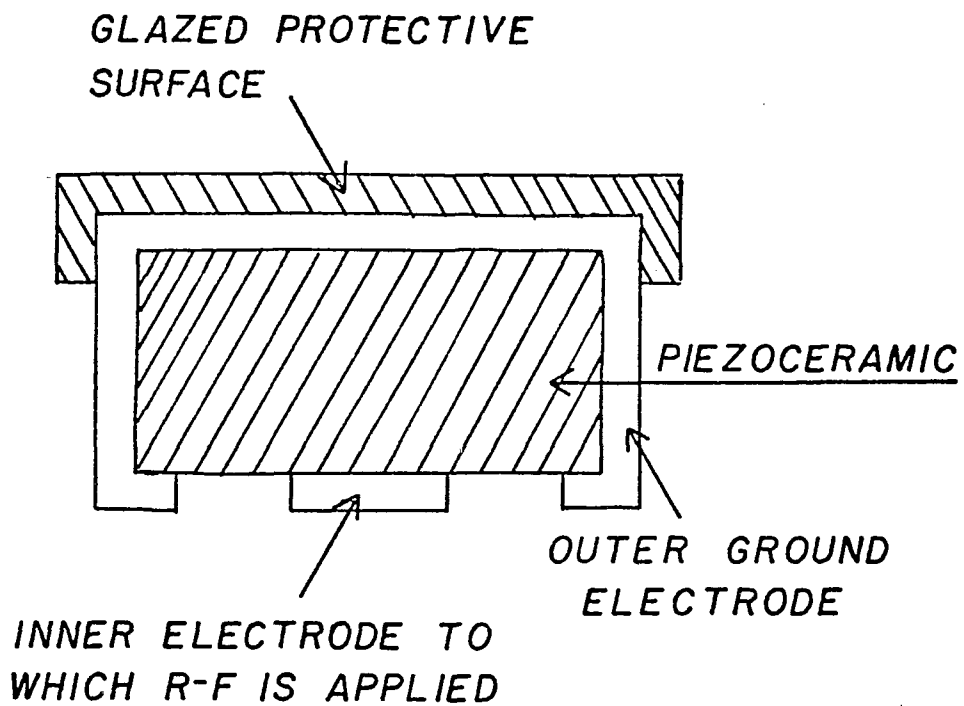

Figure 39. Cross-sectional view of piezoceramic transducer.

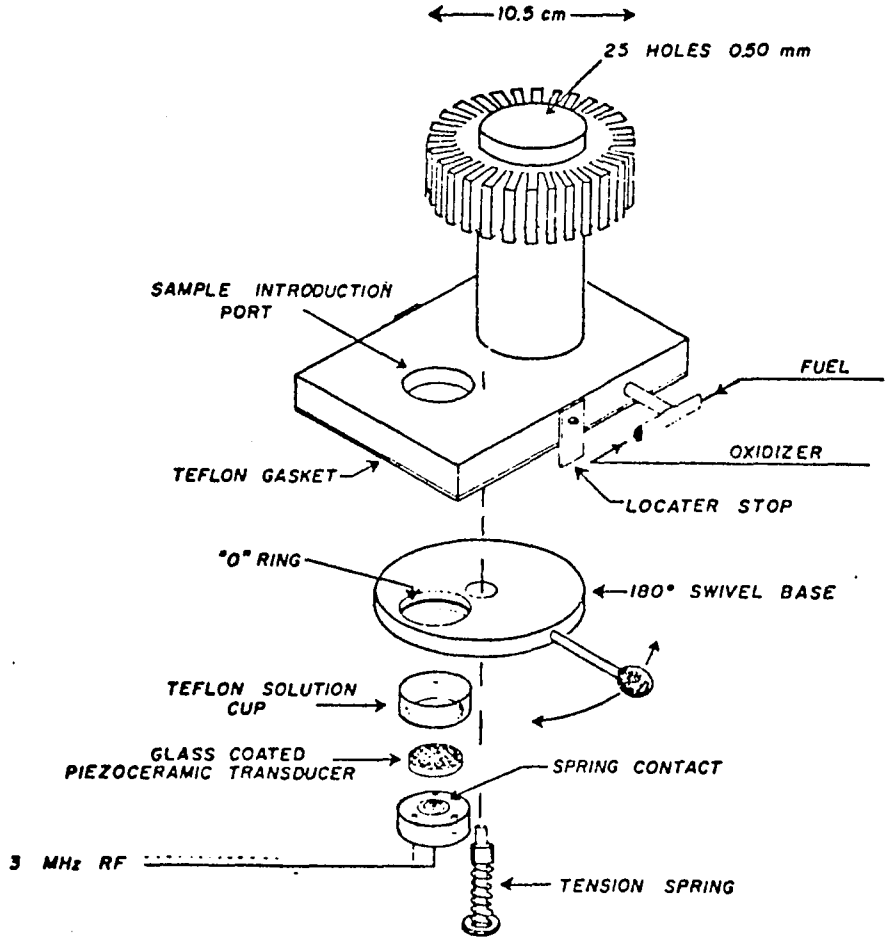

Figure 40. Detailed view of burner-nebulizer assembly.

sample cup in this position, the bottom of the mixing chamber is covered by the solid section of the base plate. A gas tight seal is obtained by using a Teflon gasket between the swivel base and the bottom of the burner. Once the sample has been applied the swivel base is rotated 180° so that the sample cup is now positioned below the mixing chamber of the burner. The sample cup reaches the same position each time by turning the base until the handle comes in contact with a locater stop. At this point the piezoceramic transducer is activated by the radio frequency generator and the aerosol produced is swept through the burner and into the flame. To run another sample requires only that the swivel base be rotated 180° in the opposite direction until the second locater stop is reached. The sample cup will now be positioned below the sample introduction port and a new sample can be applied. With this system up to three samples per minute can be run. Normal gas flow rates are: O_2:4.0 1/min and H_2:10.2 1/min measured with Dwyer flow gauges (Dwyer, Michigan City, Indiana 46360).

Experimental Arrangement

The experimental configuration used for the flame emission and atomic fluorescence investigations are shown in Figures 41 and 42. It consists of a Heath EU-700 0.4 meter Czerny-Turner monochromator, 20Å/mm reciprocal linear dispersion and EU-701-30 photometric module employing a Hamamatsu R212UH photomultiplier (Middlesex, N. J. 08846) operated at 800 volts, a log/linerar EU20-28 current module and an EU-20V variable speed recorder with a time constant of 0.039 sec/cm (Heath Company, Benton Harbor, Michigan 49022).

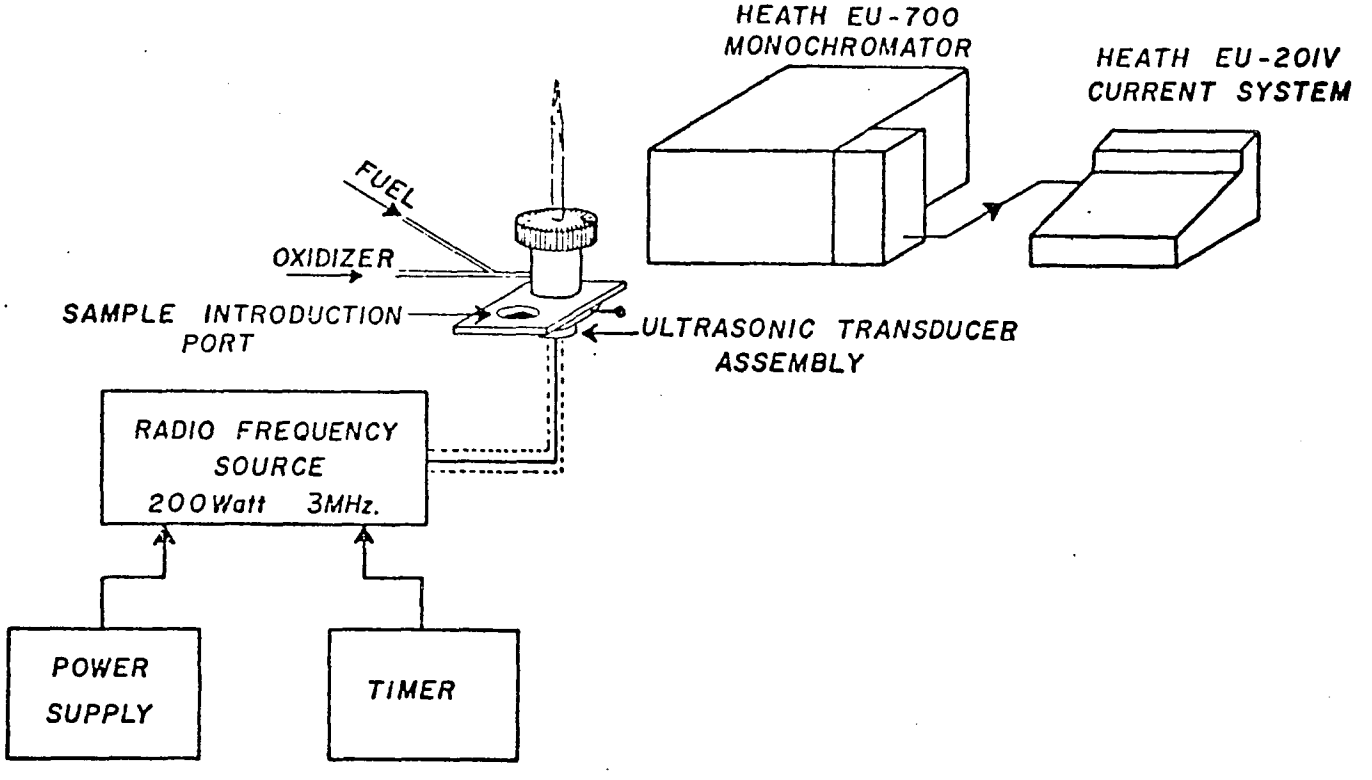

Figure 41. Experimental arrangement for flame emission using the pulse nebulizer system.

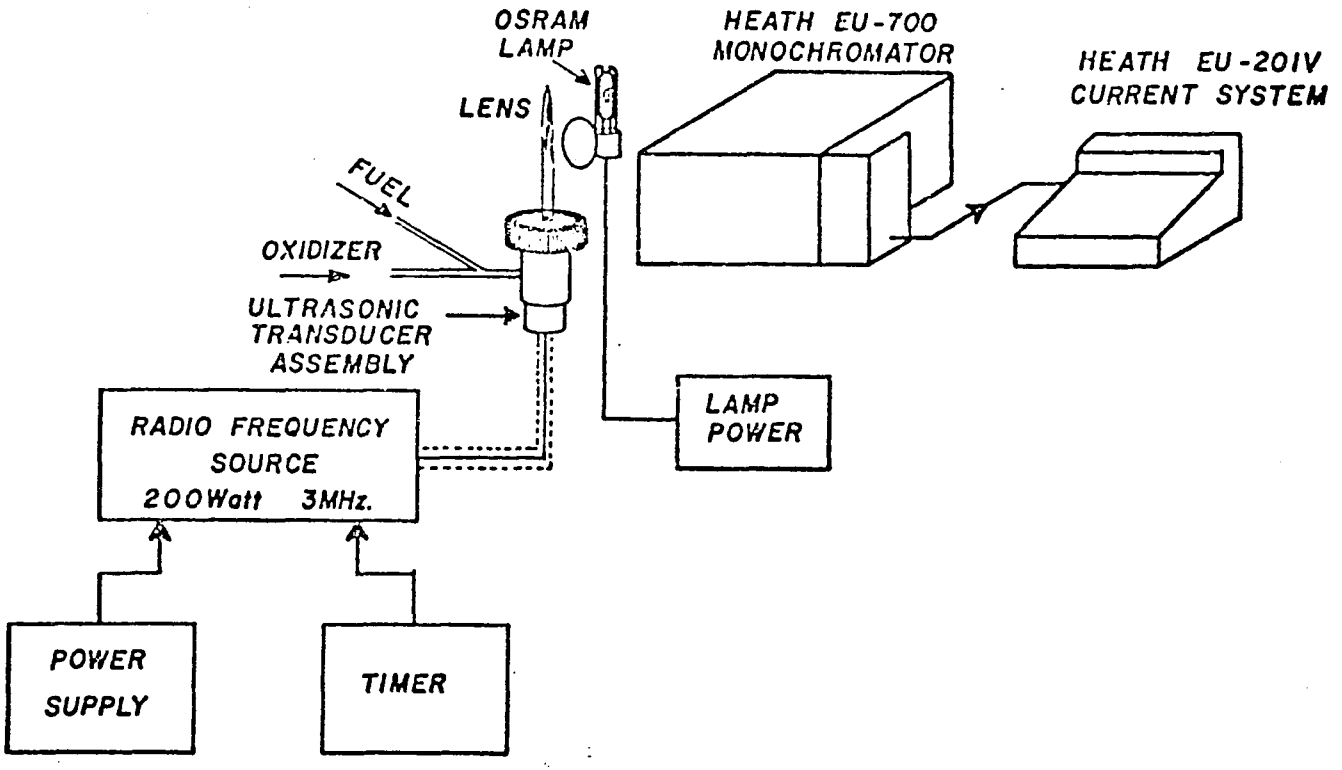

Figure 42. Experimental arrangement for atomic fluorescence using the pulse nebulizer system.

Radio Frequency Power Source

The radio frequency source used to power the piezoceramic transducer was constructed from an army surplus BC-191 transmitter (Farnsworth Television and Radio Corporation, Fort Wayne, Indiana) and a TU-5B tuning unit. Both of these units are powered by a RA-34J power supply (Radio Receptor Company, Philadelphia, Pa.). The R-F source can deliver up to 200 watts of power at 3 MHz. The radio frequency source is switched on by a monostable constructed from a Signetics (Sunnyvale, CA 94086) NE-555 timer. The system has switch selectable resistors and a 100 K-ohm ten turn potentiometer which varies the time constant in the circuit and thus the nebulization time.

Operation of the radio frequency source is initiated by turning on the filament, control and plate circuit breakers. The AC/DC switch on the transmitter should be in the AC position and the Tone/Voice/C.W. switch is set to the C.W. position. Next the main power switch of the power supply is turned on at this point and a green light should come on. The filament control voltage should be at 10.5 volts. Approximately one minute after turning on the main power switch of the power supply the plate start button should be pressed. A red light will come on indicating that voltage is being supplied to the plates in the transmitter. The actual settings used in operating the BC-191 transmitter and the TU-5B tuning unit are shown in Table 2.

Initially the frequency for maximum aerosol production was determined by operation of the nebulizer assembly in the sample loading position. Once the proper frequency for a particular transducer is

Table 2. Settings for BC 191 transmitter and TU-5B tuning unit.

Band Change Switch	M. O. Tuning	P. A. Tuning
A	B	C
1	1802	26

Ant. Coupling Switch	Ant. Ind Tuning	Ant. Circuit Switch
D	N	N
5	11	1

Ant. Cap. Tuning	Ant. Ind. Switch
0	P
35	1

determined, no further adjustments are made. At this point the time constant of the timer is set for the desired pulse length and can then be activated after the sample cup is in position as previously described.

CHAPTER 4

EVALUATION OF PULSE NEBULIZER SYSTEM

Form of Data Obtained

When a 200 µl sample of 50 µg/ml calcium is pulsed through the burner with a 2-second pulse time, a spike is obtained as shown in Figure 43. These four spikes represent four identical samples pulsed through the burner. An important point to note here is that this data was obtained with a slit width of 40 µm and when pure solvent is pulsed through the burner no spike is observed. This is important as it does not require a correction for a change in flame background emission level. Thus the peak height is proportional to the concentration of metal in the sample.

Pulse Time versus Peak Height

Investigations were conducted into factors which affect the height of the recorded spikes. The first parameter to be studied was the effect of pulse time on the emission intensity of a 200 µl Cr sample. The results of this study can be seen in Figure 44. As pulse time is increased the emission intensity is observed to increase up to a pulse time of 2 seconds at which point a plateau is reached. Pulse times longer than 2 seconds do not increase the observed emission intensity. The reason for this is that at pulse times less than 2 seconds

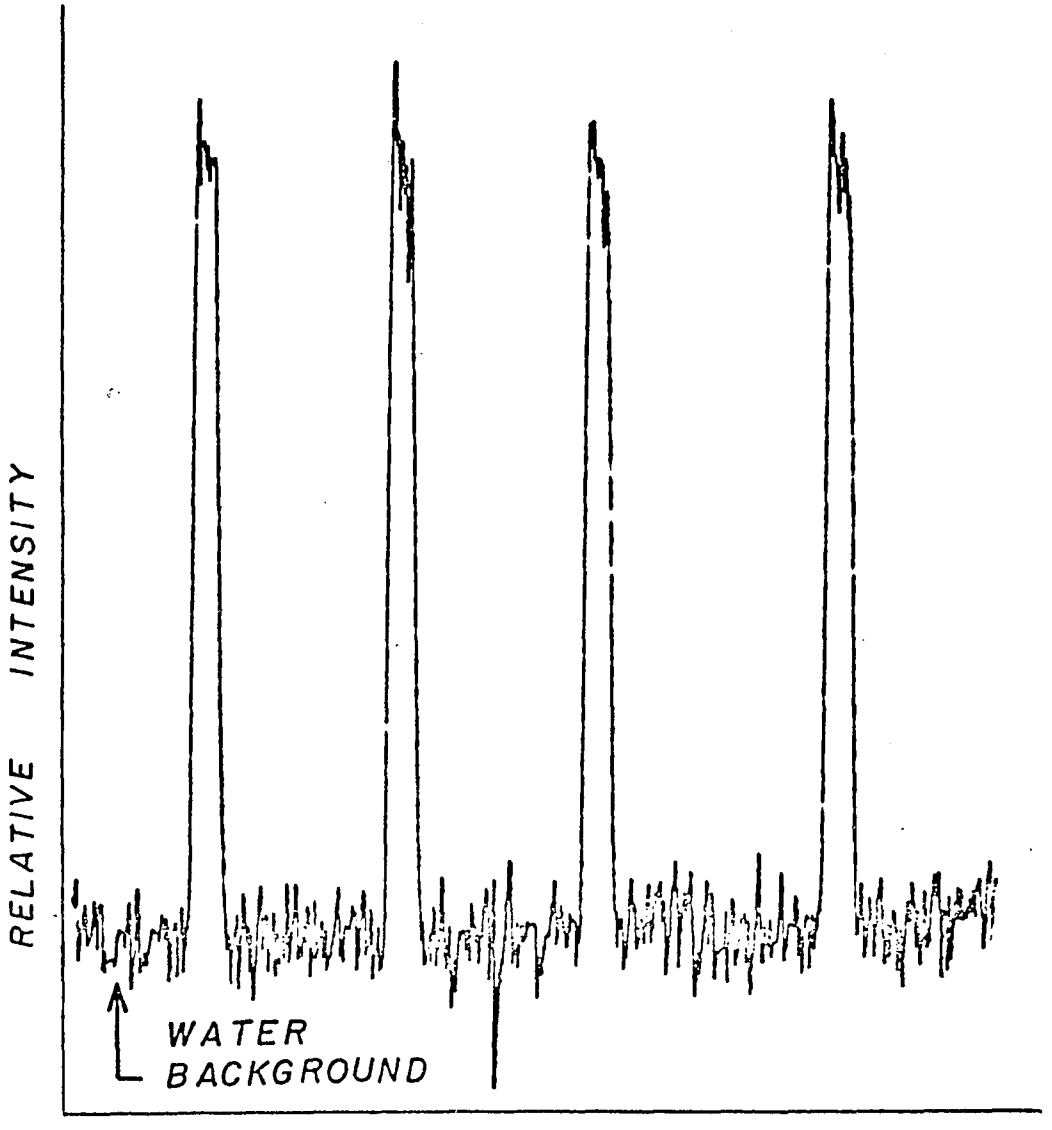

Figure 43. Recorder tracing of emission spikes obtained by pulsing 200 µl of 50 µg/ml Ca into a premixed oxygen-hydrogen flame.

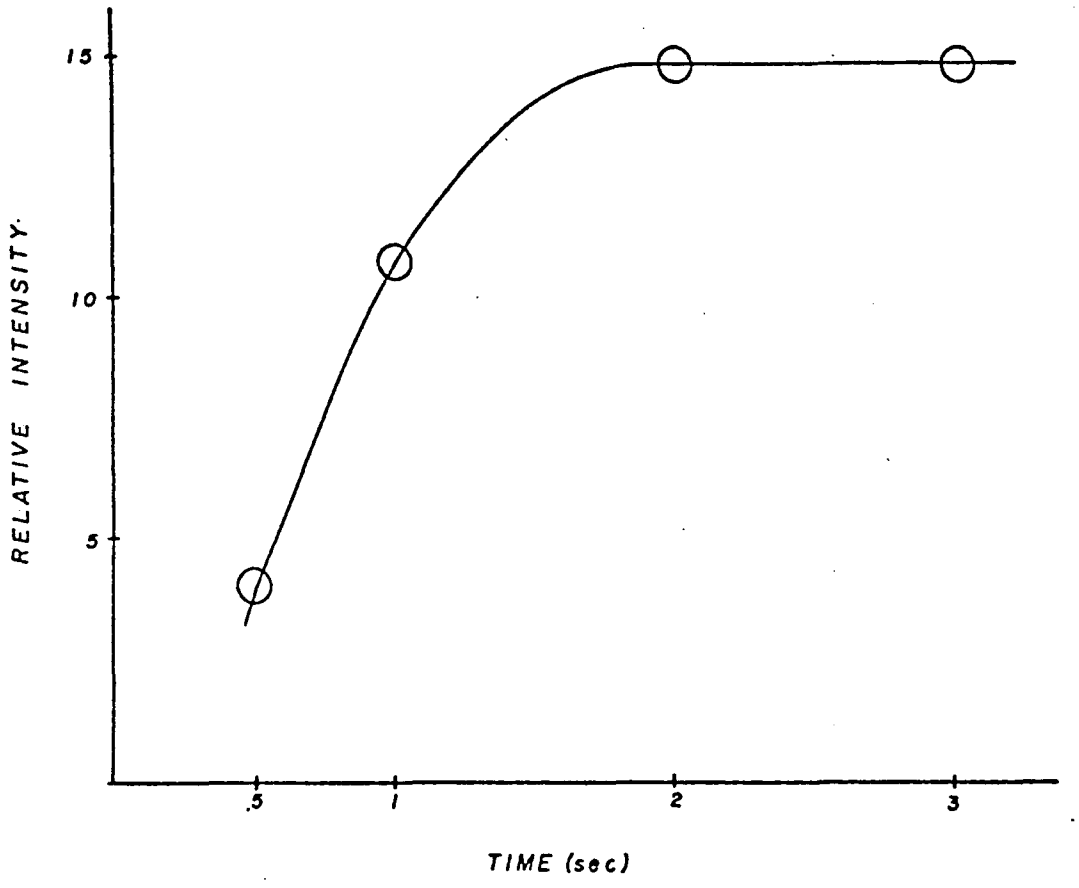

Figure 44. Effect of pulse time on emission intensity for 200 µl sample of 2 µg/ml Cr.

the nebulizer is not operating at peak efficiency in the production of aerosol. This can be visually confirmed by observing that at pulse times less than 2 seconds not all of the sample has been used and in fact some sample still remains in the sample cup. At a 2-second pulse time the entire 200 μl sample is consumed in the production of aerosol. Because the entire sample is consumed at a 2-second pulse time the use of longer pulse times does not result in an increase in emission intensity as there is no more solution present to make aerosol. Thus a plateau is reached at a 2-second pulse time. Using pulse times longer than 2 seconds, although not affecting the data, are in fact undesirable since excessive pulse times cause heating of the piezoceramic transducer which can result in depolarization in an extreme case. Pulse times longer than those to produce maximum aerosol therefore are not recommended.

Sample Volume versus Peak Height

The effect of sample volume on the emission intensity for a given pulse time was also investigated. The results of this study can be seen in Figure 45. All data were obtained with a 2 μg/ml Cr solution as in Figure 44. With a 1-second pulse time the emission intensity increases with increasing sample volume until a plateau is reached at 100 μl at which point no increase in intensity is seen. It is at this point that the transducer is producing the maximum amount of aerosol possible in the 1-second time period. Additional sample on the cup is not made into aerosol and as a result does not contribute to the emission signal. If a longer pulse time is used the emission intensity

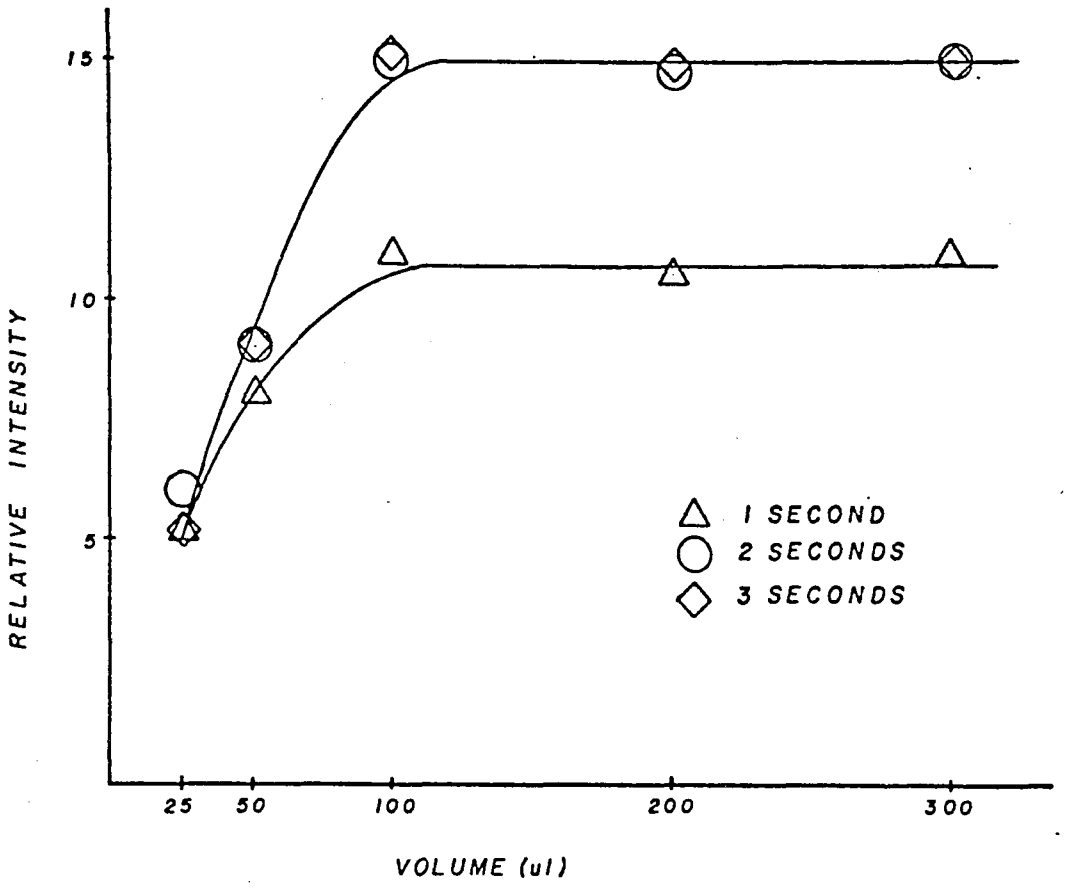

Figure 45. Effect of sample volume on emission intensity for 200 µl sample of 2 µg/ml Cr at various pulse times.

again increases as a function of volume and levels off at 100 μl as before. However, the emission intensity from the 100 μl sample is greater with a 2 or 3 second pulse time than it was with the 1-second pulse time. This is because the longer pulse time results in more aerosol being formed and thus a greater emission intensity. Placing additional samples on the transducer, such as 200 μl or 300 μl does not increase the emission signal as the transducer is producing the maximum amount of aerosol possible with the 100 μl sample. The advantage of using a 200 μl sample for analysis versus a 100 μl sample is that with 200 μl samples, one is working on a plateau and a small error in measuring the sample will not affect the height of the spike that is obtained. From Figure 45 it is apparent that if one is working in the range of 25 μl to 100 μl any error in measuring the sample volume will significantly affect the emission intensity and as a result the height of the spike.

While the total emission intensity increases with increasing sample aliquot, this increase is not a one-to-one relationship. This behavior is shown in Figure 45 where an increase by a factor of four from 25 μl to 100 μl results in a three-fold increase in emission intensity. Therefore, the best detection limits defined in concentration units are observed using aliquots exceeding 100 μl, while the best detection limits defined in terms of analyte weight are observed using small sample volumes (i.e., 25 μl). This effect can be utilized advantageously when analyzing a small sample for several species. Small

aliquots (25 μl) are utilized except for components present at such trace levels that the additional signal resulting from a larger aliquot is required for accurate analysis.

Effect of Slit Width on Peak Shape

As described in Chapter 2, the primary characteristic of a premixed oxygen-hydrogen flame is its low background emission. This allows the slits of a monochromator to be opened to a wider extent than can be done with the more conventional acetylene flames. The ramifications of using wide slit widths with a low background flame have been discussed (26, 50, 55, 69). The use of a wide slit allows one to view a greater area of the flame and thus collect more light. This works only when the background is low so that the signal increases faster than the noise as is the case when using a premixed oxygen-hydrogen flame.

One serious drawback occurs in the use of wide slits with the oxygen-hydrogen flame. That problem is at wide slit widths (> 50 μm) there is a change in background emission level when pure solvent is pulsed through the burner. This effect can be seen in Figure 46 for the analysis of strontium. The two spikes on the left side of this figure are the result of the background change when pure water is pulsed into the flame. The next two spikes are the result of a solution containing strontium at the 0.06 μg/ml level. Note that the spikes do not go down to the same level as those with pure solvent. The net emission signal which occurs from strontium in the sample is the difference between the spikes for the pure solvent and the spikes which occur as a result of a

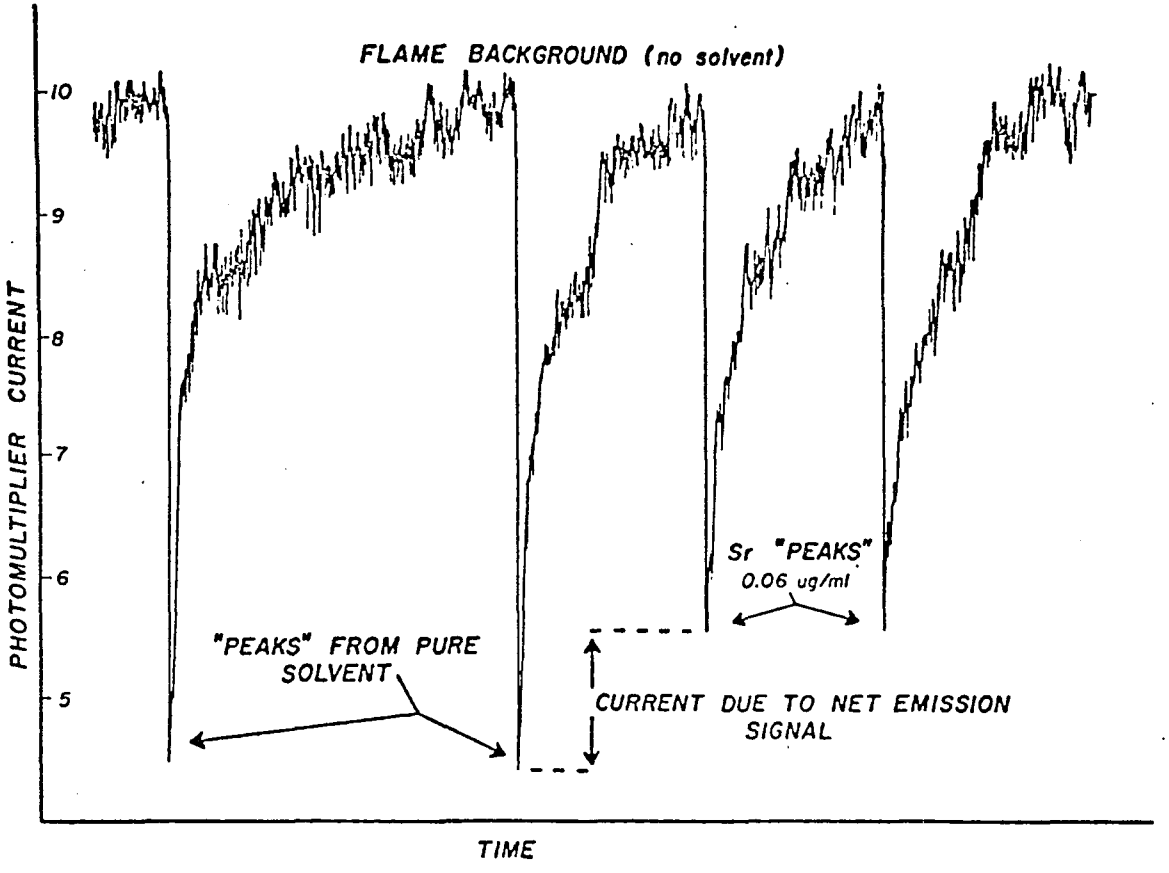

Figure 46. Change in background intensity when using a 300 μm slit width for the analysis of strontium.

solution containing strontium. This necessitates determining the background level whenever wide slit widths are employed.

The phenomena behind this background change is that at the wider slit widths the bandpass of the monochromator increases and as a result more wavelengths of the background are being monitored. When these wavelengths change the effect is additive and a net change in the background level occurs. Although at the narrow slit widths the background changes, the effect is not noticed because a smaller wavelength region is being monitored.

Detection Limits by Flame Emission and Atomic Fluorescence

Table 3 lists detection limits obtained with the element of interest dissolved in distilled, deionized water. Solutions for each element were made according to the directions of Dean and Rains (10).

In each case the detection limit was determined as twice the peak to peak background level. All detection limits were determined using a 200 μl sample and a 2-second pulse time.

The data in Table 3 show that the detection limits obtainable with the pulse system are equal to or exceed those of a turbulent oxygen-hydrogen flame. These values were obtained with slit widths of several hundred microns and as such are susceptible to interferences as a result of the increased bandpass of the monochromator. Nonetheless, it is apparent that good sensitivity is possible with this system.

Table 3. Data comparing the performance of pulse ultrasonic nebulization of 200 µl volume samples into the premixed oxygen-hydrogen flame with those obtained pneumatically nebulizing 2 ml or larger volume samples into a turbulent oxygen-hydrogen flame.*

	Line (Å)	Detection limits utilizing 200 µl sample pulse ultrasonically nebulized into the laminar oxygen-hydrogen flame		Detection limits obtained with 2 ml or more of sample pneumatically nebulized into a turbulent oxygen-hydrogen flame (27)	
		µg/ml	Slit Width (µm)	µg/ml	Slit Width (µm)
Ca	4227	0.00005	300	0.005	100
Cr	4254	0.07	250	0.05	75
Ba	5535	0.0002	300	0.25	70
Sr	4607	0.001	250	0.005	75
Tl	5351	0.5	250	0.03	75
In	4511	0.001	250	0.003	75
Cu	3274	0.5	100	0.5	40

* In each case parameters including location of flame viewed gas flow rates and slit width were optimized. Due to the high flicker noise in the turbulent flame, increased readout time constants for these values necessitated sample volumes of 2 ml or larger.

Analysis of Real World Samples

The ultimate goal in the development of any new method of analysis is its application to the analysis of "real world" type samples. It was decided to test the ability of the pulse nebulizer in the analysis of NBS bovine liver samples.

The analysis was carried out by the method of standard additions as described by Dean and Rains (10). The results are tabulated in Table 4. The standard addition curves are shown in Figures 47 through 49. As can be seen in Table 4, the experimentally obtained value using a 200 μl sample is within the confidence range certified by NBS. Only cadmium is slightly out of the confidence level. Thus the pulse nebulizer system has been shown to be an accurate method for analysis of "real world" matrix samples.

A problem often encountered with samples such as the liver is that the exit ports often will clog as a result of the high matrix content of the sample. This was found not to be a problem with the pulse system. Two factors probably account for this. First, the total sample volume being used is very small. Because of this the processes necessary to clog the exit ports do not occur since very little sample is available for this to occur. Secondly, the aerosol droplets produced by the nebulizer are of a very small diameter and as such can pass more easily through the exit ports used in this burner.

Reproducibility

Another important area to be evaluated with the pulse nebulizer is the reproducibility of the method. Figure 50 is a recorder tracing

Table 4. Analysis of NBS liver.

Element	Expt (μg/g)	NBS value (μg/g)
Ca	120.6	123 ± 10
Cd	0.324	0.27 ± .04
Zn	120.9	130 ± 10

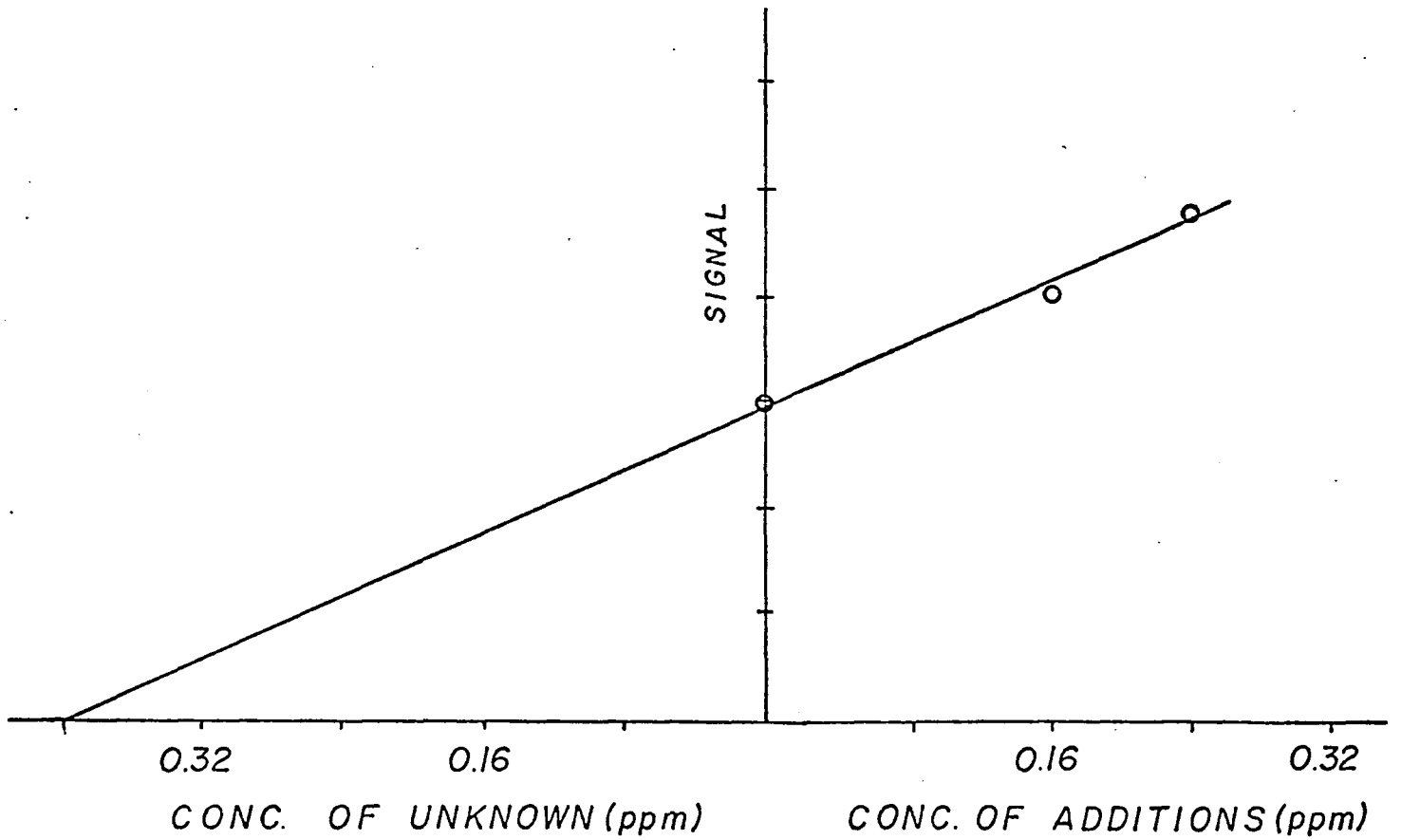

Figure 47. Standard addition curve for the analysis of Zn in NBS liver.

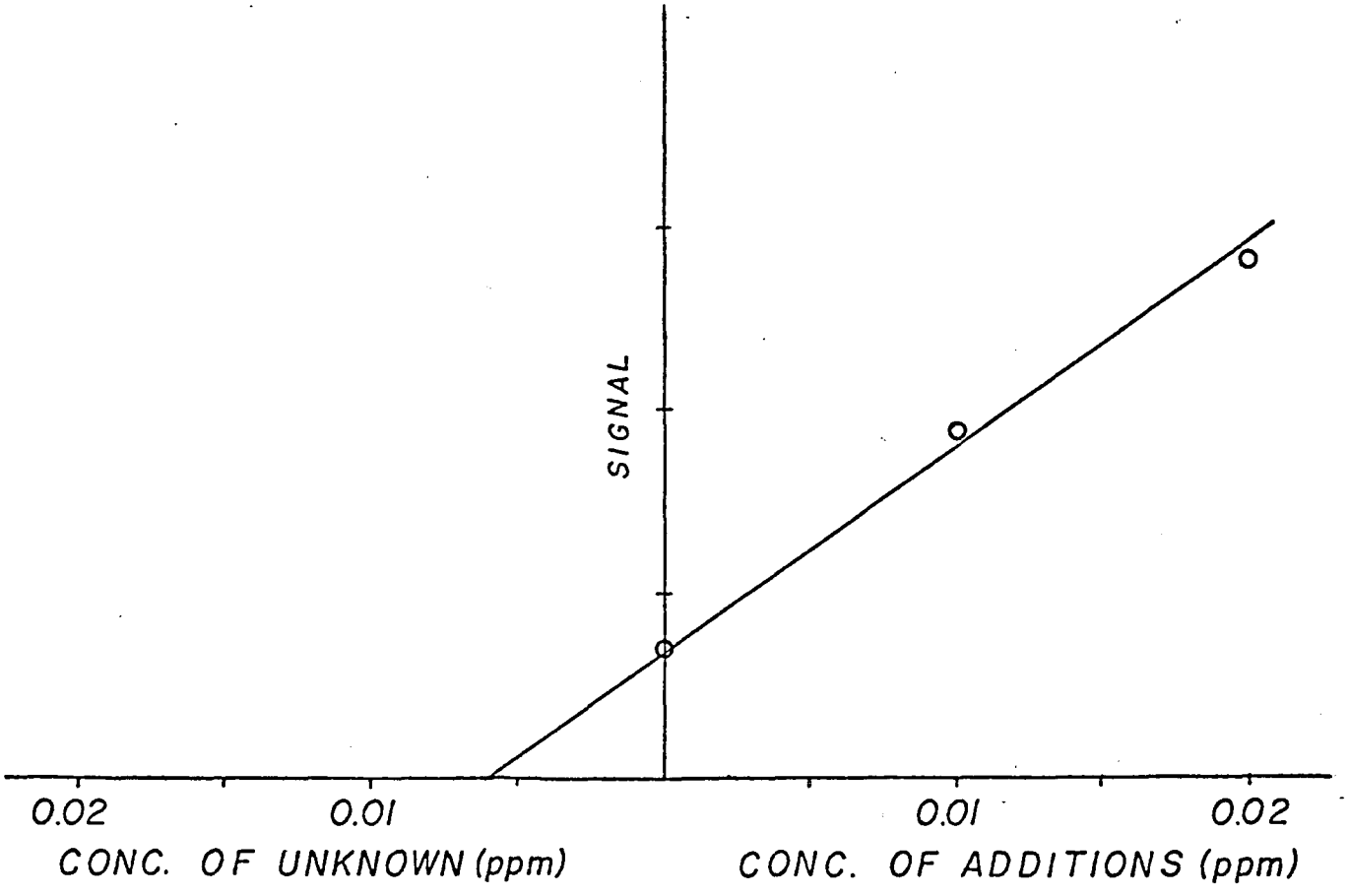

Figure 48. Standard addition curve for the analysis of Cd in NBS liver.

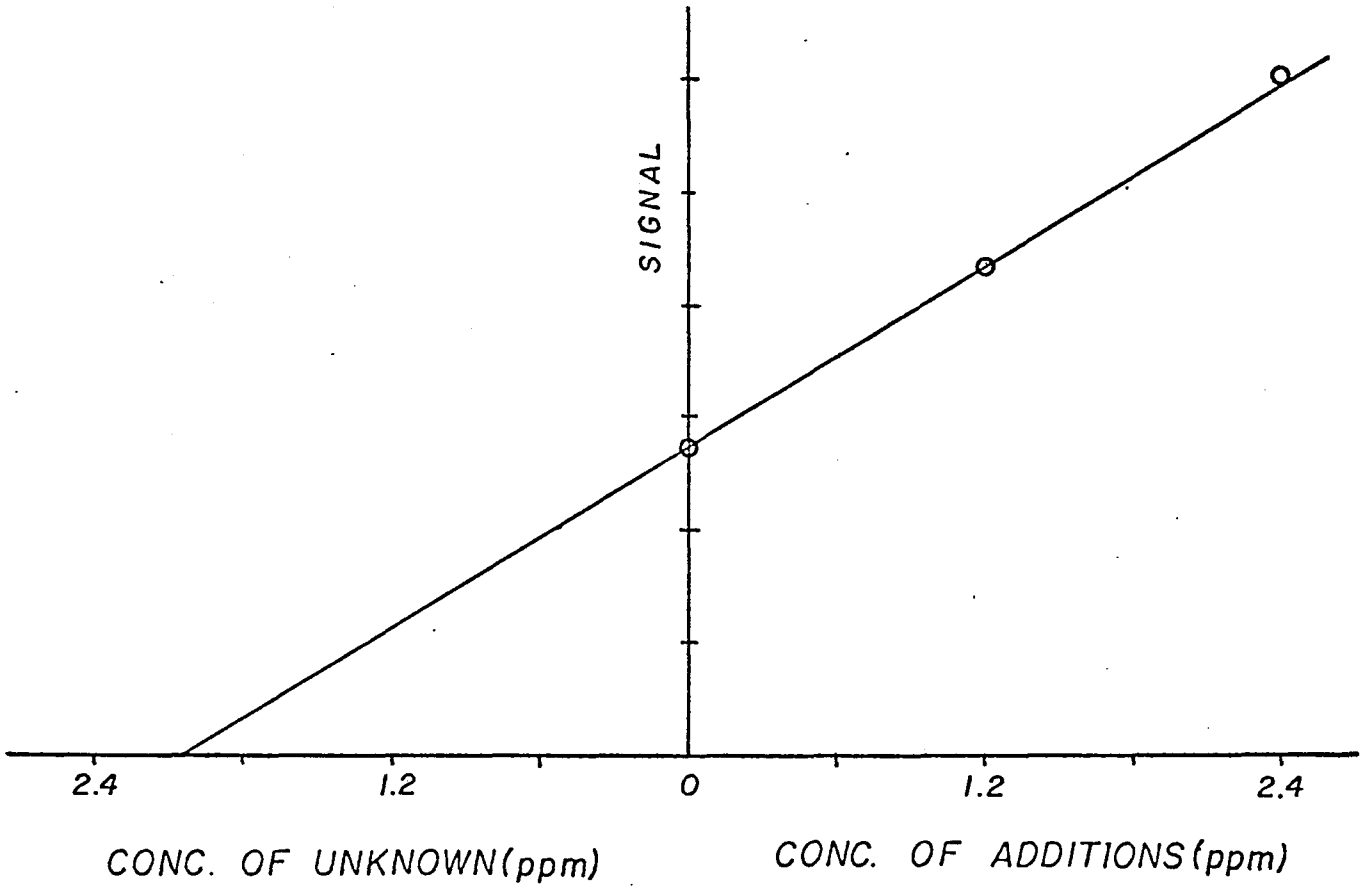

Figure 49. Standard addition curve for the analysis of Ca in NBS liver.

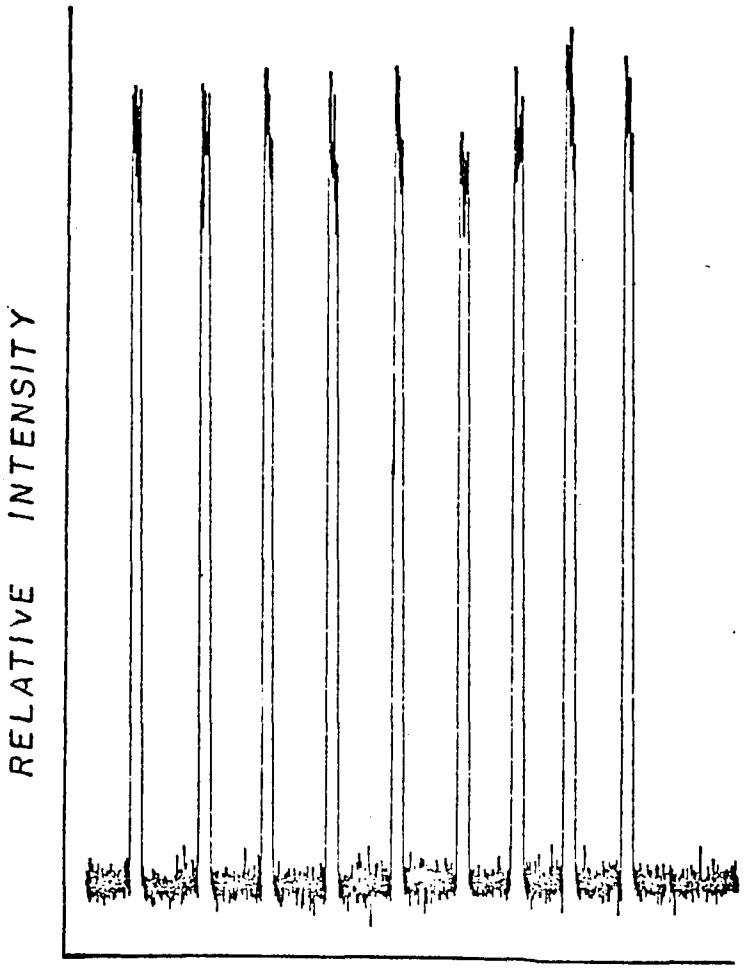

Figure 50. Reproducibility data when using a premixed oxygen-hydrogen flame with a slit width of 20 μm and a 200 μl sample of 10 μg/ml Ca.

of nine identical 200 μl samples of 10 ppm Ca pulsed into the premixed oxygen-hydrogen flame. The slit width in this case is 20 μm so no change in background is observed when pure solvent is introduced to the flame. The percent relative standard deviation for this set of data is 2.4% which compares favorably with reproducibility of other small volume techniques described in the introduction. The sixth spike of this figure is considerably lower than the others. This occurred as a result of the sample cup not being positioned correctly in the bottom of the burner. For this reason the sixth spike was not used in calculating the percent relative standard deviation reported above. If this spike is included in the percent relative standard deviation a value of 3.5% is calculated. This problem has been eliminated through the use of position stops located on the side of the burner which allow the sample cup to be accurately positioned each time a new sample is run.

As was stated earlier, to obtain the maximum sensitivity using a premixed oxygen-hydrogen flame it is necessary to open the slits up so that a larger area of the flame is viewed. However, this results in more baseline noise and less reproducible spikes. Figure 51 shows reproducibility data for 50 μm slits. As is apparent the baseline noise level is considerably greater than that in Figure 50. Since this noise is also present on top of each spike the reproducibility is degraded. The percent standard deviation for spikes in this figure is 9%. This increase in the standard deviation is the result of the increased noise level and not due to any irreproducibility of the nebulizer.

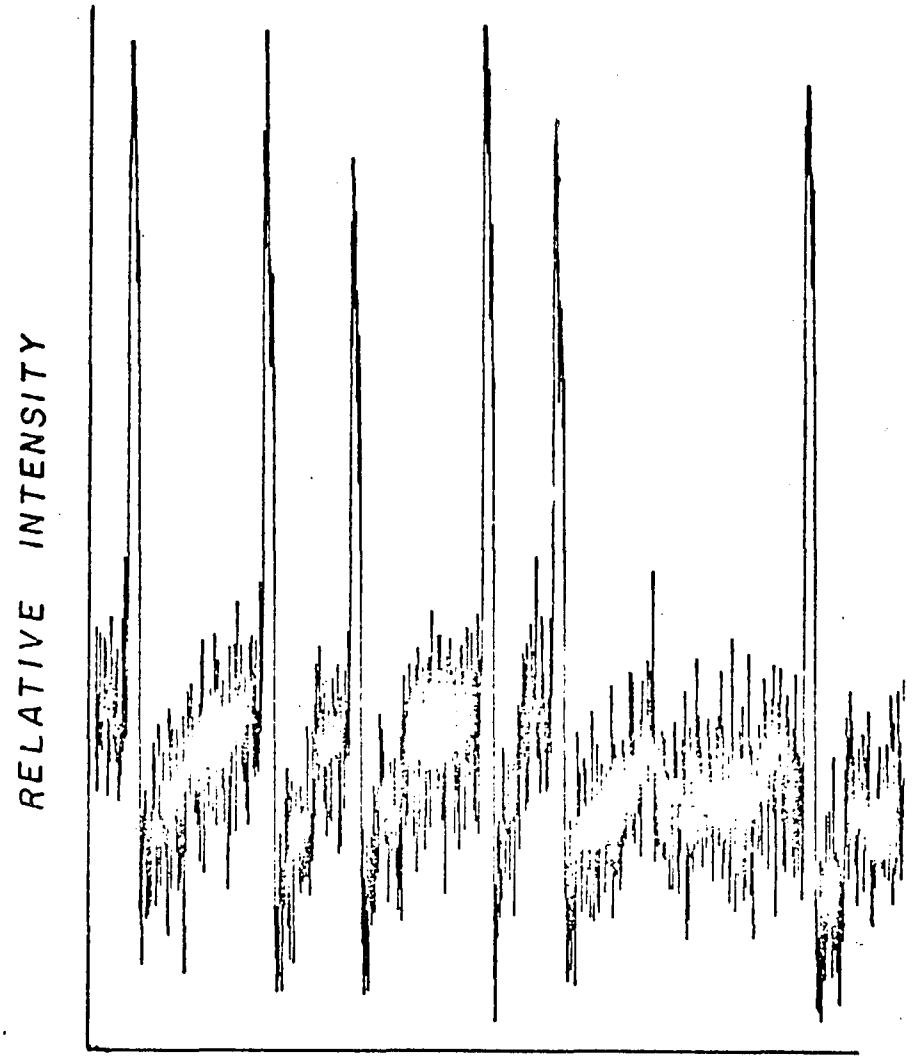

Figure 51. Reproducibility data when using a premixed oxygen-hydrogen flame with a slit width of 50 μm and a 200 μl sample of 10 μg/ml Ca.

In addition to the reproducibility data for the oxygen-hydrogen flame some data was run using a nitrous oxide-acetylene flame. The nitrous oxide-acetylene flame is characterized by a very strong background emission. Figure 52 shows the relative background emission of the oxygen-hydrogen flame versus the nitrous oxide-acetylene flame using a 50 μm slit width.

The increased background level with the nitrous oxide-acetylene flame results in less reproducible spikes than can be obtained under identical conditions with an oxygen-hydrogen flame. Figure 53 is a recorder tracing of nine 200 μl samples of 1.0 ppm Ca pulsed into a nitrous oxide-acetylene flame under experimental conditions identical to those of Figure 50. It can be readily seen when comparing these two figures that the reproducibility obtainable with the oxygen-hydrogen flame is better than that of the nitrous oxide acetylene flame. This is due to the lower background noise of the oxygen-hydrogen flame resulting in less noise being superimposed on the individual spikes. The percent standard deviation for the spikes obtained under these conditions with the nitrous oxide-acetylene flame is 6%.

It is apparent that to obtain the best reproducibility with this system the oxygen-hydrogen flame and a narrow slit width should be used. If greater sensitivity is desired, it is necessary to use a wider slit width, but this will then degrade the reproducibility.

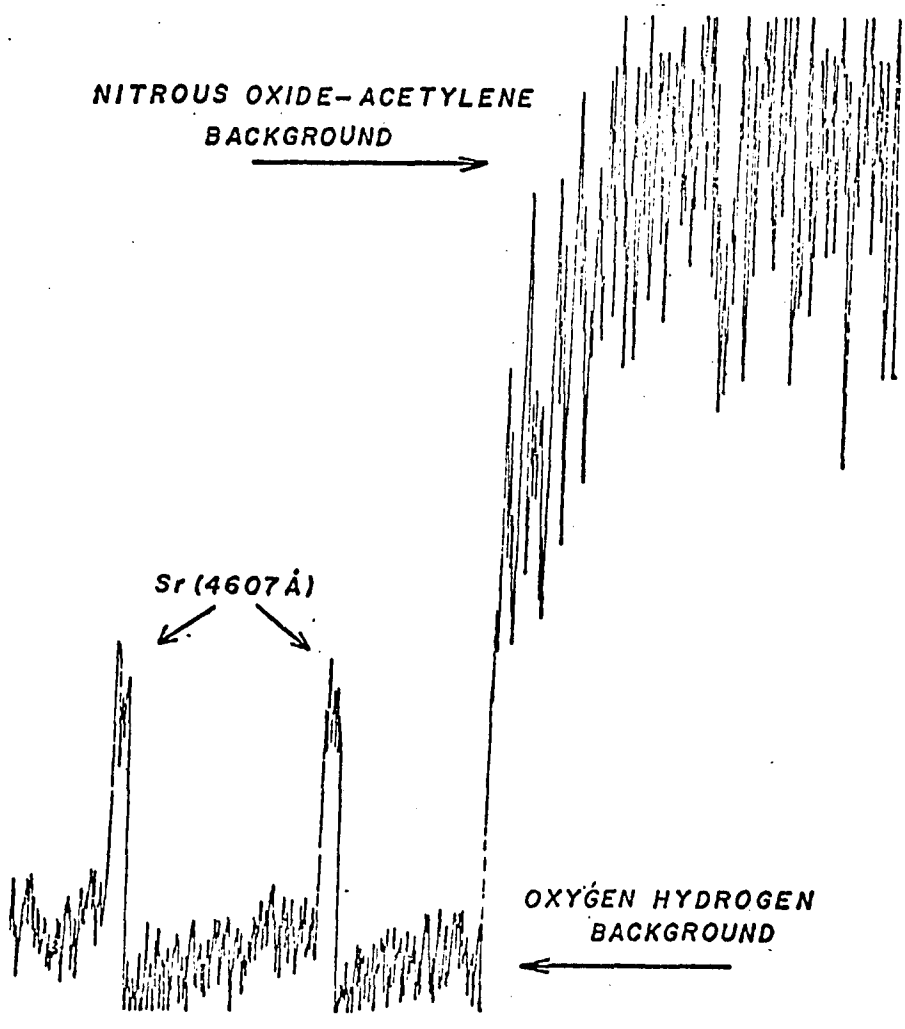

Figure 52. Relative emission backgrounds of premixed oxygen-hydrogen and premixed nitrous oxide-acetylene flames with a 50 μm slit width.

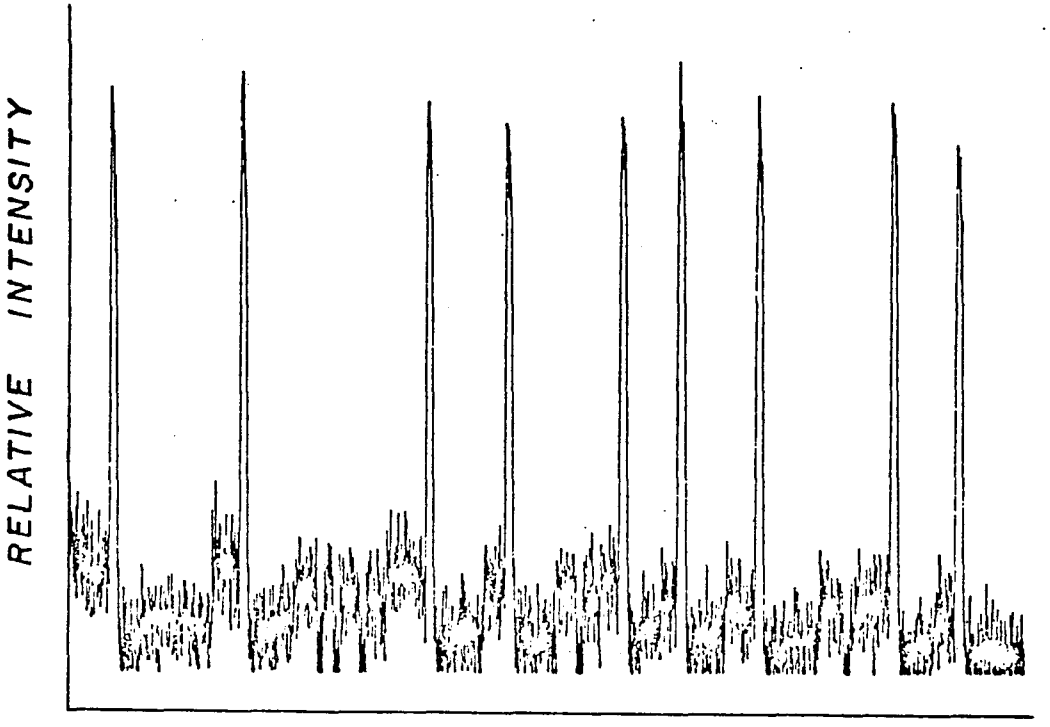

Figure 53. Reproducibility data when using a premixed nitrous oxide-acetylene flame with a slit width of 20 μm and a 200 μl sample of 1.0 μg/ml Ca.

CHAPTER 5

LASER EXCITATION FOR FLUOROMETRIC ANALYSIS

Background

When compared with conventional ultraviolet and visible sources, lasers are far superior with respect to total output power available to excite fluorescence. Table 5 shows the spectral energy distribution for a Xenon arc lamp and a Xenon-Mercury arc lamp (6). Most high wattage lamps presently in use require between 75 and 1500 watts. If the wavelength region from 200 nm to 400 nm is considered for a Xenon-Mercury lamp operating at 1500 watts only 9.5% or 142 watts of radiation is produced in this wavelength region. The nitrogen laser however operating at 337.1 nm has a peak output power of from 100 KW to 1 MW. Thus although the Xenon-Mercury lamp has an electrical input of 1500 watts, due to heat losses and the distribution of this energy over the entire spectrum from ultraviolet to infrared the output power at a given wavelength or wavelength range is much less than that which can be obtained from a laser.

As a result of the increased power available from a laser, it seems that it would be an asset as an excitation source for both atomic and molecular fluorescence. Winefordner et al. (70) have shown that up to a point the fluorescence intensity from atomic species is directly

Table 5. Spectral energy distribution of a Xenon arc lamp in % of electrical input.

Spectral Range nm	%	Xenon-Mercury Arc Lamp	%
200-400	2.5	200-400	9.5
400-700	11.8	400-700	20.5
700-1340	35.5	700-1380	20.0

dependent upon the source intensity. The integrated atomic fluorescence expression for an isolated spectral line is given by (70):

$$I_F = I_A(\varphi/4\pi)$$

where I_F is the fluorescence intensity in watts/cm^2 ster, I_A is the total intensity absorbed by the spectral line(s) which result in excitation, and φ the total power efficiency of the fluorescence transition (watts emitted to watts absorbed).

The intensity absorbed is given (70) in general by

$$I_A = \Omega_a \Sigma I_i^o A_{Ti}$$

where Ω_a is the solid angle over which excitation occurs and is determined by the entrance optics of the monochromator, I_i^o is the incident intensity of the exciting radiation in watts/cm^2 ster/sec, and A_{Ti} is the total absorption factor in sec^{-1}.

These equations indicate that a source to be useful for atomic and molecular fluorescence should be very intense over the absorption line or band. In general narrow line sources are preferred for atomic fluorescence, although the width is not as critical as it is in atomic absorption. Additionally the ideal source should have the provision for wavelength tuning. This allows it to be used for excitation of several different atomic or molecular species. It should also have good long term (no drift) and short term (minimal flicker) stability such that reproducibility is good.

With the power available from a laser it might be expected that most fluorescence systems would be saturated. Piepmeier (56, 57) has shown that to reach a limiting value of the excited atom fraction would require an infinite value of laser energy density. However, it is possible to reach a practical value of saturation with pulsed tuneable dye lasers. The exact power necessary to achieve this depends on the amount of quenching which occurs and the element of interest. In addition when working in a region of high laser energy the fluorescent to scattering ratio decreases. As the laser energy increases the scattering continues to increase while the excited state population begins to level off. This would then be detrimental to detection limits when scattered light is a significant contributor to the noise level.

The first study demonstrating the feasibility of laser excited atomic fluorescence was by Denton and Malmstadt (13). A frequency doubled ruby laser with a Q-switch cell was used to pump a dye laser of 2',7'-dichlorofluorescein. The output from the dye laser was then used to excite atomic fluorescence from a solution of barium which was nebulized into the flame. A detection limit of 1.0 ppm barium was found with this system. Scattered light from aerosol droplets was found to significantly blank the fluorescence signal when conventional nebulizers were employed. Using an ultrasonic nebulizer, which produces very small aerosol droplets, desolvation occurred much quicker with a decrease in the amount of scattered light thus improving the observation of the fluorescence signal.

Fraser and Winefordner (21, 22) used a tuneable dye laser pumped with a nitrogen laser to excite atomic fluorescence in flames. The dye laser had a peak power greater than 10 KW between 360 nm and 650 nm, a spectral half width of 0.1 to 1 nm and a repetition rate of between 1 and 25 Hz. The detection system consisted of a Heath monochromator, a photomultiplier tube and a boxcar integrator with a gate width of 10 n sec and an input resistance of 50 ohms. Analytical curves were reported for Ca, Cr, Fe, Ga, In, Mn, Sr, Al and Ti. Each of these curves was linear over a range of concentrations from three to four orders of magnitude. Detection limits were comparable to or slightly better than those obtained with conventional sources.

Another study (40) has compared detection limits obtained with a flashlamp pumped rhodamine 6G dye laser tuned to the sodium D_2 line, to those detection limits obtained with a hollow cathode or metal discharge lamp. The only special experimental modification was that the laser beam was enlarged by use of a reversed telescope such that the diameter of the beam entering the cell was 18 mm in diameter. In this study a detection limit of 0.003 ng/cm^3 was found for laser excitation which compares very well with the value of 0.5 ng/cm^3 determined for the sodium vapor lamp and 33 ng/cm^3 for the hollow cathode lamp. Thus for this nonflame study of atomic fluorescence the detection limits obtained by laser excitation are significantly better than those determined with more conventional excitation sources.

A c.w. dye laser has been used as an excitation source for the atomic fluorescence analysis of sodium (34). An output power of

approximately 50 mW was obtained when the dye laser was pumped with 1.7 W of 514.0 nm radiation from an argon ion laser. The laser beam was then focused inside the sample cell to give a diameter of 0.5 mm. A detection limit for sodium of 16 fg/cm^3 was determined with this system. A very great advantage to using a c.w. laser is that the read-out electronics necessary to monitor the fluorescence is considerably less complicated and easier to operate. It is noteworthy that the detection limit obtained with the c.w. laser is two orders of magnitude lower than that obtained with the pulse laser.

Another series of experiments (19) used a c.w. laser pumped with 1 W of 514.5 nm radiation from an argon ion laser as the excitation source for sodium vapor. The fluorescence was collected by a lens system and focused onto a photomultiplier tube which was cooled by water or dry ice. In addition, diaphragms were used inside and outside the sample cell to minimize the amount of scattered light reaching the photomultiplier tube. The laser was frequency modulated and a phase sensitive detector, registered only the fluorescence and not the background level. Using this method a working curve covering nine orders of magnitude from 10^2 $atoms/cm^3$ to 10^{11} $atoms/cm^3$ was obtained.

A study (53) has been completed comparing three different light sources: electrodeless discharge lamp, hollow cathode lamp and a frequency doubled dye (rhodamine 6G) laser for the analysis of lead atomized by a carbon rod atomizer. The output power of the laser at 283.3 nm was 400 W with a bandwidth of < 0.002 nm. Detection limits obtained with laser excitation were almost an order of magnitude better than those

obtained with the conventional sources of excitation. When compared with laser excited flame atomic fluorescence, an almost 1000 fold reduction in the detection limit was realized with the nonflame method. This reduction in detection limit using the carbon rod is probably the result, at least in part, of the greater atomic vapor density produced by the carbon rod than can be produced using a flame. In addition to the lower detection limits, the linear range of the working curve was found to be linear over an additional two orders of magnitude versus those curves obtained by the use of conventional sources.

Reports on the use of lasers as excitation sources for molecular fluorescence have also appeared in the literature (29, 63). The ideal source for molecular fluorescence should possess the following characteristics (63): 1) sufficiently intense as to result in saturation or near saturation of the excited electronic state, 2) be of sufficiently narrow tunable spectral output to enable selective excitation of molecules, and 3) safe, economical and easy to maintain and operate.

Conventional sources can be considered to meet requirement 3 and depending on the type of device used for dispersion can meet requirement 2. Although many xenon arcs, tungsten lamps, etc., may have ratings in the hundreds of watts, it must be remembered that all of this power does not go into the excitation of molecular fluorescence and therefore do not result in a condition of near saturation.

In one study (63) three compounds (quinine sulfate, fluorescein and acridine) were investigated as to the detection limit obtainable by use of dye laser excitation and that of a commercial Aminco Bowman

fluorimeter. The detection limit obtained with laser excitation equaled that of the fluorimeter for quinine sulfate, but was worse for the other two molecules. It is worth noting that the wavelengths used to excite fluorescence were not the same for both systems. For quinine sulfate the laser excitation wavelength was 365 nm while the excitation wavelength with the fluorimeter was 325 nm. In the case of acridine, the excitation wavelength was 360 nm with the laser, while it was 300 nm with the fluorimeter. Since the fluorescence intensity is very dependent on the wavelength of excitation this type of study is really not meaningful in comparing the usefulness of the two systems. The reason these authors did not use the dye laser to excite fluorescence at 300 nm for acridine and 325 nm for quinine sulfate is that when pumped with a nitrogen laser (λ = 337.1 nm) the dye laser cannot reach these wavelengths without frequency doubling. These experimental conditions are not a fair comparison when attempting to evaluate the relative merits of laser excitation.

Another paper (29) has been published using a dye laser as an excitation source for molecular fluorescence. Although this paper was principally concerned with obtaining the fluorescence spectra, one detection limit was reported for sodium fluorescein of 0.08 ng/ml. This detection limit is better than that reported by conventional excitation sources (7) of 0.3 ng/ml.

A practical application of laser excited molecular fluorescence has been reported (4), that being the analysis of aflatoxins separated on a thin layer chromatographic plate. In this application the TLC plate

was scanned with the output from a nitrogen laser. The resulting fluorescence was monitored by a photomultiplier tube with the data output being displayed on a boxcar integrator. This method shows promise as an analytical technique in that one portion of a chromatographic spot can be easily and selectively analyzed by this method. Unfortunately the linear range of the working curve was not reported.

Because of the incomplete nature of the data obtained in earlier work, studies have been undertaken to further evaluate the merits of laser excited fluorescence. Initially these studies were to be done with laser excited flame atomic fluorescence. However, because some of the studies involved changing the way in which the sample cell is illuminated which meant changing the sample cell position such that it was rotated 90^{o} and since flames do not burn well in an inverted or horizontal position the use of molecular fluorescence seemed more applicable to this study. This study also included the development and evaluation of new amplifiers for the readout stage. The testing of this equipment was made easier by the less complicated arrangement necessary for molecular fluorescence.

Molecules to be studied have their excitation maximum at 337.1 nm. For comparison studies an Aminco Bowman fluorimeter was used with the same excitation wavelength as that of the nitrogen laser. A practical problem occurs in using the nitrogen laser in that it is not tunable. However, since there are many molecules that have their excitation maximum at or near 337.1 nm and since the purpose of this study is to evaluate the merits of laser excitation in terms of sensitivity this is not a serious problem.

Nitrogen Laser

Two different experimental configurations are used for these studies. The first, shown in Figure 54, is designed to monitor the total fluorescence emission coming from the cuvette. The second system, shown in Figure 55, was constructed to allow the passage of only certain wavelengths from the cuvette to the photomultiplier tube. The results obtained with these systems will be discussed later in more detail.

The laser employed is an Avco Everett C-950 (2385 Revere Beach Parkway, Everett, Mass. 02149) pulsed nitrogen or neon gas excited laser that produces a super radiant output beam. Using operating voltages up to 18 KV the laser can generate a peak output power of 100 KW with a pulse width of approximately 10 n sec.

The laser system consists of two main sections: the laser section and the control section. The laser section contains a crossed-field channel with a stabilized electrode, and a high voltage pulser consisting of a high current hydrogen thyration and a special low inductance energy storage capacitor. Also included in this section is a capacitor charging system, thyration heater power supplies, gas and coolant pressure sensors, a channel gas pressure monitor, and gas control valves.

The control section contains AC control circuits, a high voltage power supply to supply current to the storage capacitor in the laser section, and a solid state trigger generator. The generator provides low-impedance driving pulses to the grid of the hydrogen thyratron in

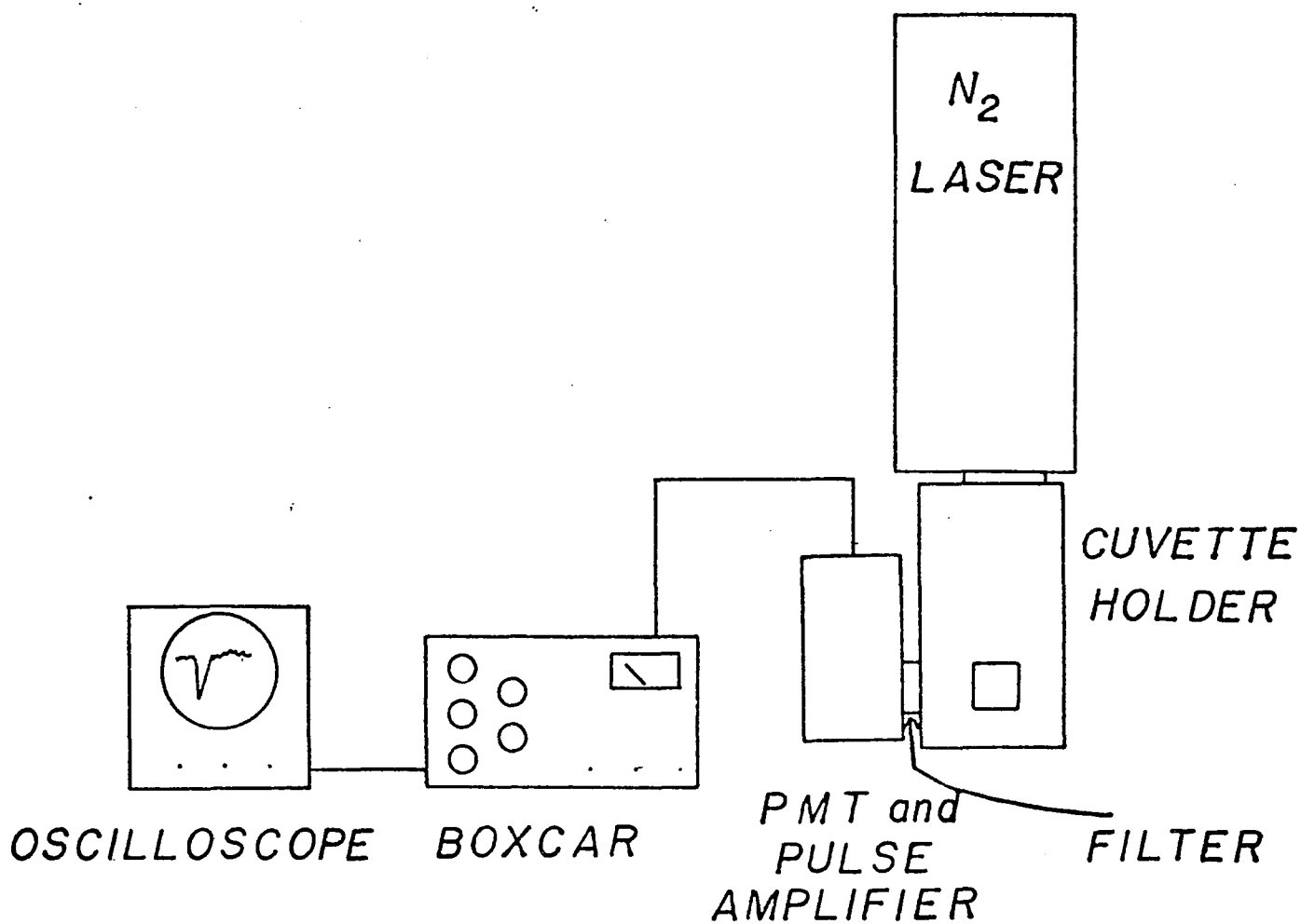

Figure 54. Experimental arrangement for analysis of total fluorescence.

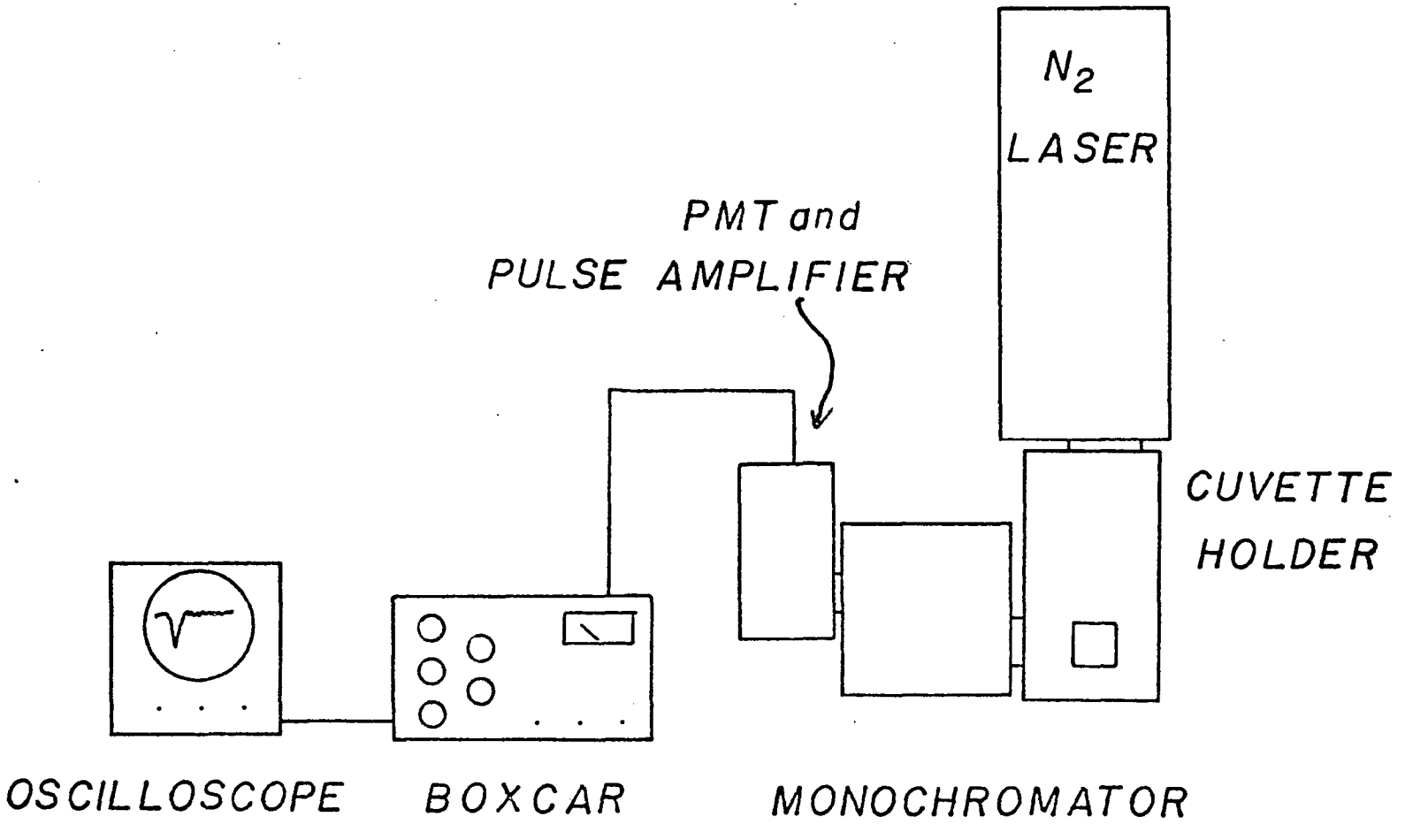

Figure 55. Experimental arrangement for fluorescence analysis using a monochromator as a dispersing device.

the laser section; the rate of these pulses may be derived from an external source or from an internal timing circuit.

Many applications require the triggering of auxiliary equipment either in sequence with or before the laser fires. Synchronization pulses are provided at the trigger generator front panel (POS. and NEG. SYNC. OUT). Characteristics of these pulses are listed in Table 6. The synchronization pulses occur one-half microsecond in advance of each laser pulse. The use of this synchronization pulse with respect to auxiliary equipment is discussed in the section on the boxcar integrator.

Upon the application of a high voltage, high current pulse to the gas within the channel, a transient population inversion is created by electron impact. When excited in this way, the laser transition has sufficient gain to produce a super-radiant output beam. Maximum output power is obtained with a single plane mirror located at one end of the laser channel, and the opposite end left open. The laser then produces an output power at the open end equal to twice the original value. Operating characteristics of the C-950 laser are given in Table 7.

The turn on procedure for the laser from a completely shutdown condition is as follows:

1. Ensure that the high voltage power supply is set for POSITIVE output voltage and that the variac is set for zero output voltage.
2. Apply line voltage to all components.
3. Turn on cooling water.

Table 6. Characteristics of synchronization pulse.

Amplitude	$\pm$ 12 volts
Impedance Level	< 50 ohms
Rise Time	50 Nanoseconds
Pulse Width	6 Microseconds

Table 7. Model C 950 pulsed gas laser specifications.

	Ultraviolet	Green
Output Wavelength	3371 Å	5401 Å
Output Bandwidth	< 1 Å	< 0.1 Å
Peak Output Power	100 KW	10 KW
Effective Pulse Width	10 n sec	3 n sec
Average Power	100 mW	3 mW
Output Beam Dimensions	0.32 cm x 5.1 cm	
Operating Gas Pressure	15-25 torr	
Maximum Supply Voltage	18 KV	
Maximum Gas Pressure	17 torr	

4. Open the cylinder main valve; set the regulator for about 3 psig.
5. Close the VENT valve.
6. Slowly open the vacuum valve to the full open position. Allow the CHANNEL PRESSURE to drop to 0 mm Hg.
7. Slowly open the input valve and admit gas to the required CHANNEL PRESSURE (generally 16 torr) not to exceed 17 torr.
8. Set the MODE selector to the TRIGGER OFF position. Before proceeding beyond step 8 approximately six minutes must be allowed for the heaters to reach operating temperature. The HEATERS READY lamp should be illuminated and all interlock lamps should be extinguished.
9. Simultaneously depress the START and HIGH VOLTAGE ON controls.
10. Adjust the power supply voltage to the desired operating level. Not to exceed 18 KV. The laser generally operates weakly at 9 KV and reaches a maximum intensity at 16 KV.
11. Set the MODE selector to the desired position.

The following is the correct shutdown procedure for the laser.

1. Reduce the main HIGH VOLTAGE control to zero.
2. Depress the MASTER STOP control.
3. Set the MODE selector to TRIGGER OFF.
4. Close the cylinder main valve and set the regulator for zero output.
5. Close the input valve.
6. Allow the channel pressure to drop to 0 mm Hg.

7. Close the VACUUM valve.
8. Remove line voltage from all components including the vacuum pump.
9. Slowly open the VENT valve to release the channel to atmosphere.
10. Turn off the cooling water.

Amplifiers

One problem associated with the use of a pulse laser system which does not occur when using a continuous source is that of amplification. An amplifier to be employed with a pulse system must have both a suitable gain and also be fast enough to respond in a linear fashion to the pulses of current coming from a photomultiplier tube. Designing and building such an amplifier is not a trivial task. As the frequency of the signal becomes greater and the current levels lower it becomes difficult to maintain an amplifier that will respond to these signals.

Two different amplifier systems were tested in this study. The first was a commercial unit from Pacific Photometric Instruments (5745 Peladeau Street, Emeryville, Ca. 94608) model 2A32. The anode of the photomultiplier tube is connected directly to the 50 ohm input resistor of the amplifier which has a gain of ten. Output current from the amplifier is carried over 50 ohm cable (RG 58/U) to the boxcar integrator. The outside shield of this cable is grounded to eliminate outside interferences. The photomultiplier tube is energized using negative high voltage of 800 volts supplied by a Power Designs Inc. (Westbury, N. Y.) model 1570 power supply.

One modification was made to this system. A string of capacitors was placed across the dynode chain to ground as shown in Figure 56. This eliminates a sudden decrease in voltage at the dynodes caused by a high current transient avalanch and has the effect of extending the upper dynamic range of linear response.

The second amplifier system was constructed from model 9816 operational amplifiers (Optical Electronics Inc., P. O. Box 11140, Tucson, Az. 85706). The operational amplifiers employed possessed a slewing rate of $\pm$ 1000 volts/μ sec, a minimum unity gain frequency of 1000 MHz and a minimum open loop gain of 60 dB.

To ensure that these amplifiers are stable at the frequencies employed, numerous precautions must be taken. First, the power supplies must be carefully bypassed at the amplifier. This prevents transient signals from the power supply, or the environment, from causing the amplifier to deviate from its normal operating characteristics. Second, wiring must be as short as possible to avoid the effects of stray inductance and capacitance. Stray inductance and capacitance can both reduce the response time of the amplifier and also cause it to go into oscillation. The third precaution to be taken is that a common ground point must be used.

Using the guidelines outlined above the amplifier shown in Figure 57 was constructed. An evaluation of this amplifier will be discussed later.

The photomultiplier tube used throughout this study was a Hamamatsu R212UH tube (Middlesex, N.J. 08846). The spectral response of

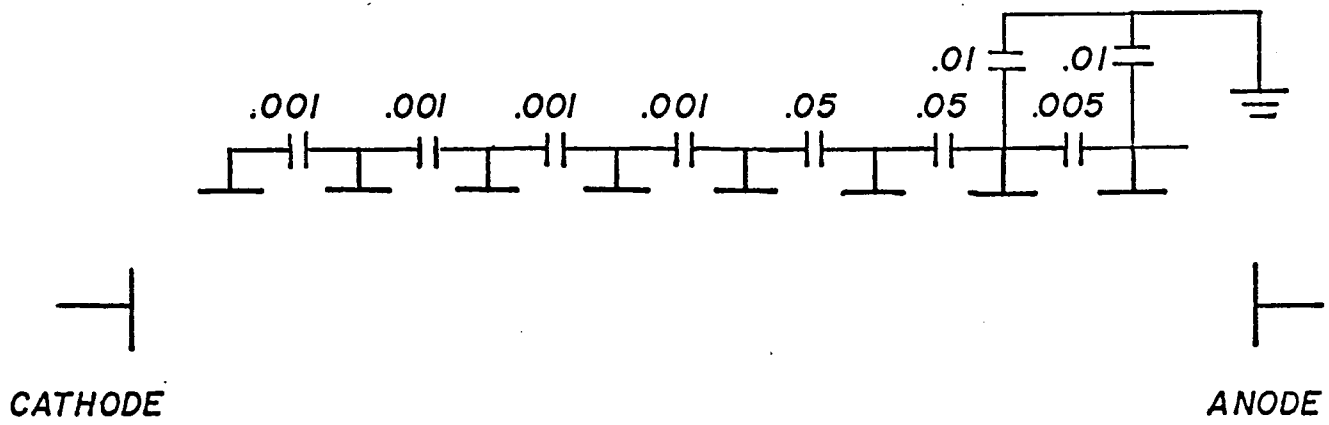

Figure 56. Capacitor string to prevent any transient signals from affecting output current of photomultiplier tube.

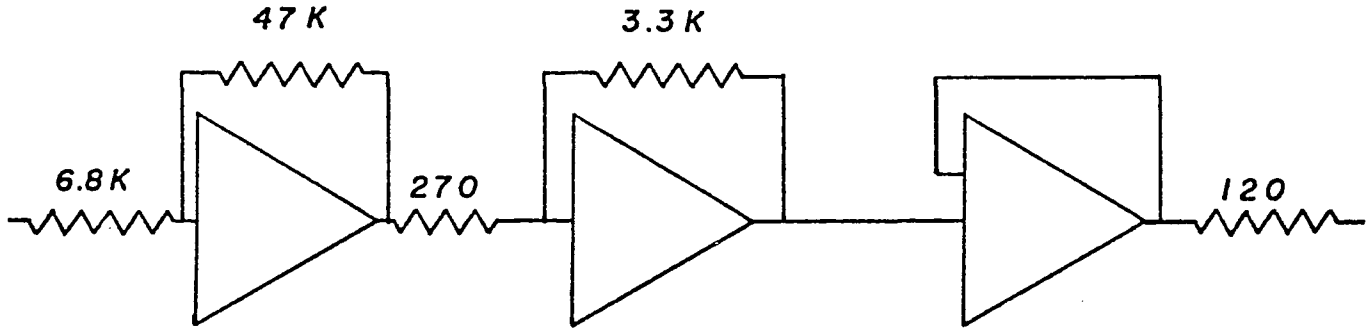

Figure 57. Schematic diagram of pulse amplifier constructed for OEI 9816 operational amplifiers.

this tube ranges from 200 nm to 700 nm with the maximum sensitivity at 340 nm.

Boxcar Integrator

The boxcar used was a PAR model 160 (Princeton Applied Research, Box 2565, Princeton, N. J. 08540). A boxcar integrator is somewhat similar to both a lockin amplifier and a signal averager. The instrument is really a single channel signal averager with a sampling gate that can be opened to measure a signal and then closed. This sampling gate can be opened in one of two ways; either recurrent or through the use of an external trigger.

Triggering

Each time the boxcar is triggered a time base ramp is generated, however the time delay between the trigger and the start of the ramp is 150 n sec. At some time after the beginning of the time base ramp the sample gate is opened for a preselected period of time, known as the aperture time. If the Delay Mode switch is set to Delay, then the delay between the start of the time base ramp and the opening of the sampling gate is determined by the setting of the Initial Delay dial. Figure 58 shows the relationship between the Trigger pulse, the time base ramp and the opening of the sampling gate.

One potential triggering problem exists with a fluorescence analysis which is excited by a pulse laser. If the boxcar is triggered at the same time as the laser is pulsed, the entire fluorescence signal will have passed by before the time base ramp is ever triggered due to

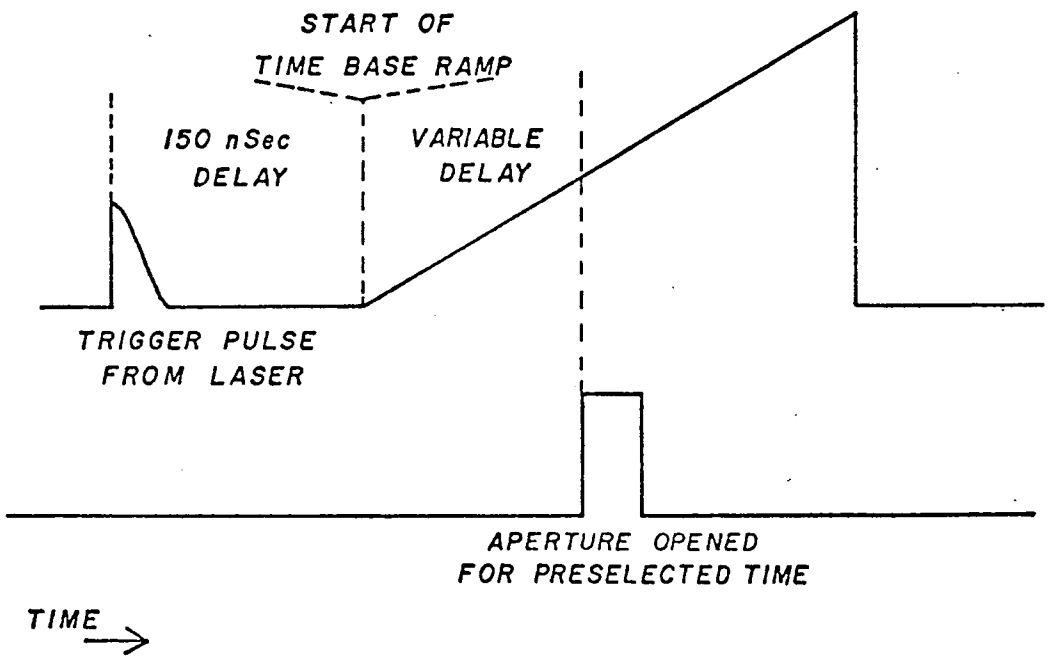

Figure 58. Triggering of PAR model 160 boxcar integrator.

the 150 n sec delay between the trigger pulse and activation of the time base ramp.

There are two methods to solve this problem. The first is to trigger the boxcar and then have a delayed pulse from the boxcar fire the laser. The other solution is to have the synchronization pulse from the laser, which will trigger the boxcar, arrive before the laser fires.

The Avco laser is designed to allow the synchronization pulse to occur approximately one-half microsecond before the laser fires. Thus the sync pulse can arrive at the boxcar, the delay can take place and the time base ramp can be initiated, all before the laser fires. In this way any problems associated with the short delay before the time base ramp is initiated are avoided.

The only important characteristic of the delay time between the sync pulse and the firing of the laser is that it be at least 150 n sec. This then allows the time base ramp to start before the laser actually fires. Once the time base ramp has started the gate can be centered over the fluorescence maximum by use of the initial delay dial. For work reported here a time base ramp of 2 μ sec was used with a delay of 23%.

If the Delay Mode switch is set to Scan, the delay between the start of the time base and the opening of the sample gate is gradually increased with the start of each new time base ramp. The rate of increase depends on the selected scan rate. The sampling gate is scanned over an interval defined by the setting of the Initial Delay and Final Delay dials. The settings are in percent delay of the total time base ramp. If the Repeat/Single switch is in the Single position, the scan will

occur only once. If it is in the repeat position the scan will be repeated.

The duration of a time base ramp is important when an entire waveform is to be recovered. If the time base ramp is too short then part of the waveform will never be seen as the sampling gate must be opened on the ramp. If one feature of a waveform is to be monitored then all that is required is that the time base ramp be of long enough duration to cover the event in question.

Aperture Time

The aperture time has a significant effect on both the shape of the waveform and the height of the recovered waveform. Figure 59 shows the waveform that is obtained with different aperture times. If a squarewave of time duration ΔT and height A is used as the input function, the identical waveform will be obtained by the boxcar when the aperture time is much less than the duration of the input function. If the aperture time is made equal to the duration of the input function a significant distortion of the waveform is seen to occur although the height of the output waveform does still reach that of the input function. Increasing the aperture time still further to a point where it is equal to twice the input function duration results in both distortion of the waveform and a reduction in the height of the output waveform. Thus if one is interested in both retaining the form of the input function and also in retaining the correct height of that function an aperture time of much shorter duration than the time scale of the input function should be employed. If however one is interested only in the height of

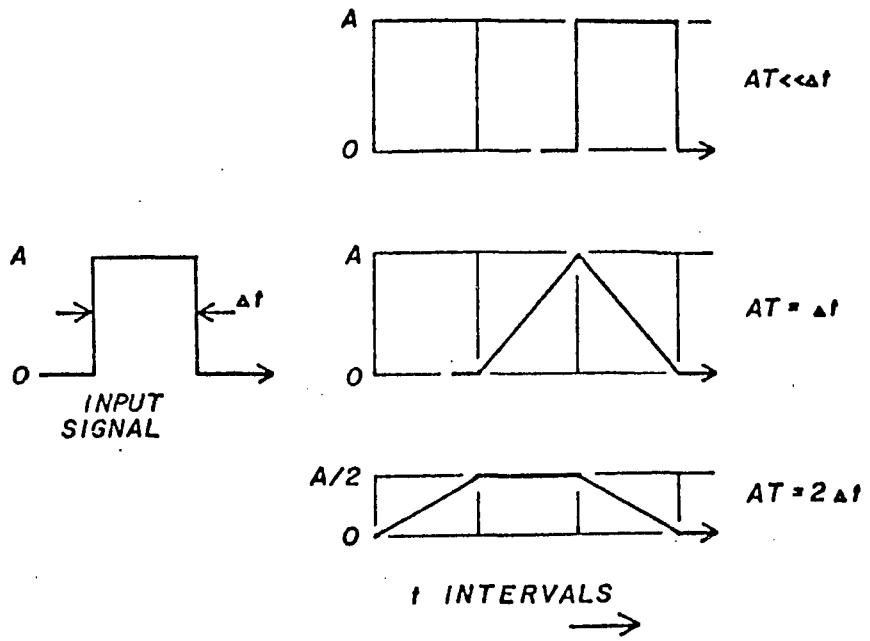

Figure 59. Effect of aperture time on recovered waveform from boxcar integrator.

the input function then any time equal to or less than the input function can be used to retain the correct height. In this work an aperture time of 10 n sec was used which is the smallest aperture time possible with this instrument. A list of all settings used with the boxcar can be seen in Table 8.

Monochromator

The monochromator is a Heath model EU-700 (Benton Harbor, Mi. 49002). It is constructed as a single pass Czerny-Turner mount with an aperture ratio of f/6.8 at 200 nm. The grating is composed of 1180 lines/mm, blazed at 250 nm. The reciprocal linear dispersion is 20Å/mm. The slits are 12 mm high and continuously variable from 5 to 200 microns.

Sample Cell Positioning

Sample cuvettes were analyzed in two different positions. A device that was constructed to hold the cuvette in a vertical position is shown in Figure 60. It consists of two sets of light baffles inside of which the cuvette is placed. The baffles help to prevent stray light from reaching the entrance slits of the monochromator. The entire assembly mounts directly to the front of the laser.

Evaluation of Laser Excitation

When using the laser as an excitation source for molecular fluorescence one would like to obtain the greatest output power so as to gain the most intense fluorescence signal. There are two easily adjusted parameters on the nitrogen laser which affect the output intensity.

Table 8. Operating condition of boxcar integrator.

Function	Setting
Trigger Mode	External
Time Base	2 μ sec
Scan/Delay Initial	23%
Scan/Delay Final	100%
Time Constant (blue)	3 n sec
Prefilter	.015

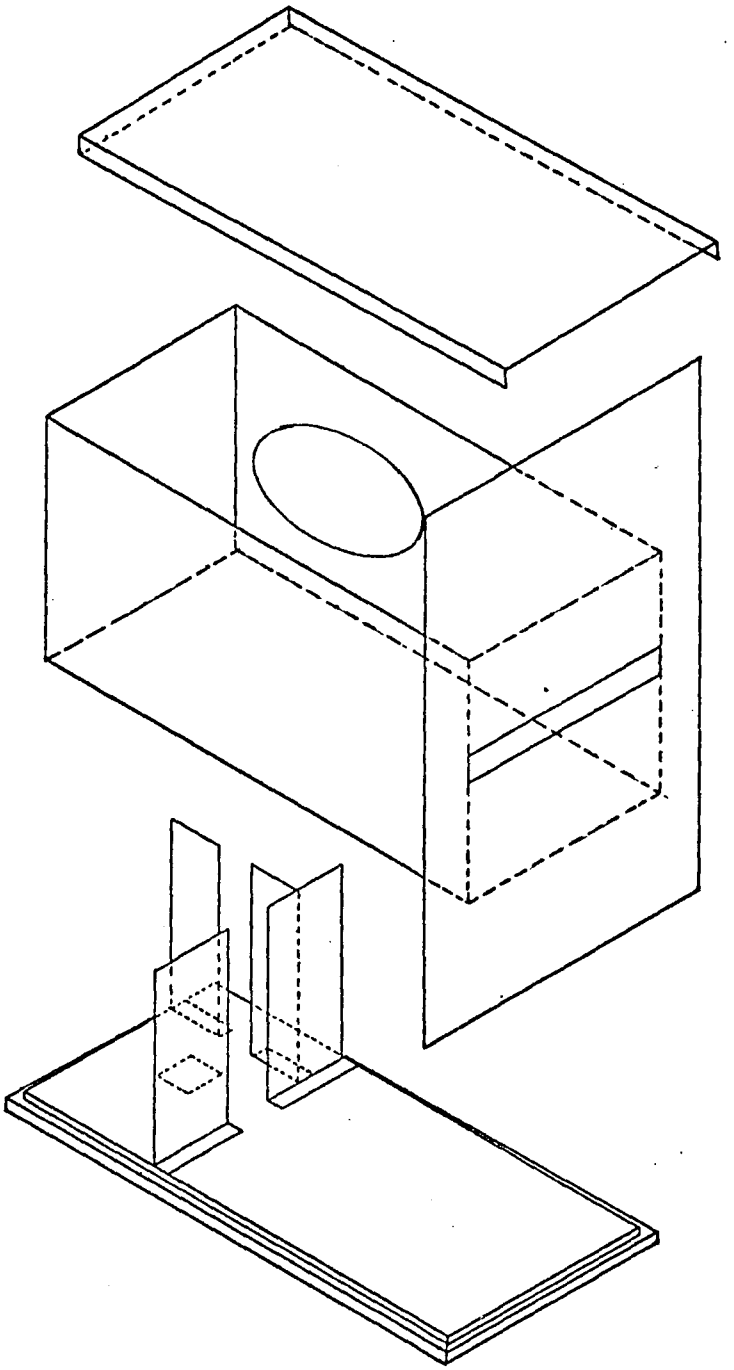

Figure 60. Diagram of cuvette housing assembly.

One of these is the voltage applied across the channel and the other is the channel pressure itself.

Applied Voltage versus Relative Output Intensity of the Nitrogen Laser

Figure 61 shows the relative output intensity as a function of voltage across the channel. This figure was obtained by placing a photodiode in front of the laser beam and monitoring the current with the boxcar integrator. To avoid saturating the photodiode a darkened piece of photographic film is placed between the laser and the photodiode. This procedure although reducing the amount of radiation falling on the diode still allows the relative output intensity to be monitored as a function of voltage. A wire mesh might be used in place of the photographic film, however the possibility of saturating the photodiode is still present as some parts of the tube will be exposed to an unattenuated portion of the beam. Therefore it is better to employ the darkened photographic film method. It was found that the laser intensity increased very rapidly from 9 KV to about 12 KV. Beyond this point the output intensity continues to increase, but at a much slower rate. At about 16 KV the intensity begins to level off. Thus to obtain the maximum laser output intensity a discharge voltage of 16 KV should be employed.

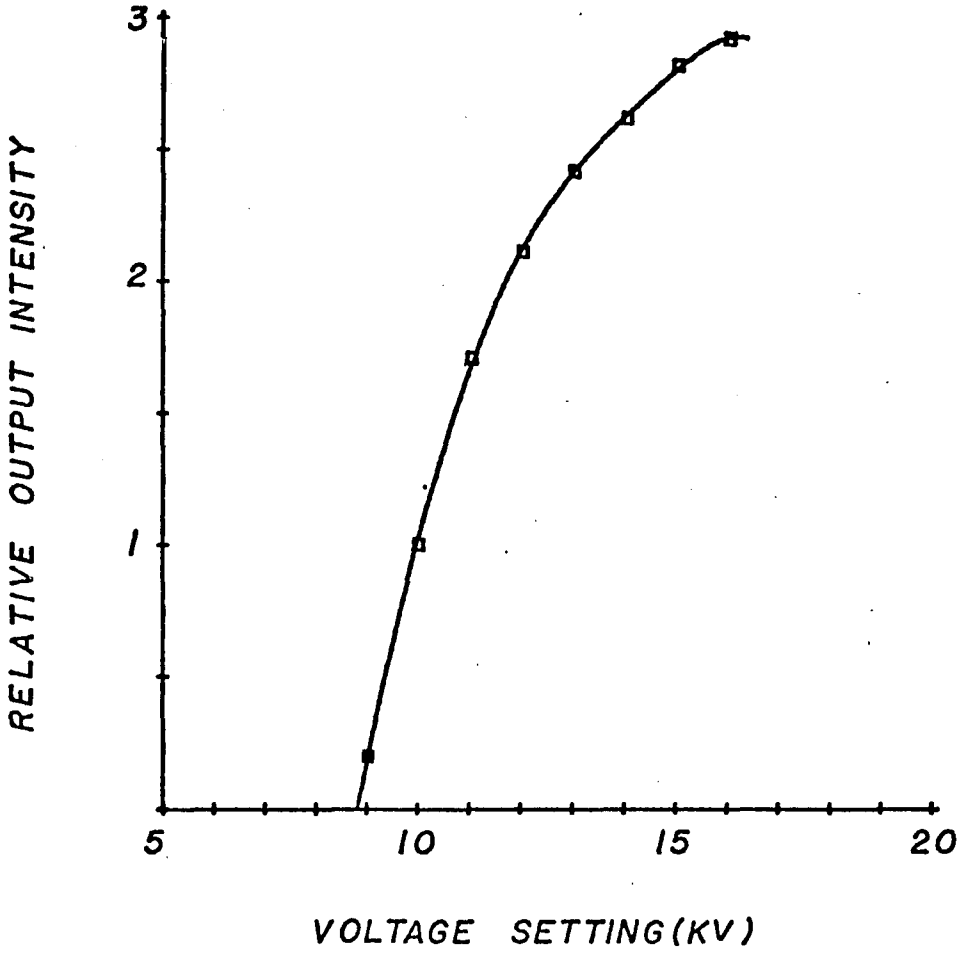

Figure 61. Variation of laser output intensity with voltage setting.

Channel Pressure versus Relative Output Intensity of the Nitrogen Laser

In addition to the voltage across the channel, the channel pressure might also affect the output intensity. Figure 62 diagrams the output intensity as the channel pressure is varied with 16 KV applied across the channel. As the pressure is changed from 11.5 mm to 17 mm no change in the output intensity occurs. Therefore when the output intensity of the laser is a critical parameter only the voltage applied across the channel has any affect on the output intensity.

Variation of Fluorescence and Background Level with Excitation Intensity

The variation of fluorescence intensity with laser intensity for a 4×10^{-6} M ethidium bromide solution is shown in Figure 63. Three curves are presented in this figure representing the background which is present partly as a result of scattered light, the monitored signal which is composed of both fluorescence and scattered light and the net fluorescence signal. By comparing the laser output intensity with the net fluorescence signal it can be seen that the fluorescence intensity is directly proportional to the laser output intensity from 9 KV to 13 KV. Beyond a channel voltage of 13 KV the fluorescence intensity begins to level off even though the laser output intensity is still increasing. At this point the photomultiplier tube has become saturated and no further increase in fluorescence intensity is observed.

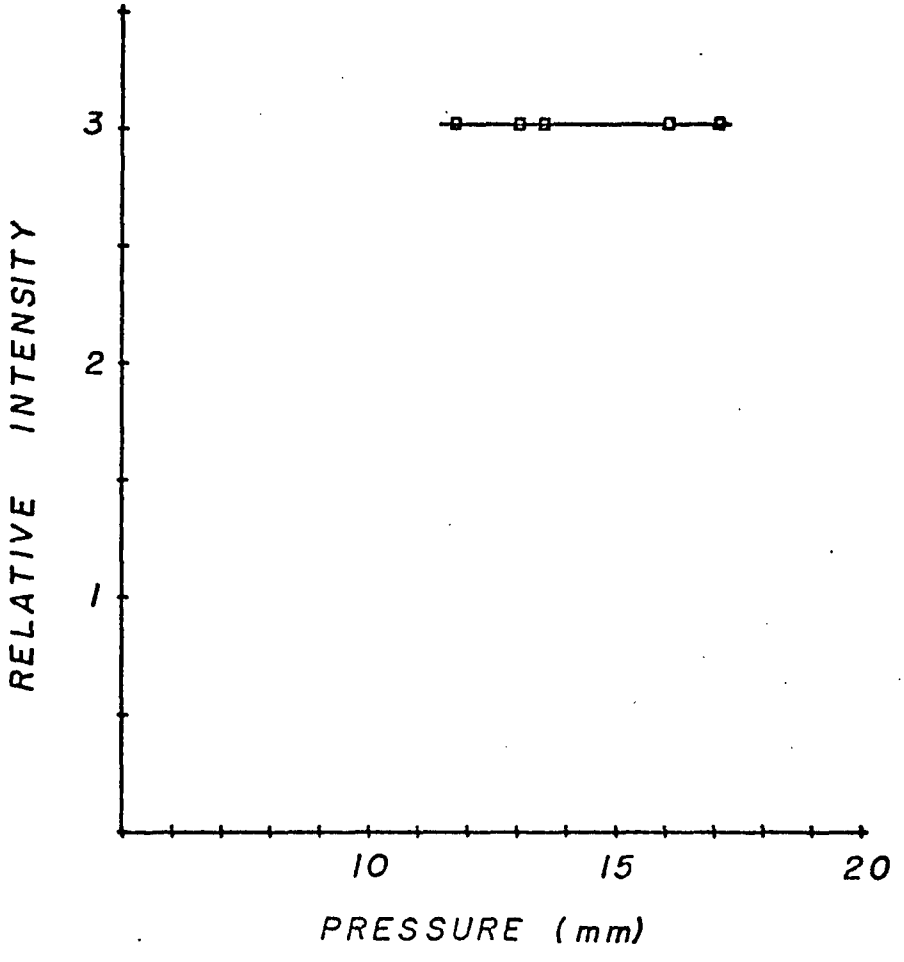

Figure 62. Variation of laser output intensity with channel pressure.

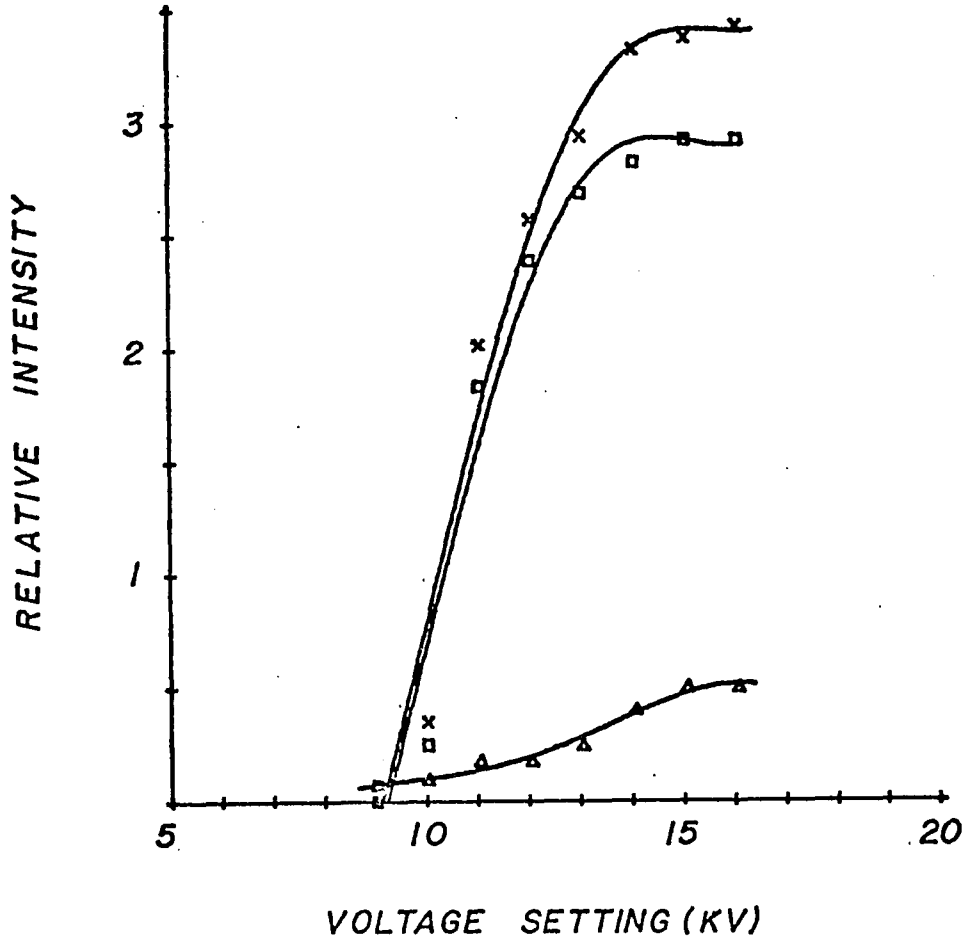

Figure 63. Variation of fluorescence, background, and total signal with laser intensity. -- X = total signal; □ = fluorescence intensity (Ethidium Bromide conc = 4×10^{-6} M); △ = background intensity.

From the above study the best laser operating conditions for fluorescence analysis are a channel pressure of 17 mm and a voltage of 16 KV.

Characteristics of Ethidium Bromide

The model compound used for this part of the study is ethidium bromide (2,7,Diamino-10-ethyl-9-phenylphenanthridinium Bromide) which is a molecule of molecular weight 394.3 the structure of which is shown below.

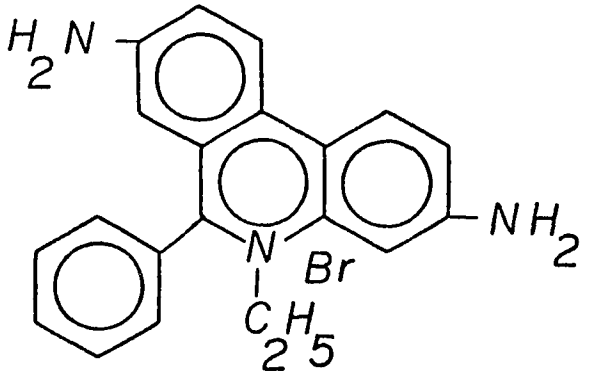

This molecule, when dissolved in water, possesses an excitation maximum at 325 nm and one at 510 nm with the fluorescence maximum occurring at 600 nm (42, 66).

Ethidium bromide has been used with great success in elucidating both the physical and chemical characteristics of nucleic acids (8, 42). Such studies generally have included the binding of ethidium bromide to the nucleic acid and observing the change in fluorescence intensity as the nucleic acid is forced to unwind or coil about itself. Information from such studies has increased what is known about interactions between bases within a given nucleic acid.

Detection Limit and Dynamic Range of Fluorescence Analysis with a Conventional System

Using an Aminco Bowman fluorimeter a detection limit of 5×10^{-7}M was found for ethidium bromide. The linear range of this working curve is slightly over two orders of magnitude long. The working curve itself is shown in Figure 64 the last point on the curve is the detection limit. A photomultiplier tube voltage of 700 V and a slit width of 2000 μm was used in obtaining this curve the excitation wavelength was 337.1 nm and the emission was monitored at 600 nm.

Total Fluorescence Analysis using Laser Excitation

If a photomultiplier tube is mounted at right angles to the excitation beam such that the fluorescence coming from the cuvette is monitored then a tremendous reduction in the detection limit for an analysis should be possible. This reduction in detection limit should result from the fact that the entire fluorescence emission band will be observed whereas in conventional fluorometry only a narrow range of selected wavelengths of fluorescence, as determined by the monochromator, are observed. Because of the possibility of scattered light a cut off filter was employed between the photomultiplier tube and the cuvette. This filter which cut off all wavelengths below 400 nm was a Kodak 2B wratten gelatin filter. The actual experimental arrangement has already been described and is shown in Figure 54.

In determining the background level with only water in the cuvette it was observed that a very intense signal was being monitored.

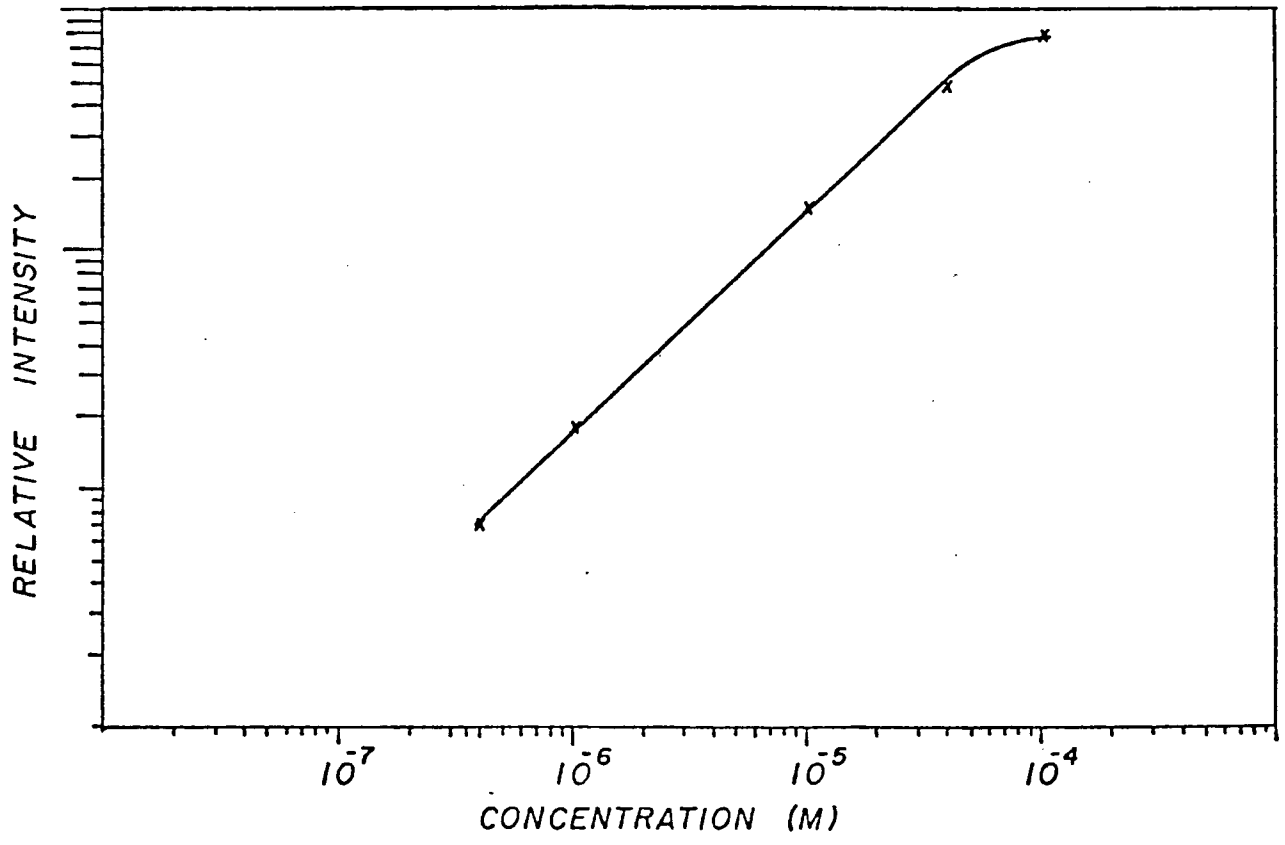

Figure 64. Ethidium bromide working curve obtained with Aminco Bowman fluorometer.

Since scattering has been a traditional problem with laser excitation at least part of the signal could be the result of scattered light. A second source of the signal could be a result of scattered light from the laser causing the filter to fluoresce. When this filter is placed directly in front of the laser beam a very bright white emission is observed. This fluorescence of the filter is obviously the cause of the large background signal being monitored.

The output current from the photomultiplier tube can be adjusted by changing the voltage applied to the photomultiplier tube. This obviously does not change the fluorescence intensity of the filter, but only the gain of the dynode chain and thus the output current. The effect of photomultiplier tube voltage on the observed fluorescence intensity from the filter is shown in Figure 65. As the photomultiplier voltage is increased a point is reached (at 200 volts) where the gain of the dynode chain is enough to result in a measurable signal. Increasing the voltage of the photomultiplier tube continues to increase the gain of the dynaode chain and the current coming from the photomultiplier tube. Using this configuration, detection limits and working curves were run at three different voltages (200, 300 and 400 volts) to determine the effect of the observed background. The results are shown in Figure 66. At a photomultiplier voltage of 200 volts a linear working curve is found from 10^{-6} M to 3×10^{-5} M. At 300 volts the detection limit and working range are both reduced, in this case the linear working curve extends from the detection limit of 5×10^{-6} M to 10^{-5} M.

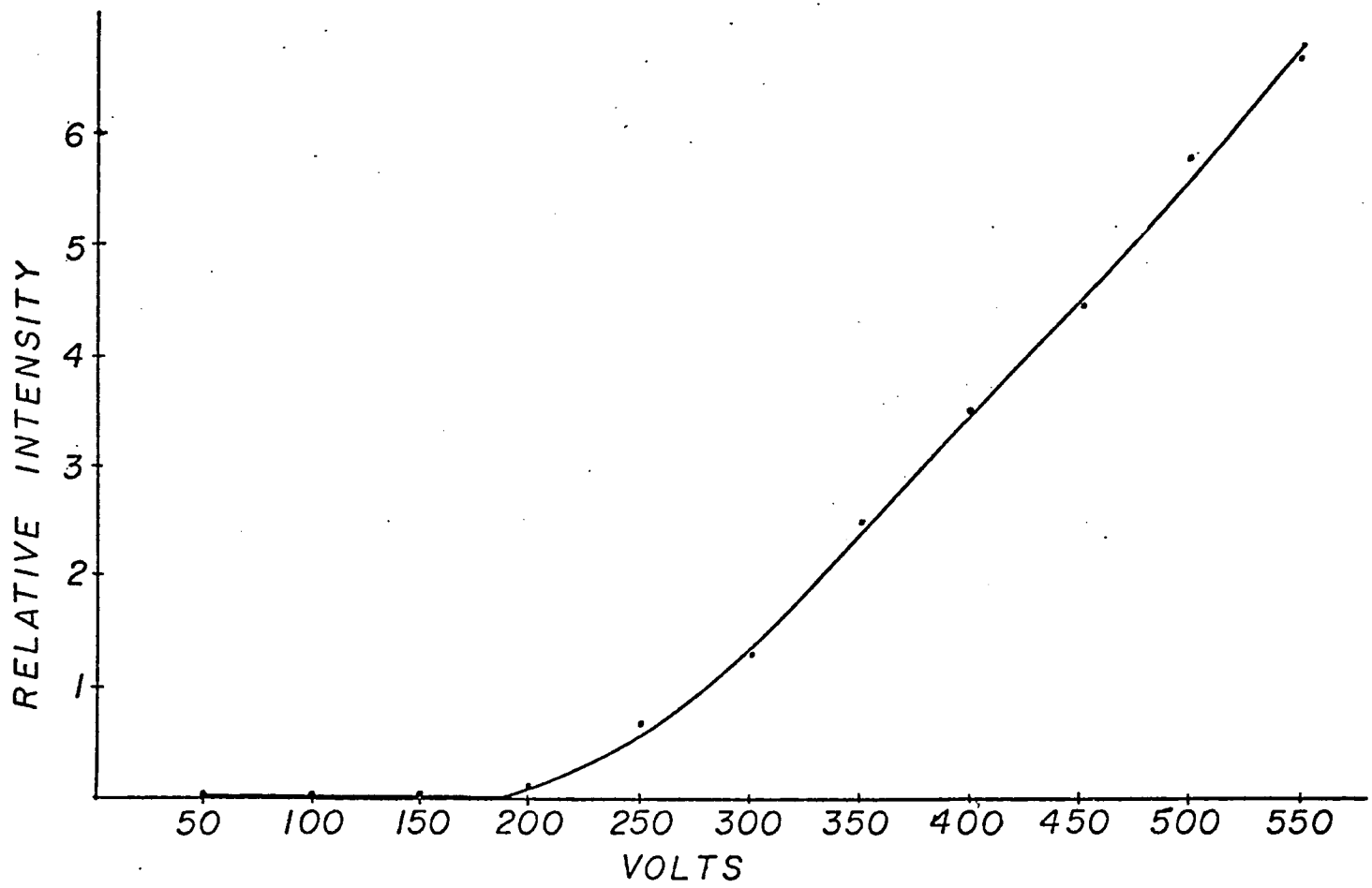

Figure 65. Variation of background intensity with photomultiplier tube voltage.

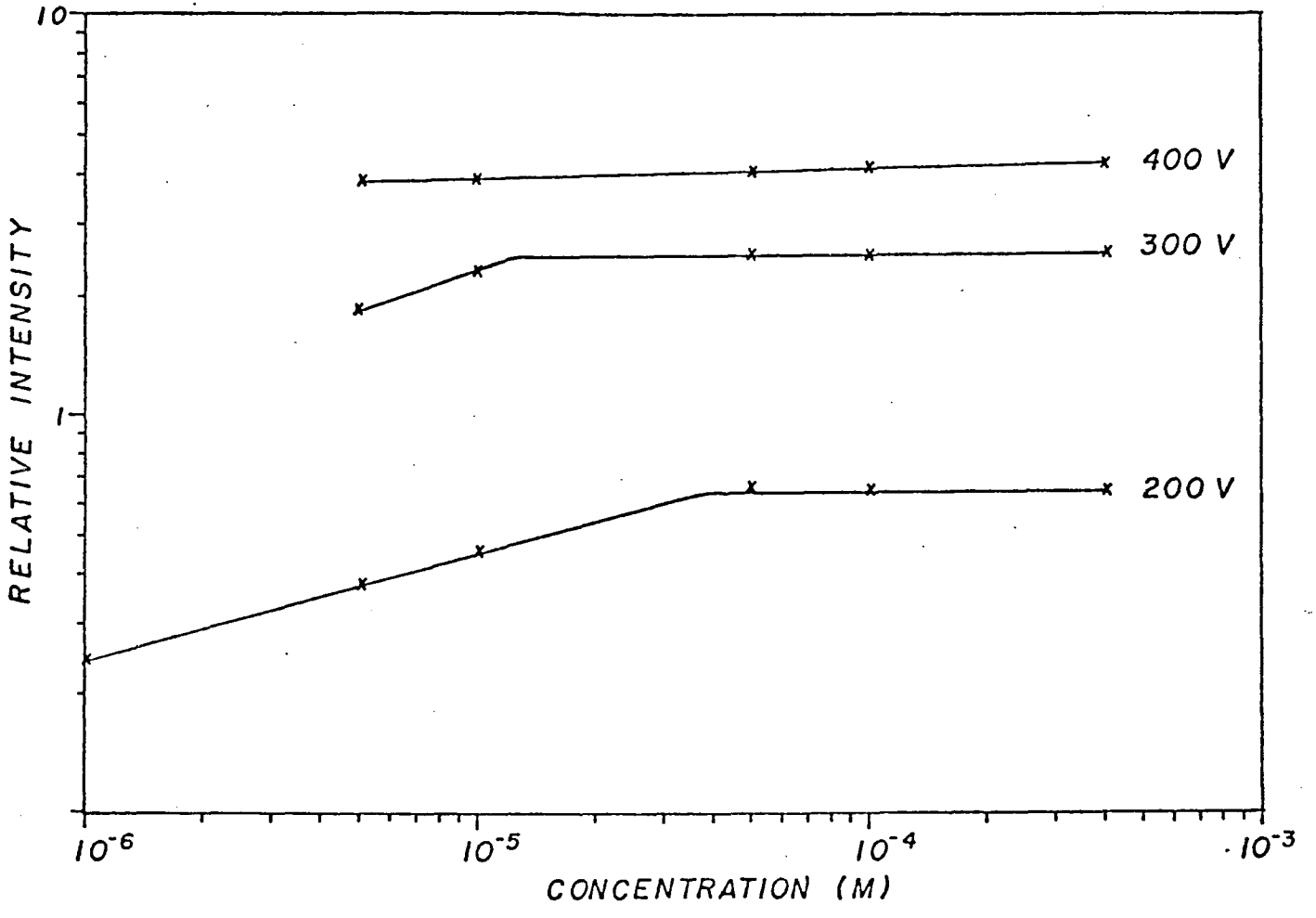

Figure 66. Ethidium bromide working curves obtained at different photomultiplier tube voltages in total fluorescence configuration.

When a voltage of 400 volts is applied to the photomultiplier tube, no analytically useful working curve is found.

From this data it is apparent that the background intensity plays a very important role in both the observed detection limit and also the useful analytical range of the working curve. Because the optimum detection limit (10^{-6} M) and the working range are both poor and since all available filters showed some level of fluorescence, no further work was attempted with this configuration.

Because the background intensity is a limiting factor in the total fluorescence method of analysis a monochromator was used in an effort to eliminate some of the scattered light from the laser. The components for this experimental arrangement were previously described and shown in Figure 55.

Scattered Light when Using a Monochromator as a Dispersing Device

The scattering signal obtained as a function of wavelength with a Heath monochromator is shown in Figure 67. A substantial scattering signal occurs from 300 nm to 480 nm with the maximum occurring at 337.1 nm. As longer wavelengths are approached the monochromator does a more effective job in eliminating the scattered light. The scattered light intensity reaches a minimum between 510 nm and 670 nm. At 674.2 nm, the second-order for 337.1 nm, the scattered intensity again rises as a spike. It is important to note that this scattered light is the result of viewing a cuvette filled with water at right angles to the laser beam,

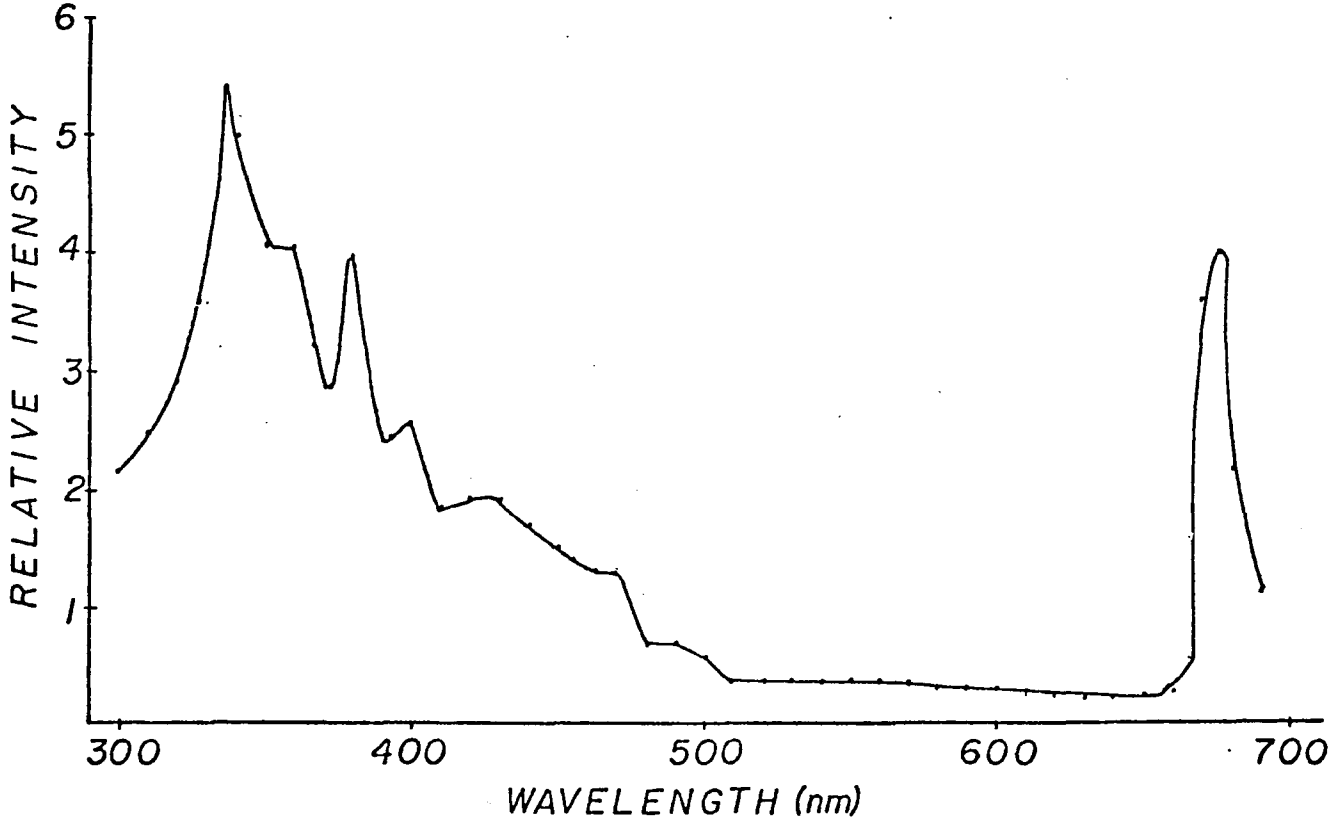

Figure 67. Intensity of scattered light versus wavelength using a Heath monochromator.

and that this background intensity will be included in any fluorescent measurement.

The possibility of using a Jarrel Ash monochromator in place of the Heath monochromator was also investigated. The Jarrel Ash, model 82/400, possesses several characteristics which make it attractive for this application. It provides a choice of two different gratings, one blazed for 300 nm and the other blazed for 600 nm. Thus if an analysis is being carried out in the red for example, a grating blazed for that part of the spectrum can be used, the same is true for the blue or ultraviolet regions. The Heath monochromator employed provides only one grating which is blazed at 250 nm. Thus with the Jarrel Ash it is possible to use the grating which will give the maximum light throughput for the region of interest. Another possible advantage of the Jarrel Ash monochromator is that the aperture ratio is smaller than that of the Heath monochromator. The Jarrel Ash being f/3.6 whereas the Heath is f/6.8. This again allows for a greater throughput of light with the Jarrel Ash system and one would expect better sensitivity.

Figure 68 shows the scattered background intensity with the Jarrel Ash monochromator. The principle area of scattering occurs between 300 nm and 380 nm and the second order at 674.2 nm. However, the background intensity is much greater at the longer wavelengths especially between 510 nm and 670 nm. Thus although a greater throughput of light is possible with this monochromator the background intensity is also much larger and because of this the Heath monochromator was used in all of the following studies.

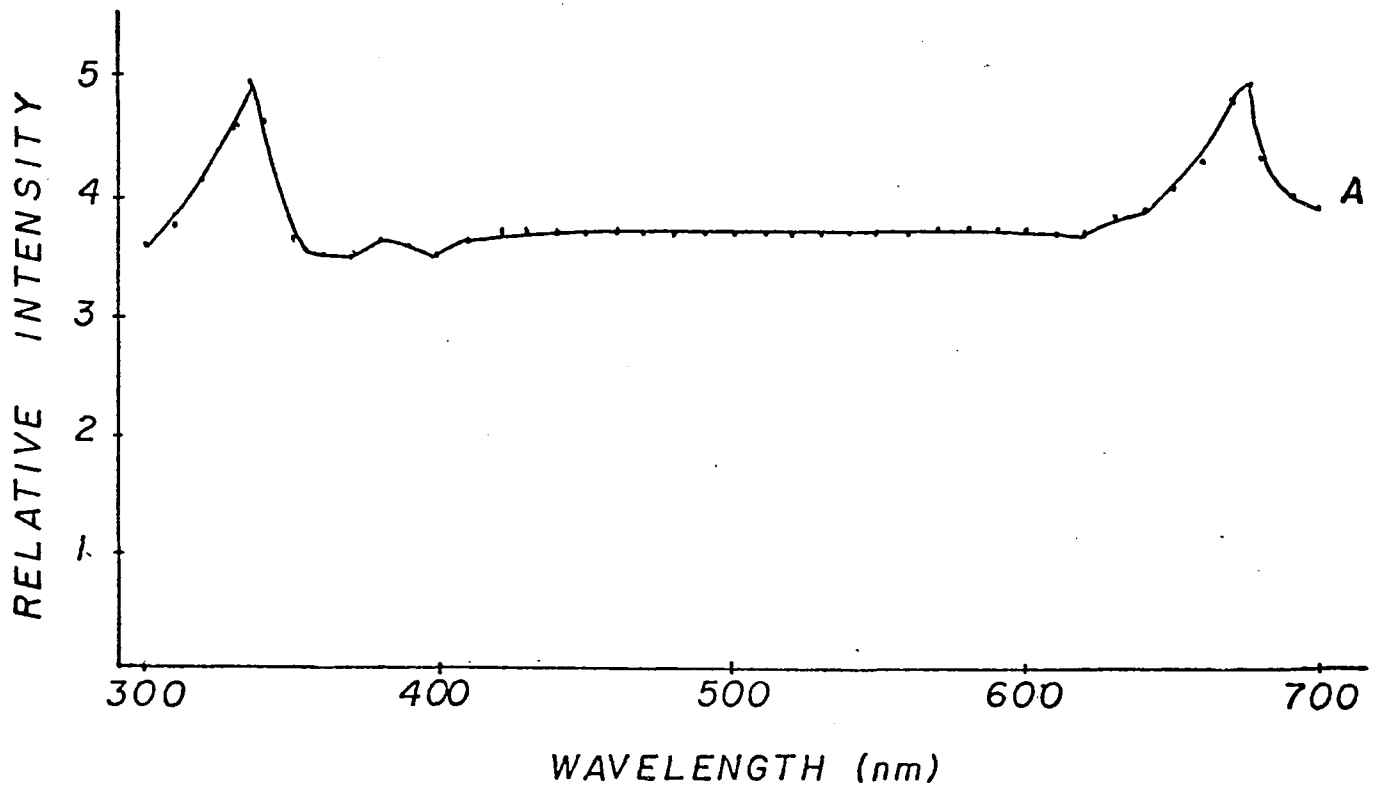

Figure 68. Intensity of scattered light versus wavelength using a Jarrel Ash monochromator.

Two different physical configurations of the monochromator and cuvette were evaluated. One with the cuvette and monochromator in their normal upright position with the length of the slits running vertically, and the other with the monochromator mounted on its side with the length of the slits in the horizontal position and the cuvette rotated 90° on its side.

Cuvette in Vertical Position

Of the two configurations the one with the cuvette mounted vertically with the laser beam passing through it as in Figure 69 could be considered the conventional method. The laser beam produced by the Avco-Everett nitrogen laser is 5.1 cm wide and .318 cm thick. As can be seen in this figure, a very small section of the cuvette is illuminated by the laser beam. The dimensions of the entrance slit to the Heath monochromator and the total illuminated area of the cuvette are shown in Figure 70. If the slit were positioned directly next to the cuvette it is apparent that only about one-quarter of the total area of the slit would be illuminated. In fact when the monochromator is moved away from the cuvette it is not the area of the slit that is important but the total viewing area as will be described later.

Cuvette in Horizontal Position

Not all light that passes through the slit will contribute to the spectral image. If it does not fall on the collimator mirror it will end up as scattered light. Therefore, it is necessary to fill as completely as possible both the slits and the collimator mirror of the

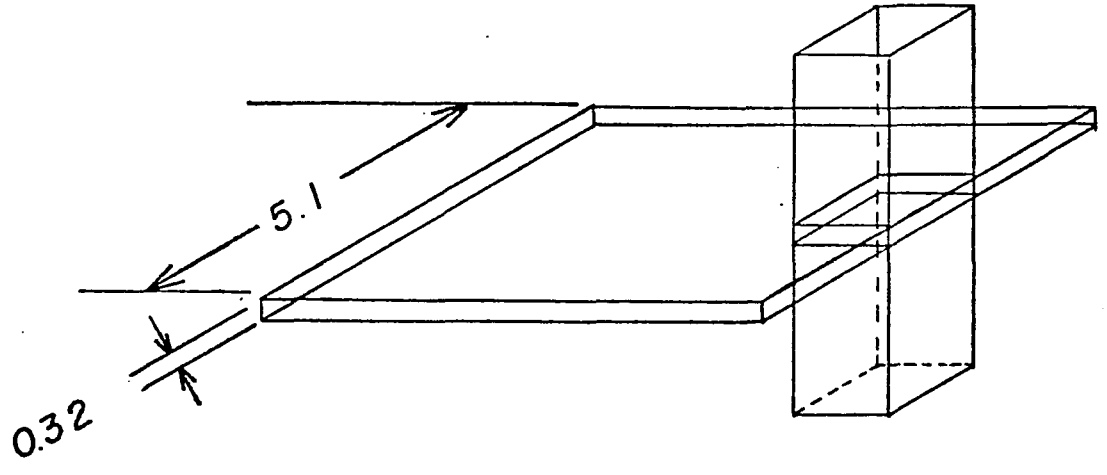

Figure 69. Orientation of the laser beam from the Avco-Everett nitrogen laser with respect to a cuvette in the vertical position.

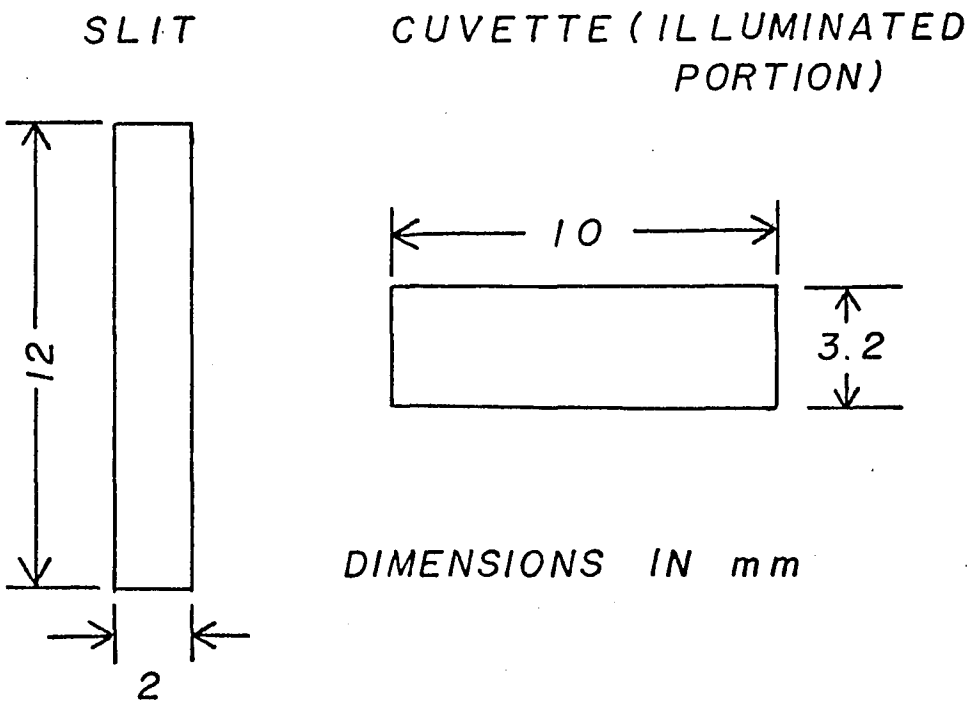

Figure 70. Size relationship between entrance slit of the Heath monochromator and the illuminated portion of a vertical cuvette.

monochromator to obtain the maximum spectral intensity. What this means is that ideally one would like a source to be either large enough or be able to bring it close enough to the slit to completely cover the angle of the collimator mirror. Figure 71 shows the angles covered by a collimator mirror in a hypothetical monochromator. If a source is large enough to cover the entire area in front of the slit described by planes x-x and y-y, then it will send the maximum amount of energy through the monochromator.

In an effort to totally fill the viewing area of the monochromator the cuvette was rotated 90 degrees as shown in Figure 72. In addition the monochromator was rotated 90 degrees such that the length of the entrance slits are now in a horizontal position in relation to the illuminated portion of the cuvette as shown in Figure 73. Thus by looking at the cuvette "end on" the entire length and width of the slits can be totally illuminated.

Evaluation of Horizontal and Vertical Viewing Positions

Several parameters are of interest in evaluating the two configurations described above, these include the net fluorescence intensity, the background intensity and the fluorescence to background ratio.

For the analysis of ethidium bromide at 600 nm the effect of slit width on the fluorescence and background intensity is shown in Figure 74. The concentration of ethidium bromide is 5×10^{-7} M and the photomultiplier tube was operated at 800 volts. In this diagram the background intensity for both the vertical and horizontal configurations

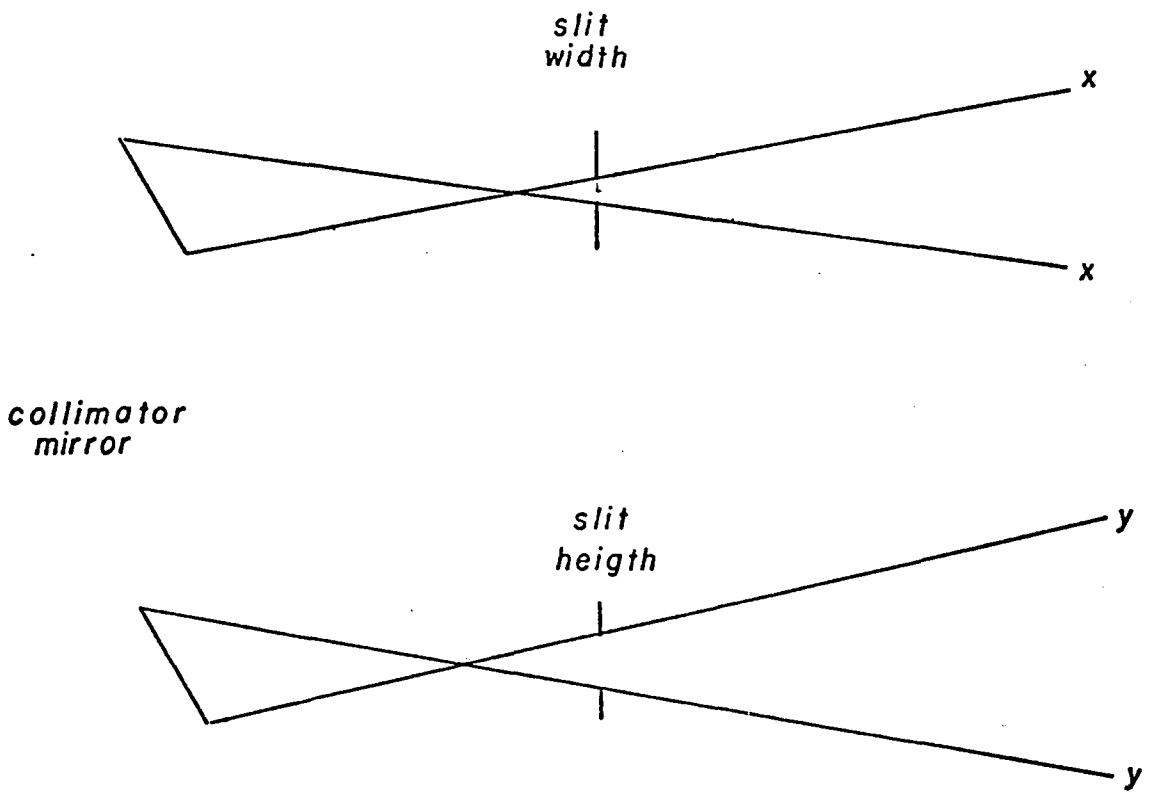

Figure 71. Viewing areas in the vertical and horizontal axis of a typical monochromator entrance slit.

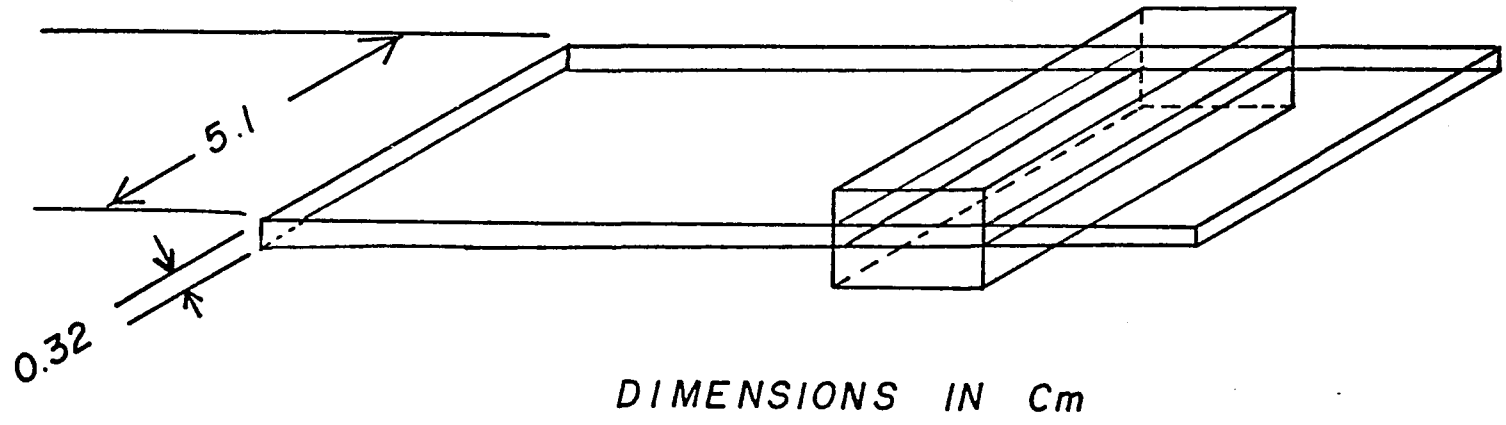

Figure 72. Orientation of the laser beam from the Avco-Everett nitrogen laser with respect to a cuvette in the horizontal position.

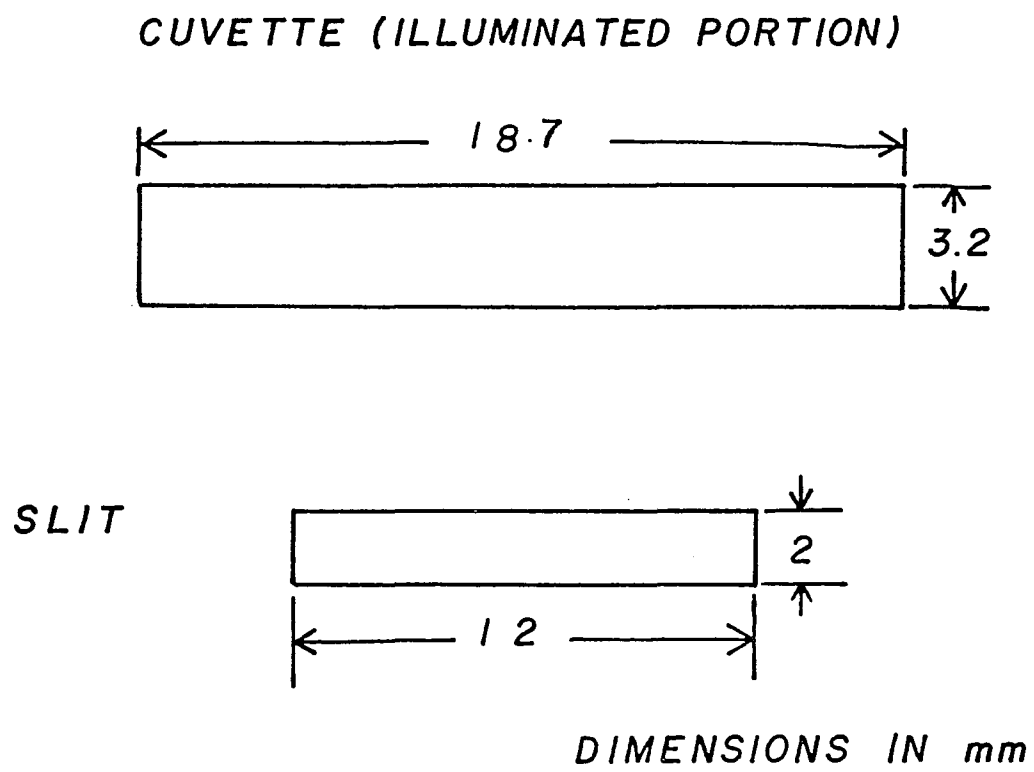

Figure 73. Size relationship between entrance slit of the Heath monochromator and the illuminated portion of a horizontal cuvette.

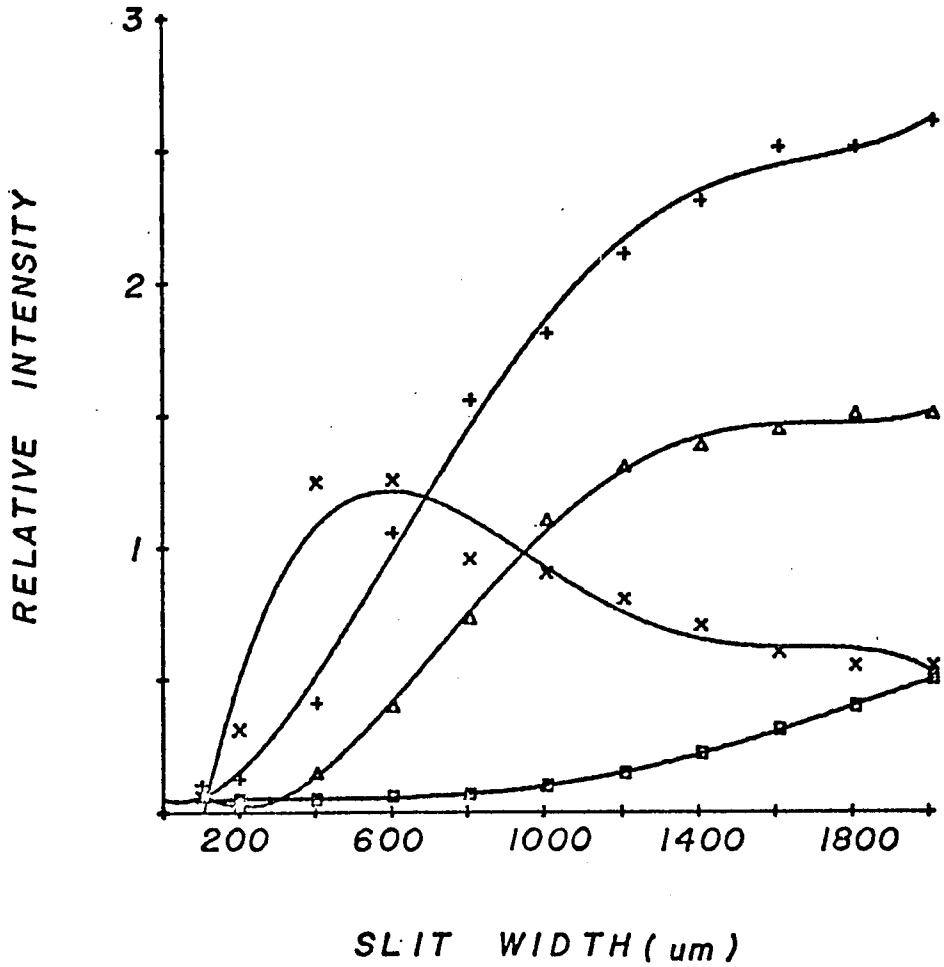

Figure 74. Background and fluorescence intensity (ethidium bromide 5 x 10^{-7} M) in both the vertical and horizontal positions with respect to slit width. -- + = background in horizontal position; □ = background in vertical position; X = fluorescence in horizontal position; △ = fluorescence in vertical position.

increases as the slit width is increased. The horizontal position shows a much larger increase in background intensity than the vertical position. This is reasonable since a larger portion of the cuvette is illuminated in the horizontal position which provides a larger scattering area for the incident beam. Although at 1400 microns both configurations show a leveling off of the scattered light intensity this never quite reaches a constant value.

The net fluorescence signal is seen to gradually increase as the slit width increases in the vertical case. This is again reasonable since a greater part of the cuvette is viewed at wider slit widths which simply means more light is being collected from the fluorescing molecules in the cuvette.

A different situation is seen to occur in the horizontal position. Here the fluorescence intensity at small slit widths is larger than that from the vertical position. This again follows since the entire slit is being filled with radiation from the cuvette and the path length through which the monochromator is viewing is longer. However, at the wider slit widths the fluorescent intensity in the horizontal position appears to decrease. This rather strange occurrence can be explained with the help of Figure 75.

Figure 75 is a diagram of the total observed signal (i.e., fluorescence and background) as a function of slit width. The total signal that is observed in the vertical position is found to continually increase as the slit width is increased. However, when looking at the total signal in the horizontal position, the signal initially increases

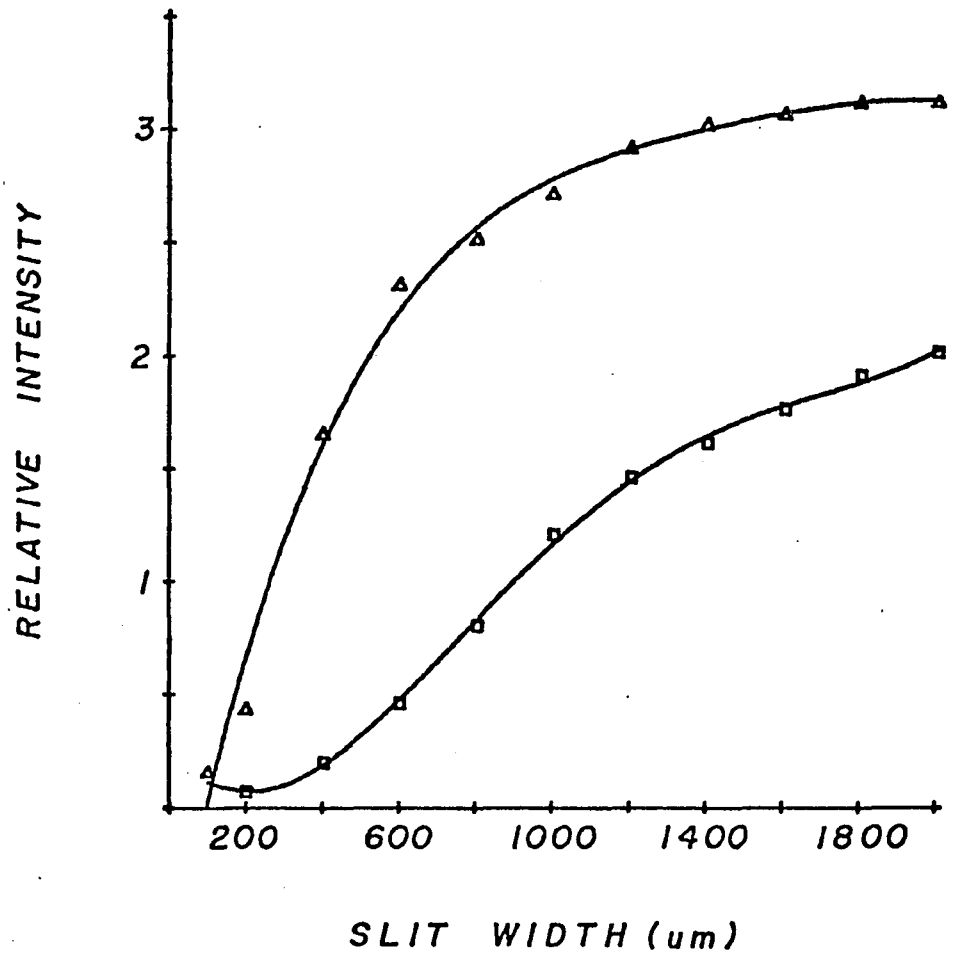

Figure 75. Total fluorescence versus slit width for ethidium bromide. -- △ = total signal in the horizontal position; □ = total signal in the vertical position.

with increasing slit width, but then levels off to a constant value at 1800 microns. At this point the photomultiplier tube has become saturated and cannot respond to any increase in intensity. When determining the net fluorescence signal the background is subtracted from the total signal. If a situation exists as shown in Figure 76 where the total signal obtained with a narrow slit is well within the range of the photomultiplier tube then both background and fluorescence can be easily determined. If however a situation exists as shown at a large slit width where the photomultiplier tube cannot respond to the entire signal (i.e., it is saturated) then when the background intensity is measured and subtracted from the total signal a fluorescent value less than the actual intensity will result. Because the fluorescent intensity decreases at large slit widths in the horizontal position and since the total signal in the horizontal position also reaches a limiting value, it appears that the photomultiplier tube is in fact being saturated in the horizontal position.

Although the net fluorescence intensity is important in determining which configuration might be best in terms of sensitivity a more useful value is the ratio of fluorescence to background. Figure 77 is a plot of the fluorescence-background ratio as a function of slit width in both the vertical and horizontal configurations. The maximum fluorescence-background ratio in the vertical position occurs at 1000 μm while in the horizontal it occurs at 400 μm. These results are not surprising as the vertical position results in less background scatter and as such allows larger slits to be employed. Referring back to Figure 74

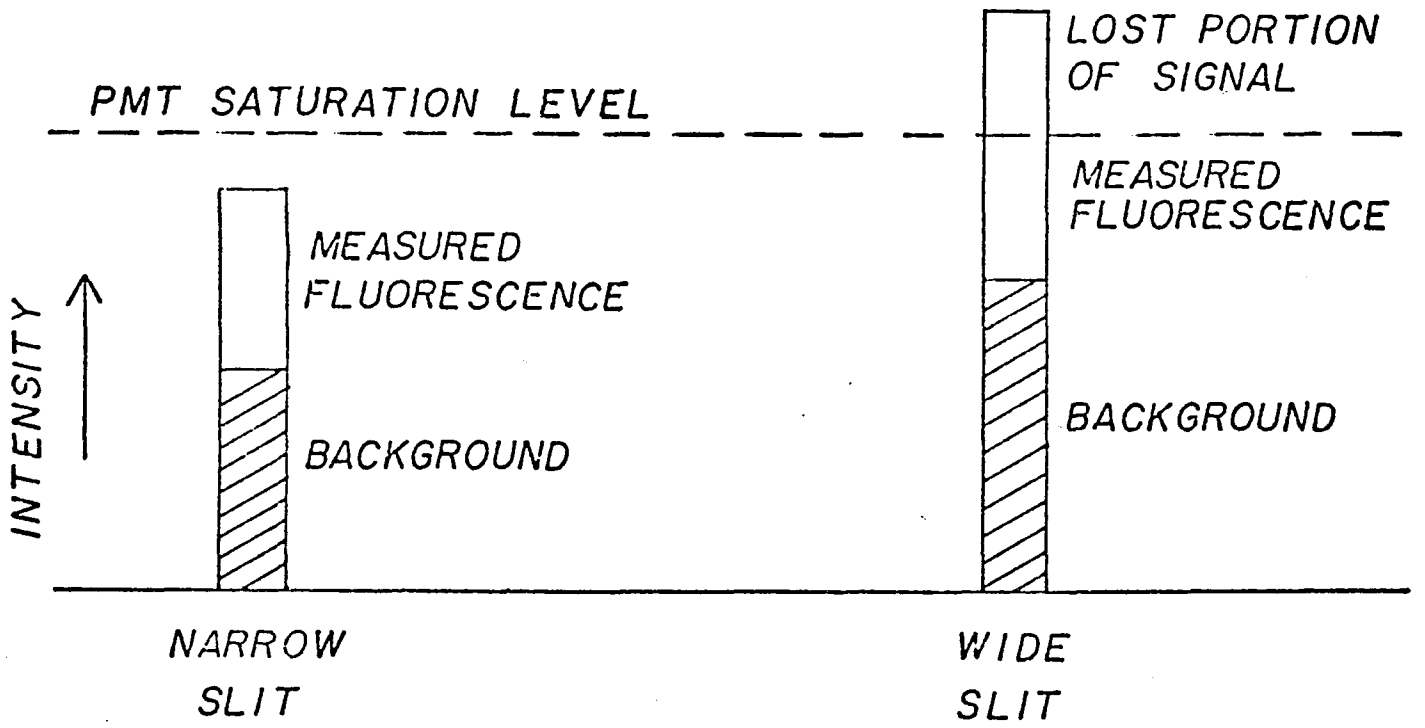

Figure 76. Diagram showing loss of fluorescence signal due to saturation of photomultiplier tube.

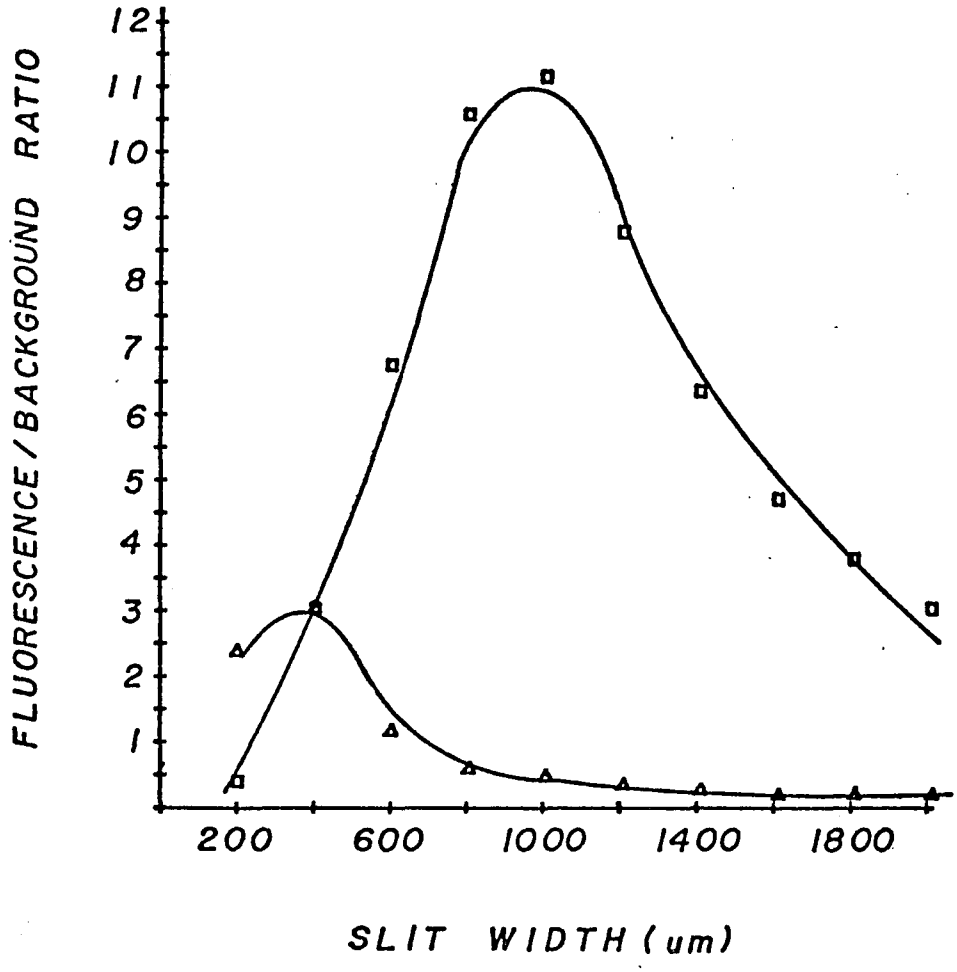

Figure 77. Fluorescence/background ratio for ethidium bromide in both the horizontal and vertical positions versus slit width. -- □ = vertical position; △ = horizontal position.

it can be seen that at 1000 μm the fluorescence signal is increasing much faster than the background. Just the opposite is true in the horizontal position. Since this configuration results in a high background level at the wider slit widths the best fluorescence-background ratio is found at the narrow slit width of 400 μm, where the background level is greatly reduced.

The advantage of operating in the vertical position at 1000 μm instead of the horizontal mode at 400 μm is reflected in the detection limits that can be obtained. The working curves for each case are shown in Figures 78 and 79 with the detection limit being the last point on the curve. In the vertical position a detection limit of 8×10^{-9} M of ethidium bromide was found as compared to 3×10^{-8} M with the horizontal position.

Referring back to Figure 67 the greatest scattered light occurs at the shorter wavelengths. Because the scattered light is greater here it might be expected that different operating parameters would be necessary to achieve optimum performance. The molecule used for this study was manadione dissolved in ethanol. The structure is shown below. This molecule has its excitation maximum at 335 nm and its fluorescence maximum at 480 nm (65).

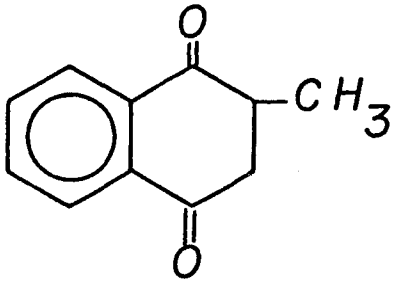

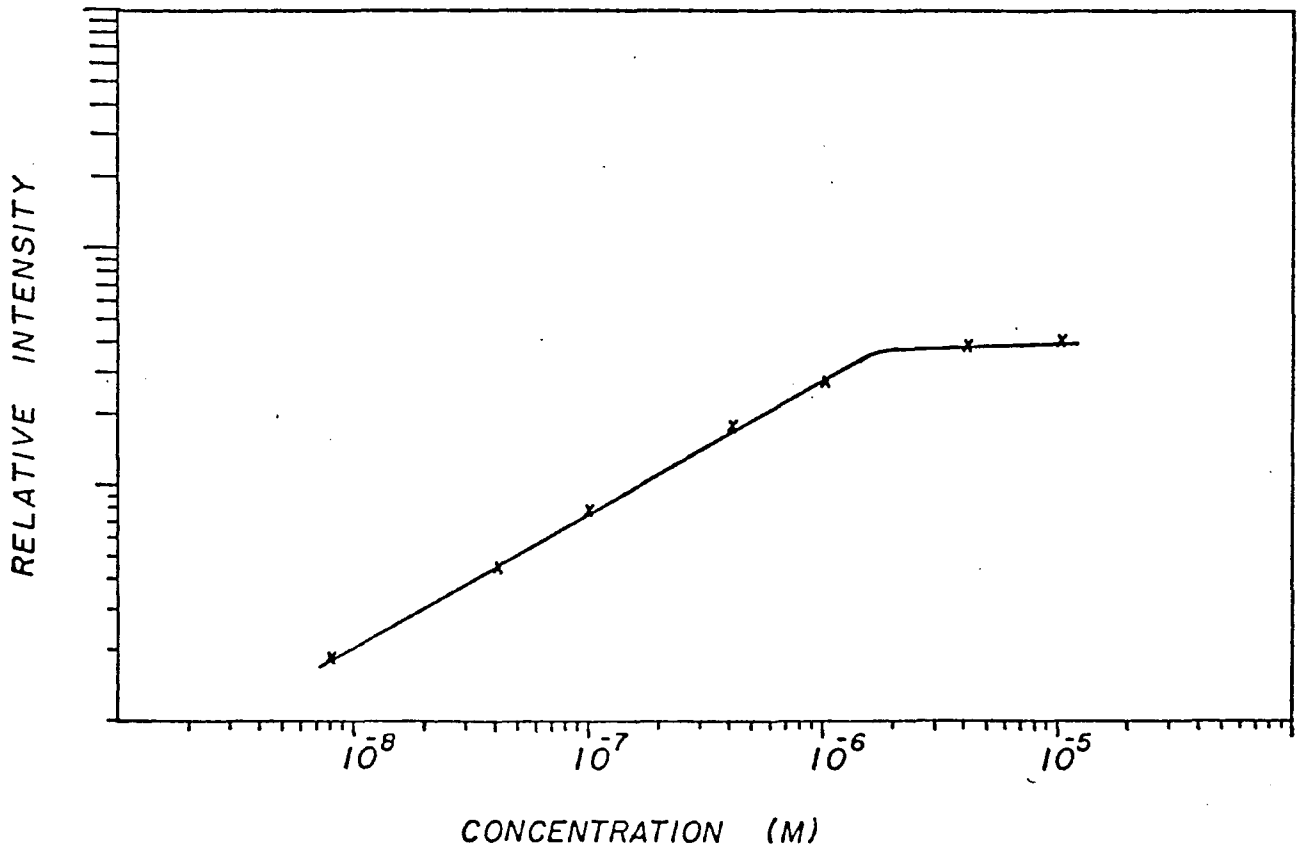

Figure 78. Working curve for ethidium bromide with the cuvette in the vertical position.

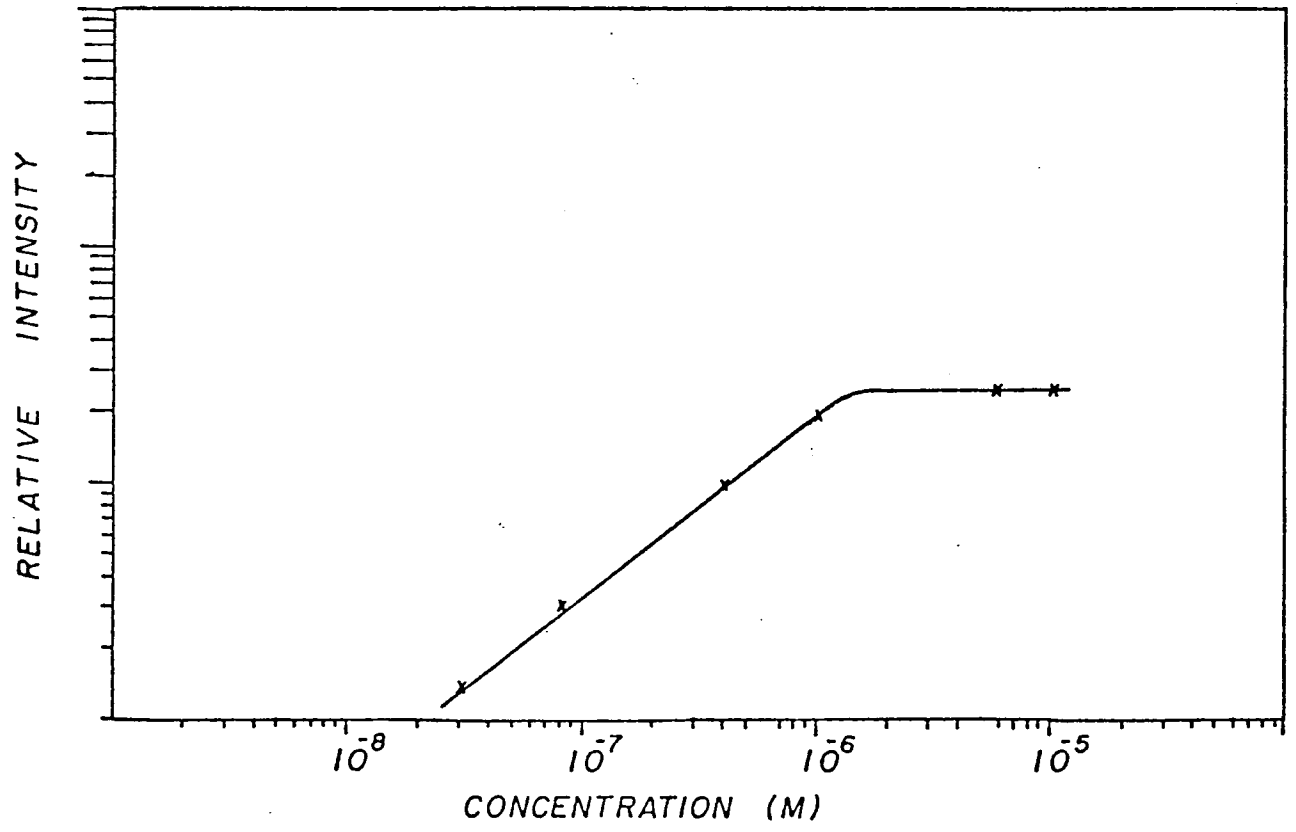

Figure 79. Working curve for ethidium bromide with the cuvette in the horizontal position.

Figure 80 shows the fluorescence and background intensities as a function of slit width for menadione in both the vertical and horizontal positions. In these experiments no filter was used. As with ethidium bromide the background intensity is much greater in the horizontal than in the vertical position. However, due to the increased background intensity at the shorter wavelengths used in this analysis the photomultiplier tube becomes saturated in both the horizontal and vertical positions. This is seen by a decrease in the apparent fluorescence intensity at 1400 μm in the vertical position. The fact that saturation again occurs at the wider slit width can be seen in Figure 81 by observing the total signal which again levels off to a constant value.

As a result of the high background level at this wavelength an interference filter was placed between the cuvette and the monochromator. The filter has a bandpass of 10 nm centered at 475 nm and is said by the manufacturer to be opaque at all other wavelengths.

With the filter in place the background and fluorescence intensities were observed as a function of slit width. The results are shown in Figure 82. As can be seen the filter does not block all of the scattered light from the cuvette. It does however reduce the intensity to a point where the photomultiplier tube is not saturated in the vertical position as was the case without the filter. Also the background is reduced to a point where it is always less than the fluorescence signal.

The effect of this on the fluorescence to background ratio can be seen in Figure 83. In the vertical position with the interference filter the best ratio is found at 1000 μm. Without the filter the

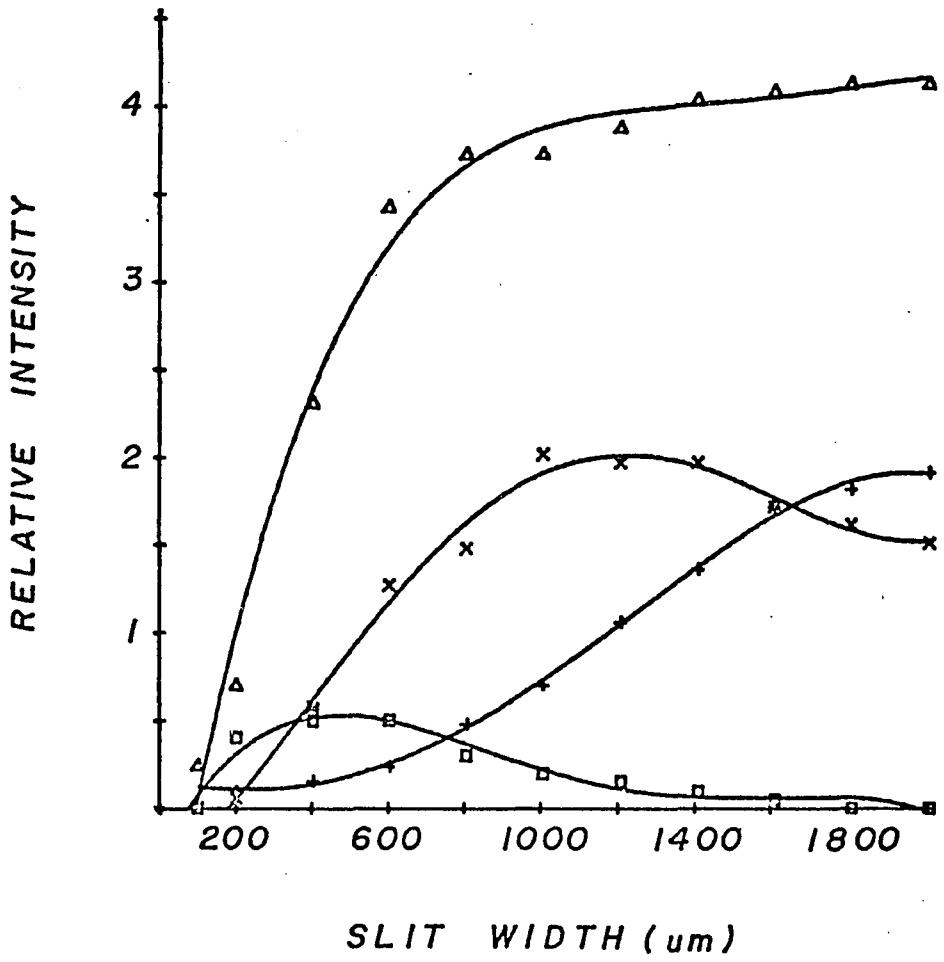

Figure 80. Background and fluorescence intensity (menadione concentration 0.5 µg/ml) without an interference filter in both the horizontal and vertical positions. -- △ = background in the horizontal position; + = background in the vertical position; X = fluorescence in the vertical position; □ = fluorescence in the horizontal position.

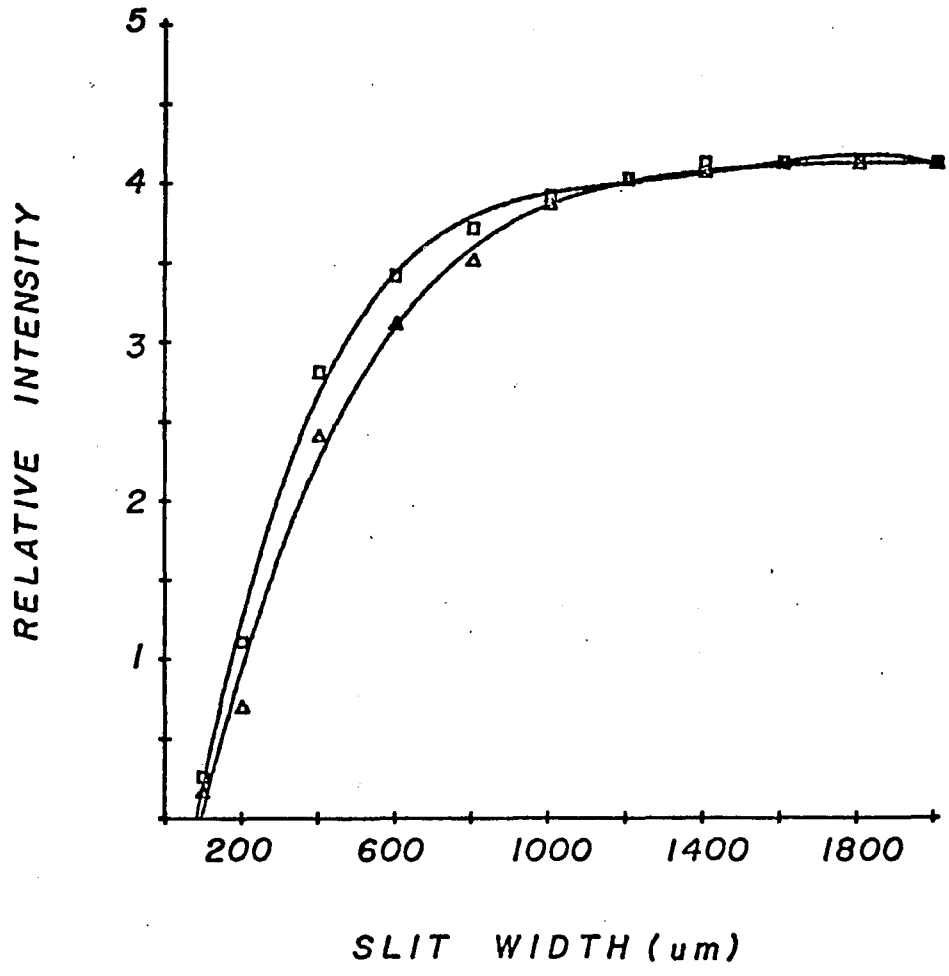

Figure 81. Total signal intensity (menadione concentration 0.5 µg/ml) in both the horizontal and vertical positions without a filter. -- □ = total signal in the horizontal position; △ = total signal in the vertical position.

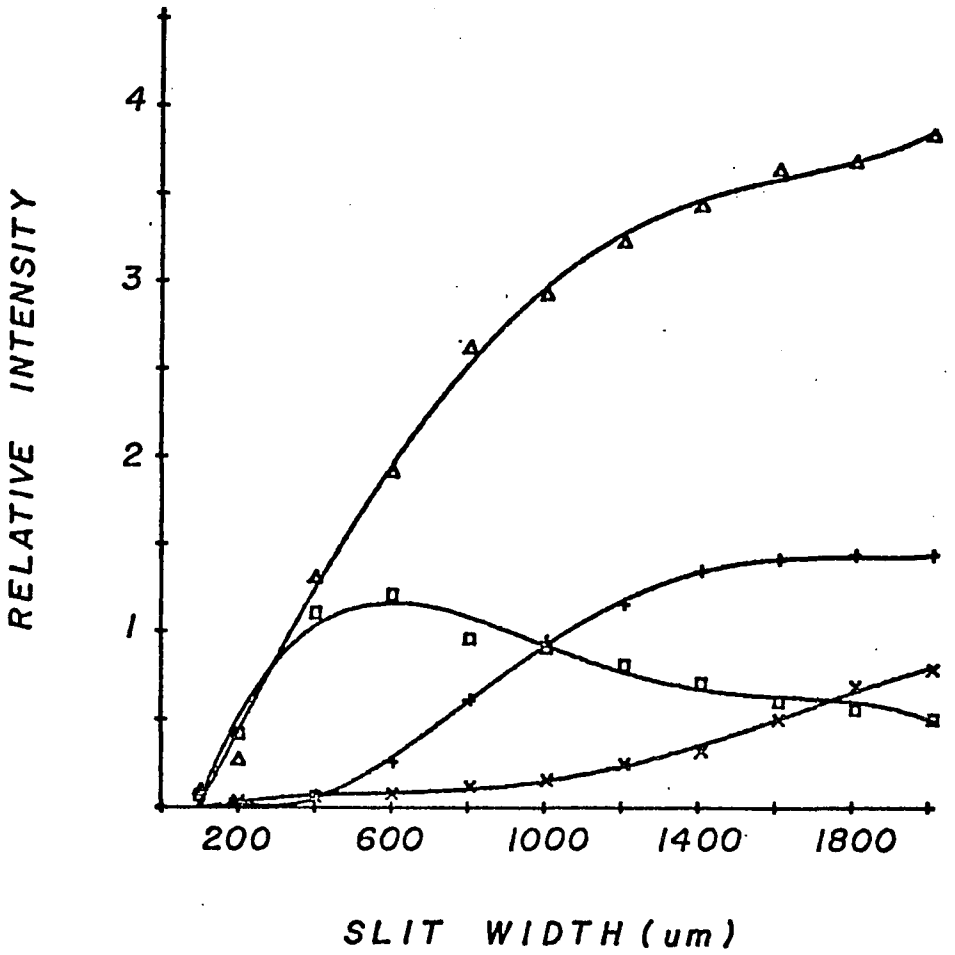

Figure 82. Variation of background and fluorescence intensity (menadione concentration 0.5 μg/ml), using an interference filter, versus slit width. -- △= background in the horizontal position; X = background in the vertical position; □ = fluorescence in the horizontal position; + = fluorescence in the vertical position.

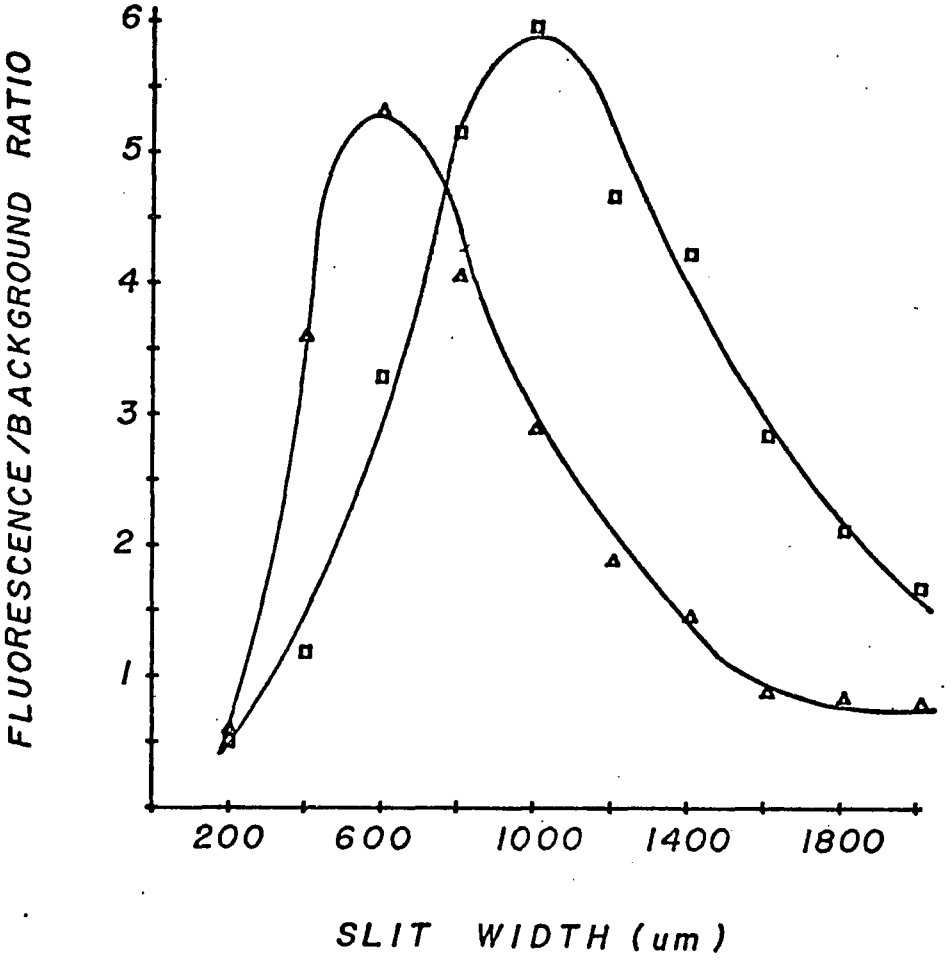

Figure 83. Fluorescence/background ratio for menadione with and without an interference filter in the vertical position. -- □ = vertical position with an interference filter; △ = vertical position without an interference filter.

optimum ratio occurs at 600 μm. The use of an interference filter affects the fluorescence-background ratio in two ways; first of all it reduces the background which results in a higher ratio and second it moves the maximum ratio to larger slit widths. The same effect can be seen in Figure 84 for the horizontal position.

Working curves and detection limits for menadione in the vertical configuration with and without the filter are shown in Figures 85 and 86. A detection limit of 0.02 μg/ml was when employing the filter. Without the filter a detection limit of 0.1 μg/ml was determined. These values are equal to or better than the value of 0.1 μg/ml as determined on the Aminco Bowman system. Thus the use of a filter to reduce background improves the sensitivity obtainable with laser excitation.

Increased Amplification of Readout Stage

In the studies reported above the amplifier used was a commercial design (Pacific Photometrics Inc.) with a gain of 10. An attempt was made to increase the gain of the amplifiers for readout employing laser excitation. The design of the amplifier has been discussed and was shown in Figure 57. Combining this amplifier with the one already in use would result in a total amplification factor of 75.

When employing both amplifiers it was expected that the total signal level would increase with a resultant decrease in the detection limit. What was found is that although the signal intensity increased the background intensity and noise level also increased. This increased noise level is partly the result of shot noise becoming a more significant factor in the total noise level.

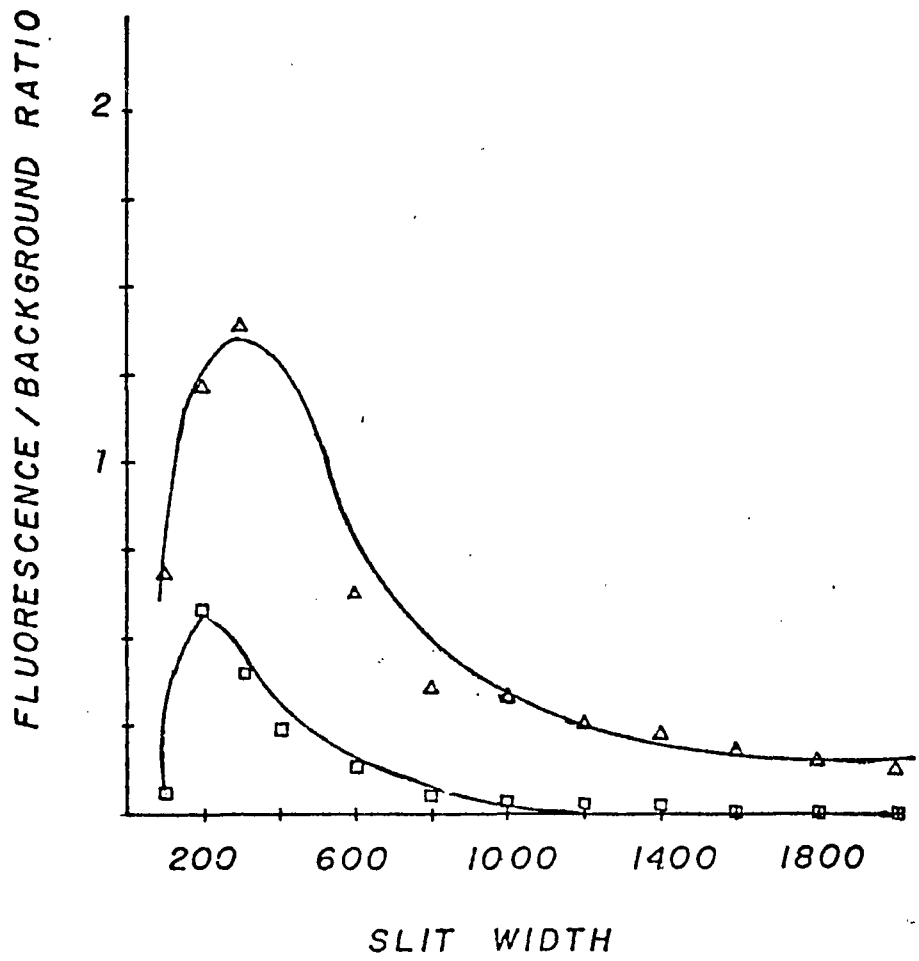

Figure 84. Fluorescence/background ratio for menadione with the cuvette in the horizontal position with and without an interference filter. -- □ = horizontal position without an interference filter; △ = horizontal position with an interference filter.

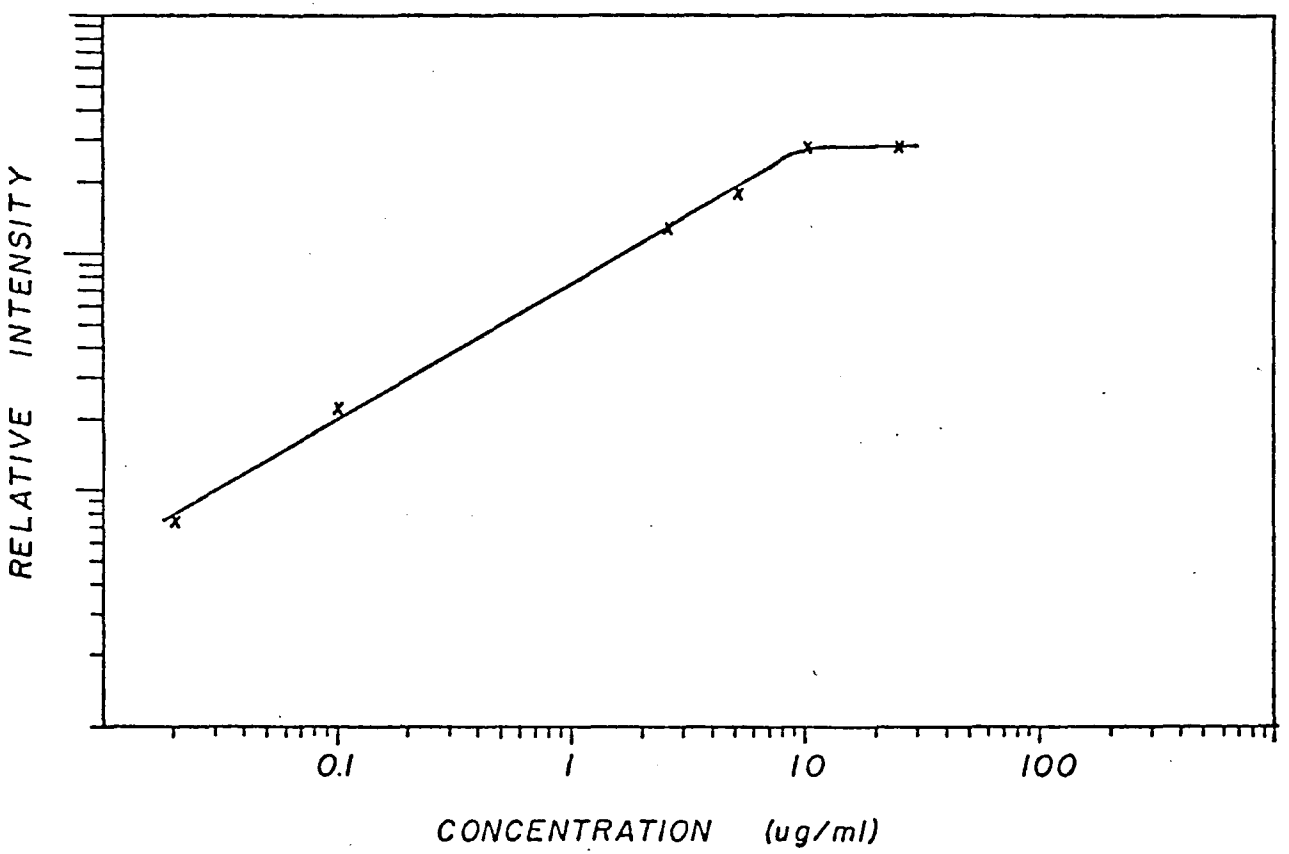

Figure 85. Working curve for menadione using an interference filter.

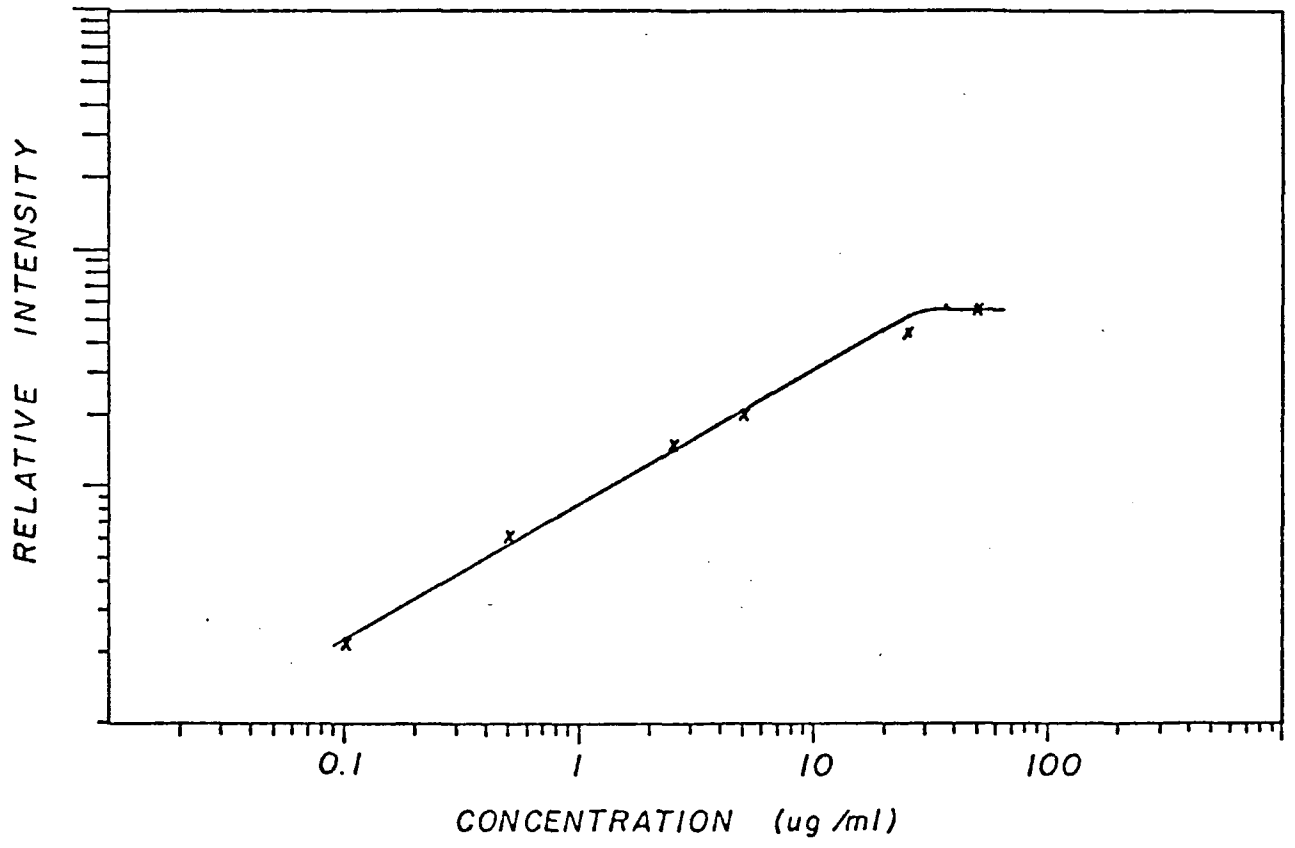

Figure 86. Working curve for menadione without the use of an interference filter.

As a result of the increased noise level the detection limit was found to be worse than before and the linear range of the working curve also decreased as shown in Figure 87 for ethidium bromide.

Conclusions

This study has shown the need for careful selection of experimental conditions to minimize the background emission level. When operating in a low scattering region such as the red a wide slit can be employed to take advantage of the full light gathering ability of a monochromator. A different set of conditions are necessary when conducting work in the blue portion of the spectrum. Here the scattered light becomes more intense and narrow slits or the use of a filter is recommended. Selection of the filter is most important Those which use a dye as the filtering agent should be avoided as fluorescence from the dye itself can be a serious background problem.

This study has also shown that the sensitivity obtainable with laser excitation can be excellent particularly when working in the red portion of the spectrum where scattered radiation from the source is not as intense. When working in this part of the spectrum it is possible to obtain detection limits which exceed those of conventional systems by a factor of 60. In the blue portion of the spectra this enhanced level of sensitivity dropped to a factor of 5 due to the increased level of scattered radiation.

The use of a horizontal arrangement to observe fluorescence from the cuvette did not result in the improved detection limit that might be expected. This again is partly the result of the increased background

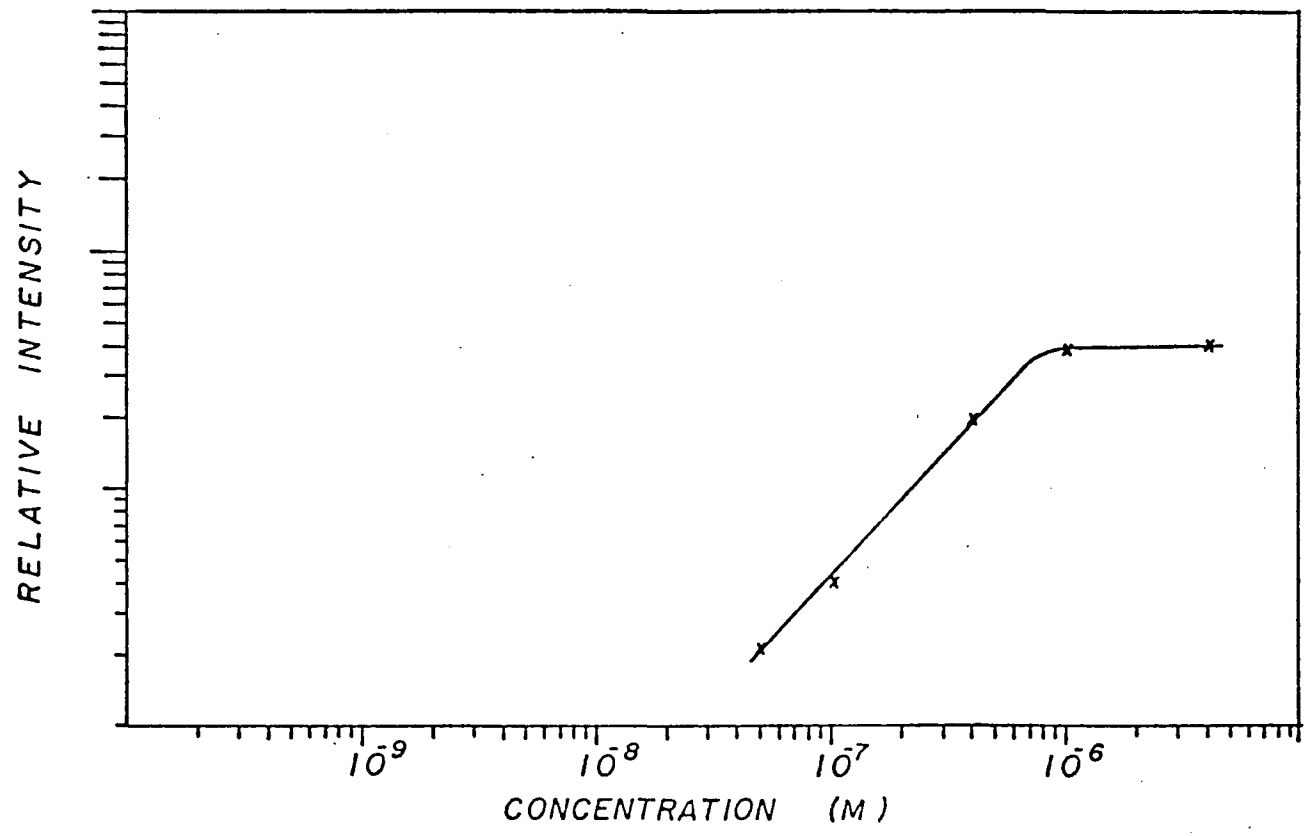

Figure 87. Working curve for ethidium bromide using additional amplification provided by the OEI amplifier system.

level which saturates the photomultiplier tube and prevents the use of wide slit widths. If this problem can be solved it would appear from the data that an increased fluorescence level would result with additional improvements in detection limits.

Suggestions for Further Research

This study has indicated that the major problem with laser excited molecular fluorescence is that the high background as a result of scattered light adversely affects the sensitivity. If this background could be greatly reduced or eliminated, additional enhanced sensitivity might very well be realized. One area of future work might involve attempts to eliminate or reduce this background which occurs as a result of scattered light. Although a better system of baffles might result in some reduction of the background, the use of a detector system that has its best response in the visible and a greatly reduced response factor in the ultraviolet might result in an improved fluorescence to background ratio. Most photomultiplier tubes unfortunately have their greatest response in the ultraviolet and blue portion of the spectrum. However, the new photosensitive semiconductor devices show the best response in the red while possessing a relatively poor response in the ultraviolet. Such devices when coupled with a monochromator might be ideally suited for analysis in the visible portion of the spectrum where heavy scattered ultraviolet radiation might also be present. In the past two years several papers have appeared in the literature describing semiconductor devices (photodiodes and phototransistors) as detection systems for flame spectrochemical analysis. Although the gain of these devices is

not as great as a photomultiplier continued research and development probably will improve this situation. At that time these devices might well result in improved sensitivity for laser excited molecular fluorescence.

Another area that needs further investigation is the use of amplifiers as part of the readout stage. The problems associated with the amplifiers in this study were due to the high frequency signals that were being measured. This prevented the construction of a variable gain amplifier which would allow the optimum amplification factor for this study to be selected. One solution to this problem would be to use a c.w. laser which would allow more conventional amplifiers to be connected to the photomultiplier tube. Cooling the photomultiplier tube with either water or ice would help reduce the problems encountered as a result of shot noise.

Additionally several possible projects are indicated from this work for laser excited flame atomic fluorescence. First, since the scattered light is such a significant factor in the background level the elimination of this from flame analysis should improve the detection limits obtainable by atomic fluorescence. The easiest and most direct way to approach this problem would be an investigation into the ease of desolvation in the flame as a function of generated aerosol droplet size. Most work done to date with laser excited flame atomic fluorescence has employed pneumatic nebulization systems. Because these nebulizers produce large droplet sizes it would be expected that, in the region of a flame normally used for analytical purposes, desolvation and

vaporization processes would be incomplete. By reducing the droplet size, through the use of ultrasonic or Babington nebulizers, the scattered signal may be reduced. As has been shown in this work reducing the scattered light allows the entrance slits to be opened wider and to collect more fluorescent radiation with a resulting decrease in detection limit.

Another investigation could be into the use of nonresonance fluorescence lines for analysis. Traditionally the resonance lines have been used because they are more intense. The laser might allow the nonresonance lines to be used and at the same time would help to eliminate problems of light scattered from the source. In the case of molecular fluorescence it has been shown that when analyzing fluorescence away from the source line that better sensitivity can be obtained.

The work reported here has shown that the pulse ultrasonic nebulizer is useful for both flame emission and atomic fluorescence analysis. To achieve maximum sensitivity it is necessary to open the slits to a wide position. This results in poorer resolution by the monochromator and in a changing background level when pure solvent is pulsed into the flame. The need for better sensitivity at smaller slit settings could be achieved by replacing the flame with an inductively coupled plasma. The higher temperature of the plasma would allow for the needed sensitivity at a smaller slit.

At the same time the small droplets of aerosol produced by the ultrasonic nebulizer would help to reduce the sample introduction problems associated with the plasma. This is because the smaller droplets

can enter the hot plasma region much easier than larger droplets. As a result more aerosol can enter the plasma with a possible decrease in detection limit. Thus the combining of these two methods might lead to some very interesting and useful results.

REFERENCES

1. Aldous, K. M., Bailey, B. W. and Rankin, J. M. Anal. Chem. 44, 19 (1972).

2. Aldous, K. M., Browner, R. F., Dagnall, R. M. and West, T. S. Anal. Chem. 42, 939 (1970).

3. Berlad, A. L. and Potter, A. E. Fifth Symposium on Combustion, Reinhold, New York, 1955, p. 728.

4. Berman, M. R. and Zare, R. N. Anal. Chem. 47, 1201 (1975).

5. Bradley, J. N. and Kistiakowsky, G. B. J. Chem. Phys. 35, 254 (1961).

6. Brand, L. and Witholt, B. Methods in Enzymology 11, 87 (1967).

7. Brand, L. and Witholt, B. Methods in Enzymology 11, 776 (1967).

8. Burns, V. W. F. Arch. Biochem. Biophys. 145, 248 (1971).

9. Calcote, H. F. Eighth Symposium on Combustion, Williams and Wilkins, Baltimore, 1962, p. 184.

10. Dean, J. A. and Rains, T. C. In Flame Emission and Atomic Absorption Spectrometry, Vol. 2, Dean, J. A. and Rains, T. C., Eds., Marcel Dekker, New York, 1971.

11. Delves, H. T. Analyst 95, 431 (1970.

12. Denton, M. B. Considerations in Laser-Excited Atomic Fluorescence Spectroscopy and Related Investigations, Ph. D. Thesis, University of Illinois, Urbana, Illinois, 1972.

13. Denton, M. B. and Malmstadt, H. V. Appl. Phys. Lett. 18, 485 (1971).

14. Denton, M. B. and Malmstadt, H. V. Anal. Chem. 44, 241 (1972).

15. Denton, M. B. and Malmstadt, H. V. Anal. Chem. 44, 1813 (1972).

16. Denton, M. B. and Swartz, D. B. Rev. Sci. Instrum. 45, 81 (1974).

17. Enikolopyan, N. S. Seventh Symposium on Combustion, Butterworths, London, 1959, p. 157.

18. Exley, D. and Sproat, D. J. Sci. Instrum. 35, 202 (1958).

19. Fairbank, W. M., Hansch, T. W. and Schawlow, A. L. J. Opt. Soc. Am. 65, 199 (1975).

20. Fiorino, J. A., Kniseley, R. N. and Fassel, V. A. Spectrochim. Acta. 23B, 413 (1968).

21. Fraser, L. M. and Winefordner, J. D. Anal. Chem. 43, 1693 (1971).

22. Fraser, L. M. and Winefordner, J. D. Anal. Chem. 44, 1444 (1972).

23. Fristrom, R. M. Ninth Symposium on Combustion, Academic, New York, 1963, p. 560.

24. Fueno, T., Mukherjee, N. R., Ree, T. and Eyring, H. Eighth Symposium on Combustion, Williams and Wilkins, Baltimore, 1962, p. 222.

25. Green, J. A. and Sugden, T. M. Ninth Symposium on Combustion, Academic, New York, 1963, p. 607.

26. Gutzler, D. E. Investigations into the Role of a Premixed Oxygen-Hydrogen Flame in Flame Emission Spectrometry, M. S. Thesis, The University of Arizona, Tucson, 1973.

27. Gutzler, D. E. and Denton, M. B. Anal. Chem. 47, 830 (1975).

28. Hand, C. W. J. Chem. Phys. 36, 2521 (1962).

29. Harrington, D. C. and Malmstadt, H. V. Anal. Chem. 47, 471 (1975).

30. Hermann, R. In Flame Emission and Atomic Absorption Spectrometry, Vol. 2, Dean, J. A. and Rains, T. C.,Eds., Marcel Dekker, New York, 1971.

31. Hieftje, G. M. Appl. Spectrosc. 25, 653 (1971).

32. Hieftje, G. M. and Malmstadt, H. V. Anal. Chem. 40, 1860 (1968).

33. Hieftje, G. M. and Malmstadt, H. V. Anal. Chem. 41, 1735 (1969).

34. Jennings, D. A. and Keller, R. A. J.A.C.S. 94, 9249 (1972).

35. Jona, F. and Shirane, G. Ferroelectric Crystals, Vol. 1, Pergamon Press, New York, 1962.

36. Kahn, H. L., Peterson, G. E. and Schallis, J. E. Atomic Absorption Newsletter 7, 35 (1968).

37. Kanzig, W. In McGraw-Hill Encyclopedia of Science and Technology, Vol. 5, McGraw-Hill Inc., New York, 1971.

38. Kistiakowsky, G. B. and Richards, L. W. J. Chem. Phys. 36, 1707 (1962).

39. Korte, N. E., Moyers, J. L. and Denton, M. B. Anal. Chem. 45, 530 (1973).

40. Kuhl, J. and Marowsky, G. Opt. Comm. 4, 125 (1971).

41. Lang, R. J. J. Acoust. Soc. Am. 34, 6 (1962).

42. Le Pecq, J. B. and Paoletti, C. J. Mol. Biol. 27, 87 (1967).

43. Lewis, B. and von Elbe, A. Combustion, Flames and Explosions of Gases, Academic, New York, 1951.

44. Lewis, B. and von Elbe, A. J. Chem. Phys. 11, 75 (1943).

45. Lobdel, D. D. J. Acoust. Soc. Am. 43, 229 (1968).

46. Lvov, B. V. Spectrochim. Acta 24B, 55 (1969).

47. Massmann, H. Spectrochim Acta 23B, 215 (1968).

48. Massmann, H. In Flame Emission and Atomic Absorption Spectrometry, Vol. 2, Dean, J. A. and Rains, T. C., Eds., Marcel Dekker, New York, 1971.

49. Mavrodineau, R. and Borteux, H. Flame Spectroscopy, John Wiley and Sons, Inc., New York, 1965, p. 18.

50. McCarthy, W. J. and Winefordner, J. D. J. Chem. Ed. 44, 136 (1967).

51. Mukherjee, N. R., Fueno, T., Eyring, H. and Ree, T. Eighth Symposium on Combustion, Williams and Wilkins, Baltimore, 1962, p. 1.

52. Muller, P. Exptl. Cell Res. Suppl. 5, 118 (1958).

53. Neumann, S. and Kriese, M. Spectrochim. Acta 29B, 127 (1974).

54. Oberg, P. A., Ulfendahl, H. R. and Wallion, B. G. Anal. Biochem. 18, 543 (1967).

55. Parsons, M. L., McCarthy, W. J. and Winefordner, J. D. J. Chem. Ed. 44, 215 (1967).

56. Piepmeier, E. H. Spectrochim. Acta 27B, 431 (1972).

57. Piepmeier, E. H. Spectrochim. Acta 27B, 445 (1972).

58. Pungor, E. and Cornides, I. In Flame Emission and Atomic Absorption Spectrometry, Vol. 1, Dean, J. A. and Rains, T. C., Eds., Marcel Dekker, New York, 1971, p. 84.

59. Ramsay, J. A. J. Exptl. Biol. 27, 407 (1950).

60. Ramsay, J. A., Brown, R. H. J. and Falloon, S. W. H. W. J. Exptl. Biol. 30, 1 (1953).

61. Ramsay, J. A., Falloon, S. W. H. W. and Machin, K. E. J. Sci. Instrum. 28, 75 (1951).

62. Ringhardtz, I. and Welz, B. Z. Anal. Chem. 243, 190 (1968).

63. Smith, B. W., Plankey, F. W., Omenetto, N., Host, L. P. and Winefordner, J. P. Spectrochim. Acta 30A, 1459 (1974).

64. Solomon, A. K. and Caton, D. C. Anal. Chem. 27, 1849 (1955).

65. Udenfriend, S., Duggan, D. E., Vasta, B. M. and Brodie, B. B. J. Pharmacol. Exptl. Therap. 120, 26 (1957).

66. Vigny, P. and Duquesne, A. Photochem. Photobiol. 20, 15 (1974).

67. von Elbe, G. and Lewis, B. Third Symposium on Combustion, Williams and Wilkins, Baltimore, 1949, p. 68.

68. Vurek, G. G. and Bowman, R. L. Sci. 149, 448 (1965).

69. Winefordner, J. D., McCarthy, W. J. and St. John, P. A. J. Chem. Ed. 44, 80 (1967).

70. Winefordner, J. D., Parsons, M. L., Mansfield, J. M. and McCarthy, W. J. Spectrochim. Acta 23B, 37 (1967).